การสังเคราะห์ตัวเร่งปฏิกิริยาพอรัสซิลิการ่วมกับนิกเกิล-ไทเทเนียมไนไตรด์สำหรับดรายรีฟอร์มิงของมีเทน

นางสาวมัสลิน โชติรัตน์

วิทยานิพนธ์นี้เป็นส่วนหนึ่งของการศึกษาตามหลักสูตรปริญญาวิทยาศาสตรดุษฎีบัณฑิต
สาขาวิชาปิโตรเคมี
คณะวิทยาศาสตร์ จุฬาลงกรณ์มหาวิทยาลัย
ปีการศึกษา 2560

SYNTHESIS OF Ni-TiN INCORPORATED POROUS SILICA CATALYSTS FOR DRY REFORMING OF METHANE

Miss Maslin Chotirach

A Dissertation Submitted in Partial Fulfillment of the Requirements
for the Degree of Doctor of Philosophy Program in Petrochemistry
Faculty of Science
Chulalongkorn University
Academic Year 2017

Thesis Title	SYNTHESIS OF Ni-TiN INCORPORATED POROUS SILICA CATALYSTS FOR DRY REFORMING OF METHANE
By	Miss Maslin Chotirach
Field of Study	Petrochemistry
Thesis Advisor	Assistant Professor Sukkaneste Tungasmita, Ph.D.
Thesis Co-Advisor	Professor Supawan Tantayanon, Ph.D.
	Duangamol Tungasmita, Ph.D.

Accepted by the Faculty of Science, Chulalongkorn University in Partial Fulfillment of the Requirements for the Doctoral Degree

.....Dean of the Faculty of Science
(Associate Professor Polkit Sangvanich, Ph.D.)

THESIS COMMITTEE

.....Chairman
(Professor Tharapong Vitidsant, Ph.D.)

.....Thesis Advisor
(Assistant Professor Sukkaneste Tungasmita, Ph.D.)

.....Thesis Co-Advisor
(Professor Supawan Tantayanon, Ph.D.)

.....Thesis Co-Advisor
(Duangamol Tungasmita, Ph.D.)

.....Examiner
(Associate Professor Warinthorn Chavasiri, Ph.D.)

.....Examiner
(Nipaka Sukpirom, Ph.D.)

.....External Examiner
(Sutheerawat Samingprai, Ph.D.)

มัสลิน โชติรัตน์ : การสังเคราะห์ตัวเร่งปฏิกิริยาพอรัสซิลิการ่วมกับนิกเกิล-ไทเทเนียมไนไตรด์สำหรับดรายรีฟอร์มิงของมีเทน (SYNTHESIS OF Ni-TiN INCORPORATED POROUS SILICA CATALYSTS FOR DRY REFORMING OF METHANE) อ.ที่ปรึกษาวิทยานิพนธ์หลัก: ผศ. ดร. สุคคเณศ ตุงคะสมิต, อ.ที่ปรึกษาวิทยานิพนธ์ร่วม: ศ. ดร. ศุภวรรณ ตันตยานนท์, ดร. ดวงกมล ตุงคะสมิต, 110 หน้า.

ตัวเร่งปฏิกิริยานิกเกิลที่มีไทเทเนียมไนไตรด์เป็นโปรโมเตอร์ชนิดใหม่ได้ถูกสังเคราะห์และทดสอบเป็นอีกหนึ่งตัวเลือกสำหรับตัวเร่งปฏิกิริยาในปฏิกิริยาดรายรีฟอร์มิงของมีเทน ตัวเร่งปฏิกิริยาชุดนี้มีนิกเกิลและไทเทเนียมไนไตรด์ในปริมาณต่างๆ ได้ถูกเตรียมโดยใช้ 2 ขั้นตอน คือ การสังเคราะห์เอสบีเอ-15 ที่มีไทเทเนียมไนไตรด์แบบขั้นตอนเดียว ตามด้วยการสังเคราะห์นิกเกิลโดยวิธีฝังตัว ผลของตัวเร่งปฏิกิริยานิกเกิลที่มีไทเทเนียมไนไตรด์เป็นโปรโมเตอร์ต่อปฏิกิริยาดรายรีฟอร์มิงของมีเทน ศึกษาที่อุณหภูมิ 700°C อัตราส่วนมีเทนต่อคาร์บอนไดออกไซด์เท่ากับ 1 เป็นระยะเวลา 4 ชั่วโมง โดยตัวเร่งปฏิกิริยาที่ดีที่ให้ค่าการเปลี่ยนของคาร์บอนไดออกไซด์และมีเทน รวมถึงการเกิดไฮโดรเจนและคาร์บอนมอนอกไซด์ที่สูง ได้ถูกนำมาศึกษาเพิ่มเติมเปรียบเทียบกับตัวเร่งปฏิกิริยานิกเกิลที่ไม่มีโปรโมเตอร์เป็นระยะเวลา 12 ชั่วโมง ผลการทดลองแสดงให้เห็นว่าประสิทธิภาพของตัวเร่งปฏิกิริยานิกเกิลได้ถูกปรับปรุงขึ้นเมื่อมีไทเทเนียมไนไตรด์ร่วมด้วย นอกจากนี้ยังพบว่าตัวรองรับเอสบีเอ-15 เหมาะสมต่อปฏิกิริยาดรายรีฟอร์มิงมากกว่าซีโอไลต์ Y โดยสภาพความเป็นเบสที่เหมาะสมเกิดจากการปรากฏของนิกเกิลและไทเทเนียมไนไตรด์บนตัวรองรับเอสบีเอ-15 ค่าการเปลี่ยนที่สูงสุดของมีเทนและคาร์บอนไดออกไซด์ได้จากตัวเร่งปฏิกิริยาที่ประกอบด้วยน้ำหนักของนิกเกิลร้อยละ 10 และน้ำหนักของไทเทเนียมไนไตรด์ร้อยละ 5 ของน้ำหนักตัวเร่งปฏิกิริยาบนตัวรองรับเอสบีเอ-15 ดังนั้นนิกเกิลไทเทเนียมไนไตรด์บนตัวรองรับเอสบีเอ-15 สามารถเป็นอีกหนึ่งตัวเลือกของตัวเร่งปฏิกิริยาสำหรับดรายรีฟอร์มิงของมีเทน

สาขาวิชา ปิโตรเคมี ลายมือชื่อนิสิต .....

ปีการศึกษา 2560 ลายมือชื่อ อ.ที่ปรึกษาหลัก .....

ลายมือชื่อ อ.ที่ปรึกษาร่วม .....

ลายมือชื่อ อ.ที่ปรึกษาร่วม .....

5572832523 : MAJOR PETROCHEMISTRY
KEYWORDS: TIANIUM NITRIDE / PROMOTER / DRY REFORMING / SBA-15 / ZEOLITE Y

MASLIN CHOTIRACH: SYNTHESIS OF Ni-TiN INCORPORATED POROUS SILICA CATALYSTS FOR DRY REFORMING OF METHANE. ADVISOR: ASST. PROF. SUKKANESTE TUNGASMITA, Ph.D., CO-ADVISOR: PROF. SUPAWAN TANTAYANON, Ph.D., DUANGAMOL TUNGASMITA, Ph.D., 110 pp.

A new titanium nitride (TiN) promoted nickel catalyst was synthesized and tested as an alternative catalyst in the dry reforming of methane (DRM). The series of this catalyst with various Ni and TiN contents was prepared in two steps, direct synthesis of SBA-15 in the presence of TiN, followed by the impregnation of Ni. The influence of TiN promoted Ni-based catalyst on dry reforming reaction was investigated at the temperature of 700ºC and atmospheric pressure for a duration of 4 h, using feed ratio of CH_4/CO_2 = 1. The promising catalysts, that gave highest CO_2 and CH_4 conversions as well as the production of H_2 and CO, were selected. These selected catalysts were compared to non-promoted Ni catalyst in the reaction for 12 h for further investigation. The results showed that the performance of Ni catalyst in the reaction was improved by incorporated TiN. Moreover, the SBA-15 support is favor to DRM reaction more than zeolite Y. The appropriate basicity was generated by the presence of both Ni and TiN supported on mesoporous silica SBA-15. The maximum CH_4 and CO_2 conversions were obtained from the catalyst containing 10 wt% Ni and ~ 5 wt% TiN supported on SBA-15. Therefore, Ni/TiN-SBA-15 could be a competitive candidate catalyst for DRM reaction.

Field of Study: Petrochemistry
Academic Year: 2017

Student's Signature .....
Advisor's Signature .....
Co-Advisor's Signature .....
Co-Advisor's Signature .....

ACKNOWLEDGEMENTS

This work cannot be completed without support, motivation and guidance from many people who contributed to this thesis. Foremost, I would like to express my greatest gratitude and sincere thank to my advisors, Assist.Prof.Dr.Sukkaneste Tungasmita, Prof.Dr.Supawan Tantayanon and Dr.Duangamol Tungasmita, for guidance, supervision and helpful suggestion throughout this research.

I am also grateful to Prof. Dr. Tharapong Vitidsant, Assist. Prof. Dr. Warinthorn Chavasiri, Dr. Nipaka Sukpirom, and Dr. Sutheerawat Samingprai for serving as chairman and members of thesis committee, respectively and for their comments and suggestions.

I would like to thank the members of DT lab for their help and suggestion in catalyst preparation and characterization. I would like to extend my deepest gratitude to Dr.Sarocha Sumrunronnasak and Dr.Thitinat Sukonkate for her help and guidance throughout this work. Many thanks are going to my friends and colleagues for their friendship and encouragement.

I gratefully acknowledge the financial support by grants from the Human Resource Development in Science Project (Science Achievement Scholarship of Thailand; SAST). The materials support from Bangkok Industrial Gas Co., Ltd. and funding support from Program of Petrochemistry and Polymer Science, and the 90th Anniversary of Chulalongkorn University Fund (Ratchadaphiseksomphot Endowment Fund).

Finally, I would like to express my gratitude to my family for their understanding, entirely care, encouragement and great support throughout my study.

CONTENTS

Page

List of Tables

List of Figures

List of Schemes

CHAPTER I
INTRODUCTION

1.1 Overview and motivations

Transition metal nitrides possess different physicochemical properties from their parent metals. The incorporation of nitrogen in the metal lattice enlarges the lattice spacing metal–metal. As a result, nitride materials can behave like platinum metals due to similarities in the electronic structure for most of the reactions. They also have the potential of being their substitute, i.e. tungsten nitride, molybdenum nitride, vanadium nitride, and chromium nitride [1-3]. In addition, metal nitrides are catalytically active for many hydrogen transfer reactions such as ammonia synthesis, hydrogenation, methanation and hydrogenolysis [2, 3].

For the applications, there are few studies about using noble metal-free to increase the performance and endurance of Ni-based catalysts in dry reforming reaction (DRM) i.e. Ni–Mo_2C/Al_2O, Ni-WC, Co_3Mo_3N and Ni/Si_3N_4 and $Ni/BN@mSiO_2$ [4-8]. Herein, titanium nitride (TiN) was one of the best candidate materials to promote Ni/SBA-15 catalyst. TiN has many unique properties, such as high chemical resistivity and functional physical properties including hardness, high melting point, low sintering tendencies and relative low-cost commercially available material [9-13].

As we known, carbon dioxide (CO_2) and methane (CH_4) are two of the major greenhouse gases that substantially contribute to the world temperature increase and the consequent effect of climate change. Growing concerns about long-term environmental impacts of anthropogenic greenhouse gas emission have prompted many attempts to reduce the amount of warming gases in the atmosphere through their utilization. Currently, dry reforming reaction of methane with CO_2, one of the utilizations of greenhouse gases, has received considerable attention. This reaction

establishes the conversion of CO_2 and CH_4, which can be converted to syngas (mixtures of H_2 and CO). It can be used as an intermediate for the preparation of valuable chemicals. This syngas, particularly with high CO production, was used as raw materials to produce oxygenated hydrocarbon i.e. dimethyl ether and methanol [14-16]. However, DRM process often depends on noble metal (Rh, Ru, Pd, Pt, and Ir) as well as Ni-based catalysts [17-20]. Due to the high cost of noble metals, Ni-based catalysts start to have attracted much interest for their high catalytic activity and low cost. Nevertheless, they have less stability than noble metal because of carbon formation over Ni-active sites, which lead to catalyst deactivation during the process [19-22]. Therefore, we focused on the development of high catalytic activity Ni-based catalyst with excellent resistance to coke.

Interestingly, several attempts have been made to suppress carbon deposition on Ni-based catalysts by the addition of a promoter to modify the basicity of the support, such as CaO or MgO which can enhance the stability and reduce carbon formation [23-27]. With these promoters, Lewis basicity was increased and so the ability to chemisorb CO_2 was improved by shifting the equilibrium toward CO ($CO_2 + C \rightarrow 2CO$) which was proposed to reduce the Boudouard reaction ($2CO \rightleftharpoons CO_2 + C$) and carbon nucleation [24-26]. Besides, the addition of a promoter could control the size and facilitate the dispersion of NiO particles into mesoporous support which could prevent the formation and growth of carbon and anti-sintering of metal catalysts [28, 29].

The type and nature of catalyst also show a significant influence on catalytic performance and carbon formation [22, 24]. In this case, mesoporous silica SBA-15 has been extensively studied; regarding to its electronically neutral framework, large pore size and high surface area which is suitable for being a support of a catalyst in dry reforming reaction. The uses of zeolite also has been intensively studied, regarding to technical applications as adsorbents, catalysts and catalyst supports with high surface area, tunable large pore and narrow pore size distribution [30-32].

To achieve the environmental and economic benefits for industrial, the development of catalyst with high catalytic performance and coke resistance is another focus point. Therefore, Ni/TiN incorporated into mesoporous silica is one of the new type catalysts for this purpose. The preparation and characterization of Ni/TiN particles embedded on the mesoporous silica SBA-15 and zeolite Y as well as the possibility of using titanium nitride (TiN) to improve the catalytic activity of Ni-based catalyst was explored in this work.

1.2 Objectives

1. To synthesize Ni and TiN incorporated porous silica as noble metal free catalysts
2. To investigate the catalytic performance of porous silica supported Ni-based catalyst with TiN promoter in dry reforming of methane
3. To compare the catalytic performance of the promoted Ni catalyst toward micro and mesoporous silica support

1.3 Scope of research

In this study, SBA-15 and TiN-SBA-15 were synthesized and characterized before Ni impregnation to form Ni/TiN-SBA-15. The catalytic performance of Ni/SBA-15 with and without TiN was tested in DRM reaction for 4 h. The superior catalysts were selected to characterize for the chemical and physical properties and test. The catalyst stability test also has been done for 12 h. Finally, the optimal content of Ni and TiN was prepared on zeolite Y support and also studied the catalytic activity.

The scope of research was briefly explained as follow:

1. Synthesis of Ni and TiN incorporated SBA-15 and zeolite Y

1.1 SBA-15 and TiN modified SBA-15 supported catalysts were prepared by direct synthesis and then Ni impregnation. As for zeolite Y supported catalyst, Zeolite Y was impregnated with TiN and Ni, respectively.

1.2 Investigate the effects of synthesis parameters on the physicochemical properties of Ni and TiN incorporated porous silica

- TiN loading; 8, 15, 22, 28 wt%
- Ni content; 2.5, 5, 7.5, 10 wt%

1.3 Investigate the as-prepared samples by various characterizations

2. Study on the catalytic performance.

2.1 Study the effectiveness of the prepared catalysts (24 samples) in DRM reaction

2.2 Investigate the effects of reaction parameters on the selected catalysts:

- Molar ratio of CH_4 : CO_2, 1:1
- Catalyst loading, 0.025, 0.05 and 0.1 g
- Reaction temperature at 450-700 °C

2.3 Determine the amount of carbon deposition by using the thermogravimetric analyzer

2.4 Study the catalytic stability

3. Study on the catalytic performance of the optimum contents of Ni and TiN on zeolite suppo

CHAPTER II
THEORY AND LITERATURE REVIEWS

2.1 Titanium nitride (TiN)

TiN is a ceramic material with high melting point, excellent thermal stability, high oxidation and chemical resistance. One of the unique characteristics of metal nitrides is their bonds in the structure, which is largely metallic with strong overlap between the metal atoms. Therefore, the interstitial sites within the metal sub-lattice are normally prone to occupy by the N atoms [1, 33]. TiN has a crystal structure of NaCl-type or face centered cubic structure (fcc). Nonetheless, the structure could exhibit different content of nitrogen; TiN_x compounds with the fraction (*x)* can vary from 0.6 to 1.2 [34].

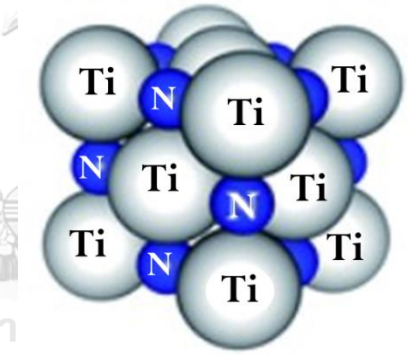

Figure 2.1 FCC structure of TiN [35]

Noteworthy, it was revealed that early-transition-metal carbides and nitrides exhibit catalytic activities that are similar to those of noble metals or platinum-group metals (PGMs) [1, 33, 36]. In case of TiN, it has not only the advantages as low costs and high availability but the catalytic applications, such as oxidation, reduction, alkylation and hydrogenolysis, were also reported [11-13, 37]. This makes it a good choice for the development of catalyst with high catalytic performance and coke resistance. Therefore, TiN is one of the most attractive promoters in many industrial applications, as the reforming of methane with carbon dioxide.

Table 2.1 Physicochemical properties of TiN [38].

Property	Information
Form	Powder
Molecular Weight (g/mol)	61.87
Particle size	< 3μm
Melting point (°C)	2930
Density (g/ml)	5.24
Crystallography	Cubic
Color	Black
Vickers Hardness (GPa)	18 to 21
Solubility In Water	Partly soluble in water

2.2 SBA-15

SBA-15 (Santa Barbara Amorphous) is a mesoporous silica material with a uniform, well-ordered structure and the pore diameter in the range of 2–50 nm. Its unique characteristics is suitable for many industrial applications i.e., catalysis, ion-exchange, separation, adsorption and nanotechnology. [39, 40] It was developed since 1998 by Zhao et al. [32].

Typical synthesis requirements of SBA-15 involve a triblock copolymer as a structure directing agent and the Tetraethyl Orthosilicate (TEOS) as a silica source. Many researchers have paid considerable attention to the development of mesoporous silica in order to design their preferred properties. In terms of material synthesis, several studies have reported the use of functionalized SBA-15 for both direct- and post-synthesis, together with organic and inorganic compositions such as NH_2-groups,

Pr-SO_3H, Al, and TiO_2 [41-46]. A comparison of all the mentioned processes has revealed that one-step direct synthesis method has many advantages over post-synthesis method, such as higher specific surface area and pore volume, which can reduce the blockage of pore channels and agglomeration on the surface, avoiding to a loss in the effectiveness of the desired mesoporous composite [47]. However, the addition of a new component to the SBA-15 structure is challenging. The key to success here is not only maintaining the hexagonal structure but also adding-up new features into the material.

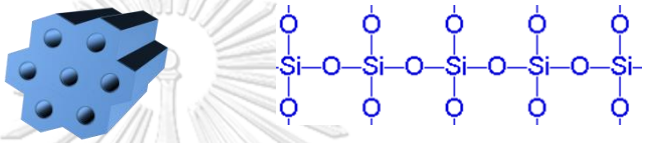

Figure 2.2 Hexagonal structure of SBA-15

2.3 Zeolite Y

Zeolites are microporous crystalline aluminosilicates, consisted of AlO_4 and SiO_4 joined into 3-dimensional frameworks. Zeolite Y exhibits the FAU (faujasite) structure, which has pores arranged perpendicular to each other. Faujasite was first discovered in 1842 by Damour and this named was for Barthélemy Faujas de Saint-Fond, a French geologist and volcanologist [48].

Zeolite Y has the largest pores over any known zeolite at 7.4 Å and the aperture is formed by a 12 member ring which results in a larger cavity of diameter 12Å [49]. The cavity is surrounded by 10 sodalite cages and the unit cell is cubic with a length of 24.7Å. It has a void volume fraction of 0.48, with a Si/Al ratio > 1.5. It has thermally decomposes temperature at 793ºC. It has some interest points to develop a metal-based catalyst for the industrial applications of CO_2 reforming of CH_4 since zeolite Y provide excellent properties (e.g. high surface area, high thermal stabilities,

and high affinities for CO_2 adsorption) so it has a potential for being a catalyst support in the DRM reaction [50-52].

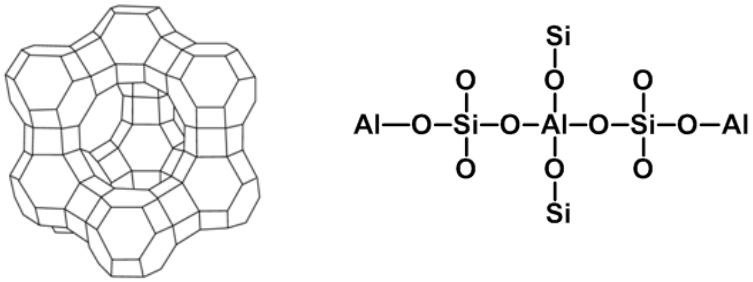

Figure 2.3 Faujasite structure of zeolite Y [53]

2.4 Dry reforming (DRM)

The increased concern on the contribution of greenhouse gases to global warming pushes the interest in the replacement of a reactant from steam to CO_2. The dry reforming reaction (DRM) can be represented by eq.1. The two most abundant greenhouse gases in the atmosphere, CO_2 and CH_4, are used as the reactants to produce syngas with H_2/CO ratio ≤ 1 which leads to higher selectivity for long chain hydrocarbons production [17].

$$CO_2 + CH_4 \rightleftharpoons 2H_2 + 2CO \qquad \Delta H°_{298} = 247 \text{ kJ mol}^{-1}$$

The reforming of CH_4 with CO_2 (DRM) has attracted considerable interest from researchers to the development for practical utilization, as it provides many advantages namely, reduction of CO_2 and CH_4, alteration of the main greenhouse gases (CH_4 and CO_2) into syngas. DRM is also an efficient usage of low-grade natural gas resources consisting of natural gas and CO_2 for valuable syngas production of high CO/H_2 ratio.

2.4.1 Reaction thermodynamics

DRM (eq.1 in Table 2.2) is a highly endothermic reforming reaction with regard to its thermodynamics of reforming with CO_2 is similar to steam reforming (SM) reaction but slightly higher endothermic than SM. Moreover, DRM produces synthesis gas lower H_2/CO ratio than SM. In addition, carbon dioxide could be counted as an oxidizing agent in DRM reaction [22] which is not oxygen or steam that requires in other reforming reactions. The chemistry and other chemical reactions involving in carbon dioxide reforming of methane are revealed as eq.1-6 in the Table 2.2.

The existing of CO_2 raises a possibility to generate carbon or coke on catalyst surface due to the reverse water gas shift (RWGS) reaction (eq.5) which not only utilize H_2 but also produce CO. Thus, the reaction equilibrium of DRM (eq.1) might affected by the simultaneous RWGS reaction, this leads to a lower of H_2/CO ratio than 1.

Table 2.2 Reaction equilibrium for syngas production from CH_4 and CO_2 [54, 55]

Reaction	$\Delta H°_{298}$	$\Delta G°$	Limiting Temperature (°C)	eq.
$CO_2 + CH_4 \rightleftharpoons 2H_2 + 2CO$ (DRM)	247	61770-67.32T	lower limit 640	1
$CH_4 + H_2O \rightleftharpoons CO + 3H_2$	206.2			2
$CH_4 \rightleftharpoons C_{ads} + 2H_2$ (methane cracking)	75	2190-26.45T	lower limit 557	3
$2CO \rightleftharpoons CO_2 + C_{ads}$ (Boudouard reaction)	-172	39810+40.87T	upper limit 700	4
$CO_2 + H_2 \rightleftharpoons CO + H_2O$ (reverse water gas shift)	41	-8545+7.84T	upper limit 820	5
$CO_2 + H_2 \rightleftharpoons C_{ads} + H_2O$ (reverse carbon gasification)	-131			6

Catalysts have been employed to reduce the energy demand for activation the reaction with regards to equilibrium calculations. Meanwhile, catalyst deactivation due to coke deposition via the Boudouard reaction (eq. 4) and/or CH_4 decomposition (eq. 3) is also a major problem. CH_4 decomposition and the RWGS are endothermic reaction and favored at higher temperatures. However, the reverse carbon gasification (eq.6) and the Boudouard reaction are exothermic reaction and favored at lower temperatures. Consequently, the results of thermodynamics analysis of these reactions indicated that carbon formation is occurred during the temperature range of 500-700°C [15, 55]. In addition, the equilibrium conversion of DRM (eq.1) could enrich at higher temperature to avoid side reactions (eq. 3, 4 and 6).

2.4.2 Reaction mechanism

Many researchers have been attempted to clarify the reaction mechanism in the carbon dioxide reforming of methane. However, the mechanism of this reaction over supported metal catalyst depends on various factors for example; the type of catalyst and support, temperature and the ratio of reactants. In brief, CH_4 is adsorbed on metal surface and then dissociated to hydrogen and hydrocarbon species, CH_x (x = 0–4), the number of x depends on temperature and the type of substrate. After CH_x and H atoms are resided on the active sites of metal, hydrogen species are recombined to form hydrogen molecule and gradually desorbed into hydrogen gas.

However, types of support also provide different mechanism. As for acidic supports, the reactants both CO_2 and CH_4 are only accelerated on the active sites of metal and produce the carbon soot which could block the metal active sites. In case of the basic supports, CO_2 is activated on the support into a carbonate species then it is reduced by CH_x species to generate carbon monoxide (CO). Furthermore, loading another metal or a promoter could play an important role to promote the mechanism [15, 54]. The possible proposed reaction mechanism in DRM process with catalyst is presented in Figure. 2.2 and Table 2.2.

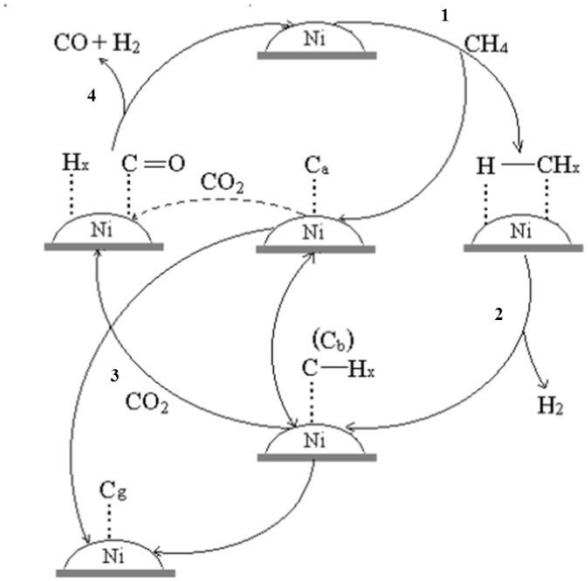

Figure 2.4 Mechanism of DRM reaction via the nickel catalyst (C_a: carbidic species (C_α), C_b: carbonaceous species (C_β), C_g: carbidic clusters species ($C\gamma$). Dotted line is the less possible pathway) [56].

Table 2.3 Reaction mechanism of DRM reaction over the supported metal catalyst [54].

Catalyst composition	**Proposed mechanism**
Metal active site ; $M_{(as)}$	$CH_4 + 2M_{(as)} \rightleftharpoons CH_3{-}M_{(as)} + H{-}M_{(as)}$
	$CH_3{-}M_{(as)}{-}M_{(as)} \rightleftharpoons CH_2{-}M_{(as)} + H{-}M_{(as)}$
	$CH_2{-}M_{(as)}{-}M_{(as)} \rightleftharpoons CH{-}M_{(as)} + H{-}M_{(as)}$
	$CH{-}M_{(as)}{-}M_{(as)} \rightleftharpoons C{-}M_{(as)} + H{-}M_{(as)}$
	$2H{-}M_{(as)} \rightleftharpoons H_{2(g)}{-}M_{(as)}$
Support	• **Acidic support:** $CO_{2(g)} \rightleftharpoons CO_{2(metal)}$ $CO_{2(metal)} \rightleftharpoons CO_{(metal)} + O_{(metal)}$ $CO_{2(metal)} \rightleftharpoons CO_{(gas)}$
	• **Basic support:** $CO_{2(g)} \rightleftharpoons CO_{2(support)}$ $CO_{2(support)} + O^{2-}{}_{(support)} \rightleftharpoons CO_3{}^{2-}{}_{(support)}$ $2H_{(metal)} \rightleftharpoons 2H_{(support)}$ $CO_3{}^{2-}{}_{(support)} + 2H_{(support)} \rightleftharpoons HCO_2{}^{-}{}_{(support)} + OH^{-}{}_{(support)}$ $CO_{(support)} \rightleftharpoons CO_{(gas)}$
Promoter	$CO_{2(g)} \rightleftharpoons O_{(promoter)} + CO_{(support)}$ $O_{(promoter)} + C_{(metal)} \rightleftharpoons CO_{(gas)}$

2.5 Catalyst for DRM

2.5.1 Metal (active species)

Accordingly, dry reforming is a strongly endothermic reaction which requires high temperatures, this leads to the rapid deactivation of the catalyst by carbon deposition and/or metal sintering. It is well-known that noble metals; Ru, Rh, Pd and Pt catalysts are very active in this reaction [19-22]. Regarding a high expense of noble metals, they are not suitable to apply as a large scale in industries. Interestingly, Non-noble (Ni, Co and Fe) metal catalysts also show high catalytic activities [57]. Ni seems to be the most outstanding choice because it is cheaper, and comparatively more active and selective. However Ni based catalysts have a tendency to deactivate by coking [21, 22]. Thus, a current challenge is to find a noble-metal-free catalyst that is resistant towards coking.

2.5.2 Support

Besides the active metal, the catalyst support is also an important parameter for dry reforming. Several studies have shown that the nature of support influences in terms of surface area, acid-basic sites and metal support interaction which affects the catalytic activity and coke deposition [22]. In this case, the oxide supports (CeO_2, ZrO_2, MgO, SiO_2, TiO_2 Al_2O_3, etc) greatly impact the catalyst activity due to their large surface area and basic property. From the previous studies, silica oxide especially SBA-15 and zeolite-Y have potential properties for being supported in dry reforming reaction due to their porous structure, high surface area and more resistance to deactivation by coking [15, 51, 58].

2.5.3 Promoter

An additive without its own catalytic properties but improves the catalytic activity is called a promoter. In general, CO_2 adsorption and dissociation take place on catalysts surface during the DRM process. As for CO_2 is an acid gas so these steps

could enhance by a basic catalyst. Therefore, the addition of an alkali or a basic promoter (MgO, CaO, TiO_2, Y_2O_3, etc) to the catalysts was productive in mitigation of coking [24, 28, 59, 60]. Moreover, a small amount of noble metals were also introduced into the catalysts as a promoter regarding to their high catalytic activity and less coke formation.

2.5.4 Carbon formation

Various types of carbon were formed during the DRM reaction which relates to the reactivity. Generally, there are three types of carbonaceous species presented on the Ni catalysts; carbidic species (α-C), carbonaceous species (β-C), carbidic clusters species (γ-C) (see in Figure. 2.2). The α-C was considered for CO formation, while the less active carbon types (β- C and γ-C) affected to catalyst deactivation. The previous studies revealed that different types of carbon represented alternation roles in the DRM reaction. The less reactive (β-C) was suggested as a main contribution in the catalyst deactivation. In case of α-C, it was enlarged with the continued DRM reaction. However, this linear relation brings to the conclusion that α-C could play as a reaction intermediate [24, 61]. These unstable surface carbides are subsequently decomposes into filamentous and encapsulating carbon as shown in Fig 2.3 [62]. For filamentous carbon, metal particles often appear at the tips of the growth carbon due to weak interaction between metal and support [62, 63]. In case of the encapsulating carbon, the graphitic layers are formed around the whole surface of metal particles. These lead to blockage of the active sites and deactivate the catalysts [64].

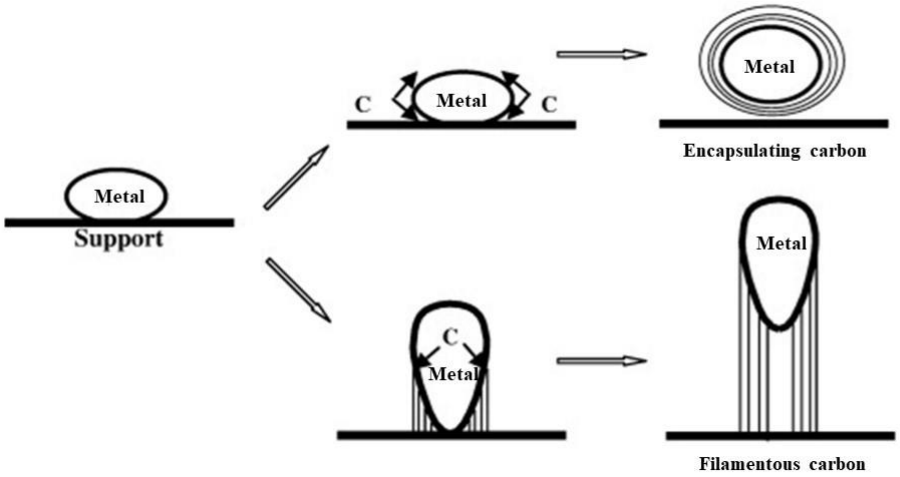

Figure 2.5 Schematic diagram of carbon formation; encapsulating and filamentous carbon [63].

2.6 Literature reviews

- TiN

Yao. et al. [11] and Fischer. et al. [12] suggested that TiN was found to have a strong tendency to catalyse the alkylation of ketones with alcohols and yield unsaturated compounds. Interestingly, TiN was proved to be the most effective catalyst with almost 90% yield. TiN nanoparticles synthesized through the urea route were more active than those produced through the C_3N_4 route. This can be related to their relatively lower amount of residual carbon.

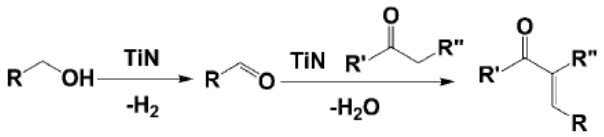

Scheme 2.1 Alkylation of ketones with alcohols, catalysed by mesoporous titanium nitride.

Molinari et. Al. [13] synthesized TiN-Ni and applied as a catalyst for hydrogenolysis of aryl ethers as models for lignin. They prepared TiN as a support to enhance the catalytic activity of Ni for the first time. TiN-Ni can successfully cleave diphenyl ether with highly competitive to the commercial hydrogenation catalysts such as Pd/C and Raney Ni.

Ham and Lee [65] studied the efficiency of transition metal carbides (TMCs) and transition metal nitrides (TMNs) as electrocatalysts which could replace the noble metals. They found that TMNs have a possibility for oxygen reduction reaction (ORR) higher than TMCs. TMNs has been known for a promotion of the 4-electron pathway, and enhancement of stability via strong interaction with various metals. However, TMCs are more active as anode catalysts for oxidation of fuels.

- Dry reforming of methane

Wu and Chou [66] prepared BN-supported Rh–Ni catalysts for dry reforming reaction of methane with carbon dioxide. They found that BN exhibited a unique property of minimum metal-support interference, due to the inert nature of BN, which allowed the metal cluster to migrate freely and form Rh-Ni [19]. Therefore, yield of hydrogen was improved with higher conversion of methane. Moreover, Coke formation was slightly reduced on BN due to the strong metal support interaction.

Cai et. Al. [67] reported that the addition of a small amount of Rh promoted the reducibility of Ni particles and decreased the Ni particle size of Rh–Ni/SBA-15 catalyst. In addition, the Rh–Ni bimetallic catalysts showed high activity and stability in the dry reforming of methane when compared with Ni/SBA-15 catalyst.

Luengnaruemitchaiet. Al. [51] investigated the catalytic performance of Ni based on various types of zeolites (zeolite A, zeolite X, zeolite Y, and ZSM-5) which prepared by incipient wetness impregnation for the catalytic carbon dioxide reforming of methane into synthesis gas at 700 °C, at atmospheric pressure, and at a CH_4/CO_2 ratio of 1. They found that Ni loading at 7 wt% showed the best catalytic activity on

each zeolite support but the highest amount of coke was obtained. Moreover, the stability of the Ni/zeolite Y was greatly considerably to the other catalysts with a high CH_4 conversion (91.6%). Therefore, they suggested zeolite Y has very good potential for being a support for Ni catalysts in the dry reforming of CH_4.

Amin et. Al. [68] studied the activity of Ni supported on different mesoporosus; SBA-15, MCM-41, KIT-6, and γ-Al_2O_3, as catalysts for methane dry reforming. After 20 h time on stream, the activity sequence in terms of CH_4 conversion was as following: Ni/SBA-15 (84%) > Ni/KIT-6 (77%) > Ni/γ-Al_2O_3 (67%) > Ni/MCM-41(51%). The rate of carbon deposition on the catalysts was as follows: Ni/KIT-6 < Ni/MCM-41] < Ni/SBA-15 < Ni/γ-Al_2O_3. They suggested that Ni/SBA-15 exhibited excellent catalytic performance in terms of catalytic conversion and long-term stability. In addition, the activity for the silica framework catalysts correlated strongly with their surface area and pore diameter.

Yasyerliet. Al. [69] investigated dry reforming of methane over the Ru and Mg incorporated Ni-MCM-41 catalysts at low temperature (500-600 °C). They found that H_2 selectivity significantly increased with increasing temperature, while CO selectivity slightly decreased. However, reverse water gas shift reaction becomes quite significant at lower temperatures.

CHAPTER III
EXPERIMENTAL

The experimental section is divided into three categories as follow:

- Catalyst Synthesis
- Catalyst Characterization
- Investigation of Catalytic Activity

3.1 Catalyst Synthesis

3.1.1 Synthesis of pure SBA-15

Mesoporous SBA-15 was prepared according to the methods as described by Zhao et al. [32]. To obtain the gel composition of 1.0 TEOS: 0.017 P123: 6.370 HCl : 40.857 H_2O; 4 g of P123 was dissolved in 30 g of DI water and 120 g of 2.0 M HCl by stirring the mixture at room temperature for 60 min. Then, 8.5 g of tetraethyl orthosilicate (TEOS) was gradually added and stirred for 60 min. The mixture solution was continuously stirred and aged at 40°C for 48 h. The white gel solution was transferred into Teflon–PARR autoclave for crystallization at 100°C for 48 h. Next, the white solid was filtered and washed with DI water to neutral pH value and finally calcined at 550°C for 5 h.

3.1.2 Synthesis of TiN-SBA-15

TiN modified SBA-15 was prepared using a modified hydrothermal method. The different amounts of the TiN powder (TiN <3 μm, Sigma Aldrich) were directly dispersed into an acidic mixture solution of the triblock copolymer Pluronic P123 ($EO_{20}PO_{70}EO_{20}$, M_n ~ 5800; Sigma Aldrich), 2M HCl, DI water and TEOS. Next, the mixture was continuously stirred at 35°C for 20 h and aged at 90°C for 24 h. Then, a similar procedure was applied as the typical synthesis of SBA-15 for crystallization

and filtration. The as-synthesized TiN–SBA-15 was obtained, and the organic template was successfully removed by calcination at 550°C in a N_2 atmosphere for 4 h. The sequence of TiN-SBA-15 preparation is shown in diagram 3.1.

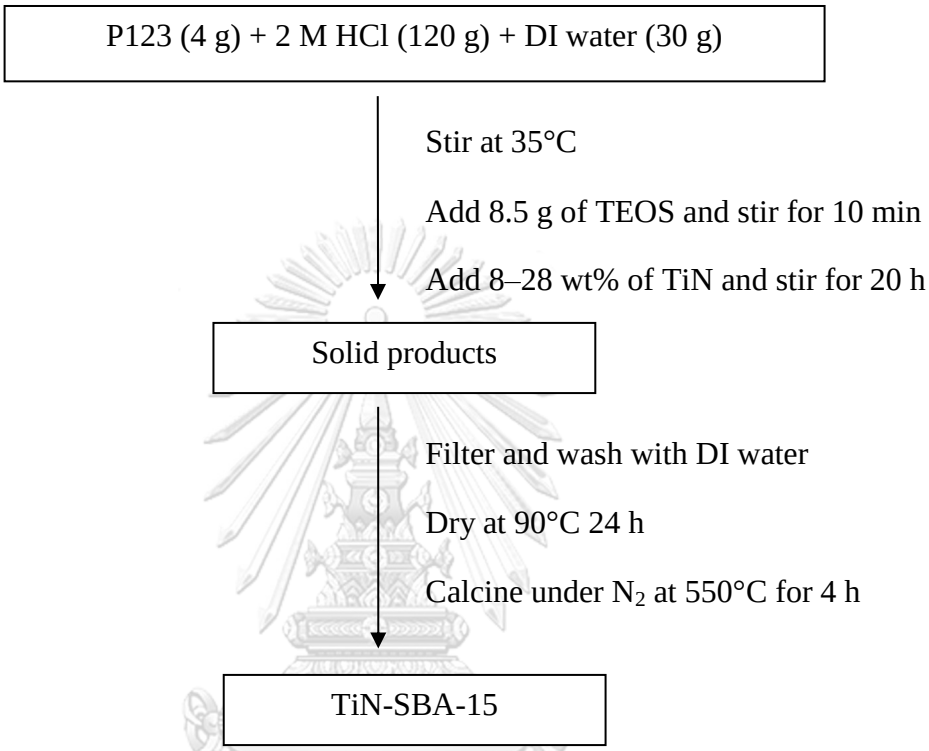

Scheme 3.1 TiN preparation method

3.1.3 Synthesis of Ni/TiN-SBA-15

Nickel (II) nitrate hexahydrate $Ni(NO_3)_2.6H_2O$ was dissolve in 15 mL of ethanol and then it was added a drop wise to TiN-SBA-15. The suspension was stirred overnight after that the solvent was slowly evaporated until obtained a homogeneous grey powder. The powder was calcined under N_2 flow with at 500 °C for 3 h. The prepared catalysts were denoted as xNi/yTiN-SBA-15 where x is the wt% of Ni (x = 2.5, 5, 7.5 and 10%) and y is the wt% of TiN containing in SBA-15; 5, 10, 15 and 18%, respectively.

3.1.4 Synthesis of Ni/TiN-Zeolite Y

TiN was dissolved in 15 mL of ethanol and then impregnated into zeolite Y (Si/Al =5.5, TOSOH). The mixture was stirred overnight and slowly evaporated to obtain a homogeneous grey powder. Nickel (II) nitrate hexahydrate $Ni(NO_3)_2.6H_2O$ in 15 mL of ethanol was also impregnated a drop wise to TiN-Zeolite Y. Next, the similar procedure was applied as the calcination of Ni/TiN-SBA-15.

3.2. Catalyst Characterizations

3.2.1 X-ray diffraction (XRD)

The structured of prepared sample was characterized using a Rigaku D/MAX-2200 Ultima$^+$ X-ray diffractometer (XRD) equipped with Cu K_α radiation (40 kV, 30 mA) and a monochromator. The scattering slit, divergent slit and receiving were fixed at 0.5 degree, 0.5 degree and 0.15 mm, respectively. The measurement was done at 2 theta angle between 0.7 to 3.0 degree and 10 to 80 degree.

3.2.2 Scanning Electron coupled with Energy Dispersive X-Ray Spectrometer (SEM-EDS)

The morphology of catalysts and the composition of Ti, O and Si were analyzed by JEOL JSM-7610F Field Emission Scanning Electron Microscope equipped with Energy Dispersive X-Ray Spectroscopy attachment (FESEM-EDS). The powder samples were distributed uniformly on the double sided carbon adhesive tape stuck on the microscope specimen holder.

3.2.3. Fourier transform infrared spectroscopy (FTIR)

NICOLET 6700 FT-IR spectrometer was used to investigate the incorporated of TiN in SBA-15 framework. The samples were prepared by the KBr-pellet technique and analyzed in the wave number 400-4000 cm^{-1} with 4 cm^{-1} resolution.

3.2.4 Nitrogen adsorption-desorption technique

Specific surface area, total pore volume and mean pore diameter were measured by N_2 adsorption-desorption isotherm at liquid N_2 temperature (-196°C) with using highly pure nitrogen as an adsorbate. About 40 mg of sample was pretreated at 400°C for 3 h under vacuum before analysis by BELSORP-mini instrument. The surface area and pore size distribution were calculated by the BET and BJH method [70].

3.2.5 Temperature program reduction and desorption (TPR and TPD)

The reduction and desorption temperature of catalysts were investigated by Thermo Finigan, TPDRO 1100. In TPR, about 0.2 g of catalyst was treated at 400°C in N_2 for 1 h then cooled down to room temperature. Next, the catalyst was annealed at 10°C/min up to 800°C in 5% H_2/N_2 and held for 1 h. The amount of hydrogen consumption was recorded as a function of temperature.

For the interaction of carbon dioxide, the catalyst was also treated at 400°C in N_2 for 1 h. Then the catalyst was annealed at 10°C/min up to 950°C in CO_2 and held for 0.5 h. After that, the saturation CO_2 was removed by purging with helium at flow rate 30 mL/min. The amount of CO_2 desorption was recorded as a function of temperature.

3.2.6 X-Ray Fluorescence Spectrometer (WDXRF)

The elemental compositions of some catalysts were analyzed by WDXRF (S8 Tiger). The samples were pelleted before the measurement. The data was reported in terms of % metal containing in the prepared catalyst.

3.2.7 X-ray photoelectron spectroscopy (XPS)

X-ray photoelectron spectroscopy (XPS) was performed by a JEOL JPS-9010MC, equipped with an Al Kα (1487 eV) X-ray source. The charging effected from the measurement was corrected by setting the binding energy of carbon (C 1s) at 284.8 eV. The XPS spectrum can give the information about the surface chemistry of a material i.e. binding energy, chemical state and electronic state of the elements that exist within a material.

3.2.8 Transmission electron microscopy (TEM)

The microstructure of some samples was visualized by using JEOL JEM-2010 TEM, operated at accelerated voltage of 200 kV. The particle size and the distribution of catalysts were obtained.

3.2.9 Thermogravity analysis (TGA)

After the reaction, the amount of coke formation on the catalyst surface during the experiment was measured by Thermogravimetric Analyzer (209 F3 Tarsus). The spent catalyst was annealed in air from room temperature up to 800°C in order to achieve the mass loss by the oxidation and removal of carbon.

3.2.10 Gas Chromatograph Analyzer (GC)

Gas chromatography (GC) on-line analysis of gas-phase reaction products was performed on PR2100 Perichrom equipped with automatic sampling valves. The carrier gas carried the mixed feed gas: CH_4, CO_2, CO and H_2 at pressure of 50 kPa, and flowed pass through the Porapack Q column then entering into the serial-arranged a molecular sieve (13x) for H_2 and CO separation. The thermal conductivity detector (TCD) was used to detect the filtered gasses by the temperature measurement. The temperature of gas inlet, detector and oven were set up at 100°C, 120°C and 35-150 °C, respectively. The composition of permeation gas was analyzed by calculation of

the peak area which compared to the standards from the calibration curve. The data acquisition and analysis was performed by clarity computer software.

3.3 Catalytic activity investigation

The catalytic activity of the catalysts in dry reforming of methane and carbon dioxide into synthesis gas was performed in batch reactor by using a homemade 316L stainless steel reactor with 1/4″ ID and 50 cm in length. Prior to the experiment, 0.5 g of fresh catalyst was covered by quartz wool to get a catalyst bed height of ~2 cm then packed into the reactor. N_2 was introduced into the reactor from room temperature before switching to reduce the catalysts in 10% H_2/Ar at 600°C for 1 h. Subsequently, the temperature was raise up to 700ºC and then purged the reactant gas with ratio of CH_4/CO_2 = 1 with the flow rate of 20 mL/min at atmospheric pressure with reaction time 4 h. The synthesized products were analyzed by gas chromatography (GC) with TCD, for determination % yield of H_2, and CO together with % conversion and % selectivity of CH_4 and CO_2 as follow equations:

$$\text{DRM} = CO_2 + CH_4 \leftrightarrow 2H_2 + 2CO$$

$$\%CH_4 \text{ conversion} = 100 \times ([CH_4]_{in} - [CH_4]_{out})/ [CH_4]_{in}$$

$$\% CO_2 \text{ conversion} = 100 \times ([CO_2]_{in} - [CO_2]_{out})/ [CO_2]_{in}$$

$$\% H_2 \text{ yield} = 100 \times 1/2[H_2]_{out}/ [CH_4]_{in}$$

$$\% \text{ CO yield} = 100 \times [CO]_{out} / ([CH_4]_{in} + [CO_2]_{in})$$

$$\% H_2 \text{ selectivity} = 100 \times 1/2[H_2]_{out} / ([CH_4]_{in} - [CH_4]_{out})$$

$$\% \text{ CO selectivity} = 100 \times [CO]_{out} / (([CH_4]_{in} - [CH_4]_{out}) + ([CO_2]_{in} - [CO_2]_{out}))$$

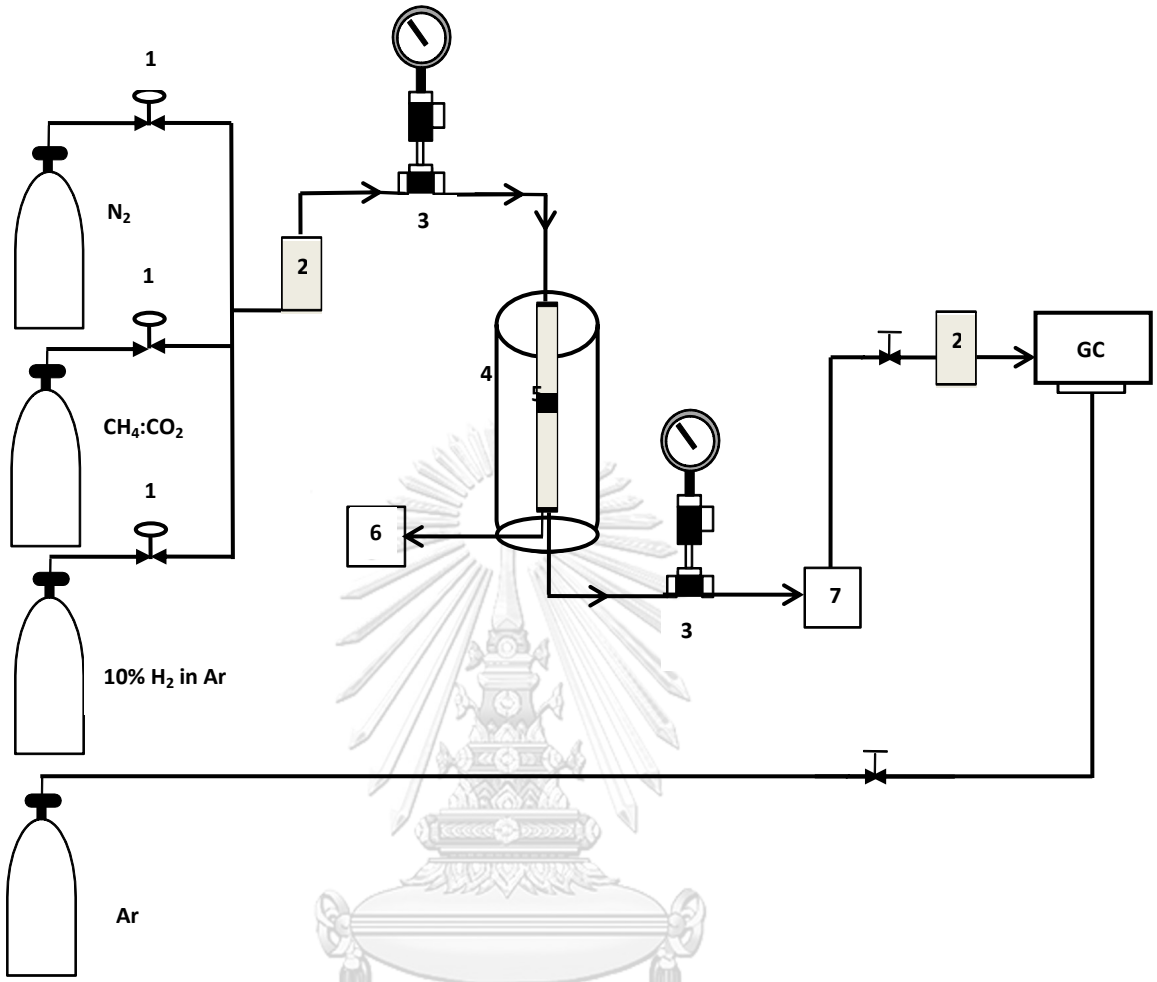

Figure 3.1 A schematic diagram of experimental apparatus for dry reforming reaction

1. Ball valve
2. Digital flow meter
3. Pressure gauge
4. Furnace
5. 316 L Stainless steel fixed bed reactor
6. Temperature controller
7. Cold trap

CHAPTER IV
RESULTS AND DISCUSSION

This chapter consists of three parts. The first part explains about the synthesis and materials characteristics of SBA-15, TiN-SBA-15 and Ni/TiN-SBA-15. The second part presents the catalytic activity of DRM reaction at 4 h using Ni/SBA-15 catalysts together with and without TiN. Moreover, the prominent catalysts were selected to investigate the catalytic performance and their stability at 12 h on stream. The last part presents the effects of support on the catalytic activity for zeolite Y (microporous), compared with SBA-15 (mesoporous).

4.1 Characteristics and Properties of SBA-15, TiN-SBA-15 and Ni/TiN-SBA-15

4.1.1 X-ray diffraction (XRD)

X-ray diffractograms at low 2θ range of SBA-15 and TiN-SBA-15 were shown in Fig.4.1 (a). All materials exhibited three well-resolved diffraction peaks, which can be indexed as (100), (110), and (200) reflections. These corresponded to the well-ordered structure of p6mm space group of the SBA-15 characteristics [71]. Note that the (100) peak of TiN-SBA-15 showed a reduction in the intensity and shifted toward a higher angle with an increasing amount of incorporated TiN. It was due to the dilution of TiN with the silica oxide framework [72]. Emphasizing that TiN content has an impact on the order of the mesoporous structure. However, TiN incorporated SBA-15 (TiN-SBA-15) can still maintain mesoscopic pore structure of SBA-15.

Fig. 4.1(b) showed the x-ray diffractograms at 2θ between 10°−80° of TiN loadings with different content of TiN in SBA-15. The broad peak around 2θ = 22° was the typical amorphous silica [47]. The diffraction peaks can be assigned to (111), (200), (220), (311), and (222) of TiN (PDF-01-071-0299), confirming the existing of TiN on the surface of SBA-15. Moreover, the small amount of rutile TiO_2 (PDF-01-

072-1148) was also apparent. This could be due to the oxidation of TiN during calcination of the as-synthesized materials in N_2 atmosphere, and also the ability of TiN to form oxides of titanium; the adsorbed oxygen could easily react with TiN at high temperatures [73]. The weight fraction TiN/TiO_2 of the prepared samples was calculated using the Topas3 software, shown in Table 4.1. Well-dispersed TiN particles in the silica framework were found in the samples with a low amount of TiN, whereas the aggregation of high TiN loading was clearly observed with SEM-EDS mapping. Highly dispersed TiN particles were easily oxidized to form TiO_2. This was confirmed by the TiN/TiO_2 weight fraction, which was less than or almost equal to 1/1 in case of (5TiN-SBA-15, 10TiN-SBA-15 and 15TiN-SBA-15) but nearly 3/1 for 18TiN-SBA-15.

Fig.4.2 shows the x-ray diffractograms for Ni/SBA-15 and Ni/TiN-SBA-15 samples. All samples exhibited three well-resolved characteristic peaks which can be indexed to the (111), (200), and (220) of face-centered cubic phase NiO (JCPDS card no. #47-1049). The presence of TiN on the surface of SBA-15 was confirmed by the diffraction peaks (111), (200) and (220) of TiN (PDF-01-071-0299) and the small amount of rutile TiO_2 (PDF-01-072-1148) was also observed.

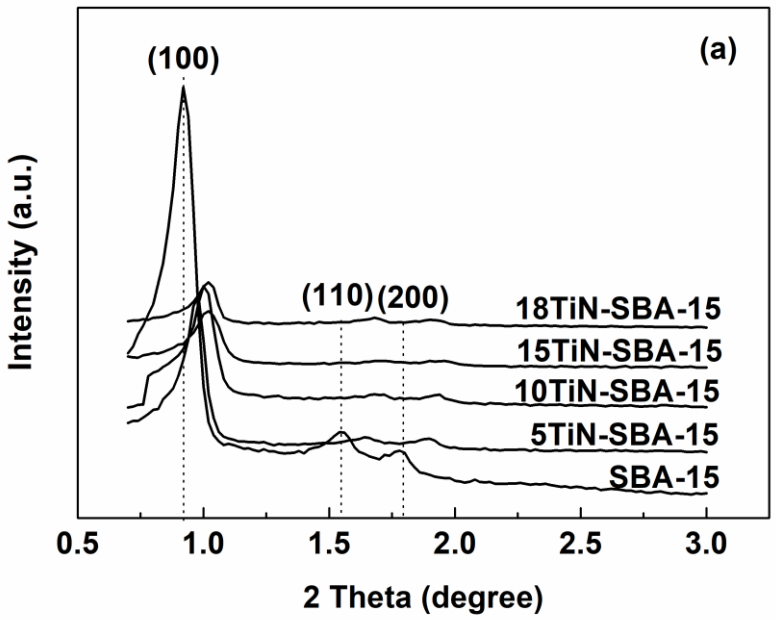

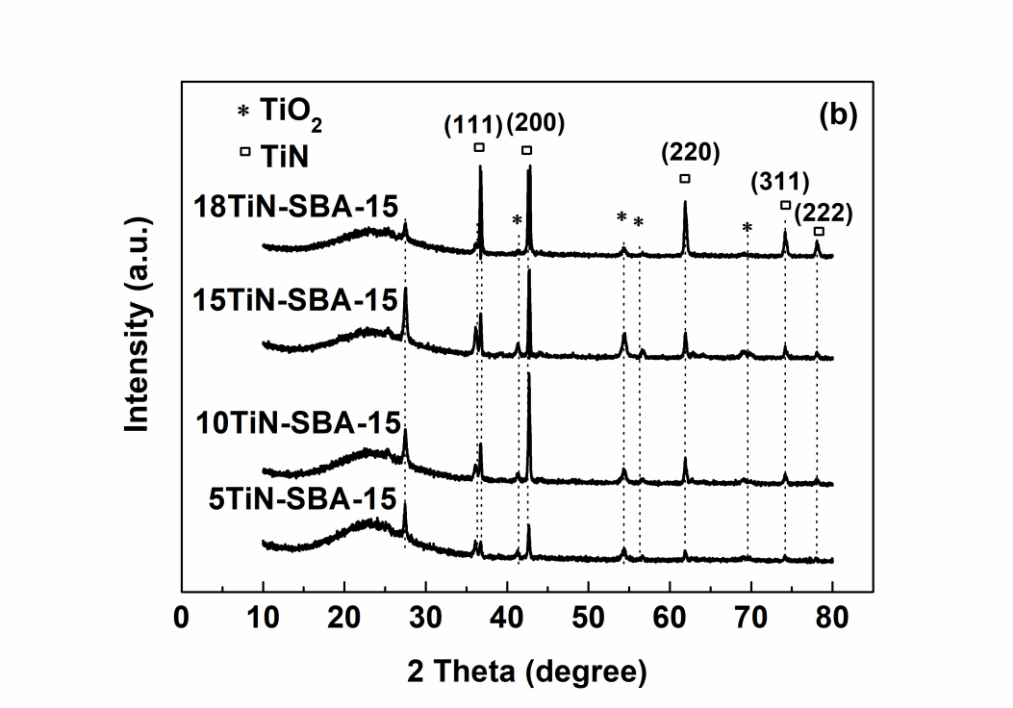

Figure 4.1 x-ray diffractograms (a) low-2θ and (b) 2θ between 10°−80° of pure SBA-15 and TiN modified SBA-15.

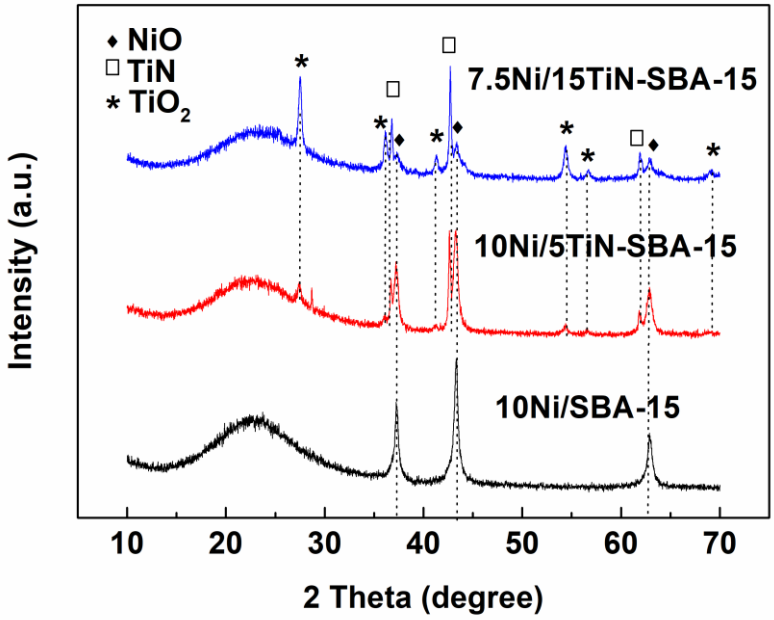

Figure 4.2 X-ray diffractograms of Ni based-catalyst both with and without TiN.

4.1.2 Wavelength Dispersive X-ray Fluorescence (WDXRF)

An elemental analysis of the TiN incorporated in SBA-15 and containing of both Ni and TiN in SBA-15 were summarized in Table 4.1. The estimated composition of TiN was measured from Ti content. The value measurement of samples at the same amount of TiN or Ni should be equivalent to other as-prepared samples which was not characterized.

Table 4.1 Chemical composition of fresh catalysts.

Sample	Composition by WDXRF (wt%)			TiN/TiO_2(wt%) (Topas3)
	Ti	TiN (calculation)	Ni	
5TiN-SBA-15	3.8	4.9	-	44.2:55.8
10TiN-SBA-15	7.2	9.3	-	42.7:57.3
15TiN-SBA-15	11.2	14.5	-	30.6:69.4
18TiN-SBA-15	13.9	17.9	-	74.3:25.7
10Ni/SBA-15	-	-	10.7	-
10Ni/5TiN-SBA-15	3.6	4.6	10.6	
7.5Ni/10TiN-SBA-15	7.6	9.8	7.6	-
5Ni/5TiN-SBA-15	4.0	5.2	5.3	-
2.5Ni/10TiN-SBA-15	7.7	9.9	2.6	-

4.1.3 X-ray photoelectron spectroscopy (XPS)

The XPS was performed to investigate the binding energy and chemical information for the incorporation of TiN on the silica surface. The XPS peaks were calibrated based on the C1s peak at 284.8 eV of the carbon peak reference. Fig. 4.3 (a) shows the Ti2p XPS spectra. For pure TiN, the Ti2p can be divided into 4 peaks of TiN and TiO_2 due to TiN is easily oxidized. The energy peak positions for TiN were found at 455.7 and 460.0 eV whereas the best fitted binding energy of TiO_2 were 458.2, 464.3 and 463.9 eV which were in agreement with the reported literatures [37, 74-79]. However, the broadening spectrum of Ti2p could be the overlapping signals of different Ti intermediate phases from the oxidation of TiN itself i.e. TiN, TiO_2 and TiN_xO_y [37, 75, 80]. It is obviously that TiO_2 is the most abundant species on the surface of the samples after the formation of TiN-SBA-15. The shift of $Ti2p_{1/2}$ and $Ti2p_{3/2}$ from 464.2 to 463.9 eV and 458.4 to 458.2 eV with increasing TiN loading was due to the agglomeration against the oxidation of TiN particles as revealed by EDS results.

The sharp and intensive peak centered at ca.533 eV in Fig 4.3 (b) is the typical binding energy of O1s XPS spectra of SBA-15, indicating that the Ti was incorporated into the SBA-15 framework with Si–O–Ti cross-linking bonds [37, 74, 81, 82]. Another peak at about 529 eV can be seen only pure TiN and 18TiN-SBA-15 due to high TiN amount facilitated the formation of TiO_2 clusters as a second phase [77, 81, 82]. However, a BE value at 531.0 eV is clearly observed on the surface of pure TiN which related to the bonding of O to Ti by surface-adsorbed oxygen on TiN or Ti-OH bond of the normal TiN sample [76, 77, 81, 83, 84]. It is noteworthy that these observations are in accordance with the EDS and XRD results.

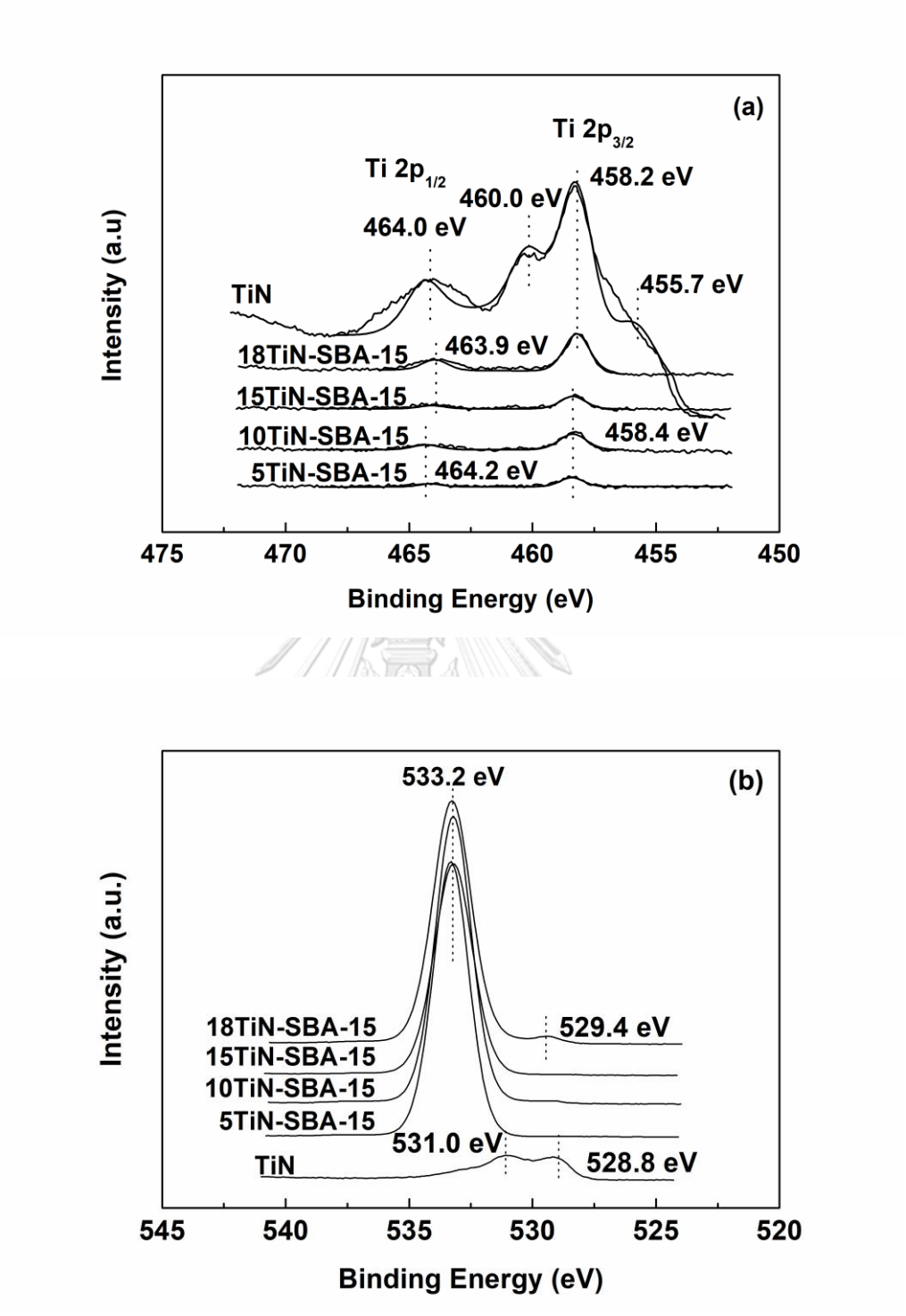

Figure 4.3 XPS spectra of (a) Ti2p and (b) O1s of pure TiN and TiN-SBA-15.

In case of the mesoporous silica surface modified with TiN and Ni particles, the XPS spectra were presented in Fig. 4.4. The peak position of $Ti2p_{1/2}$ was shifted from 464.3 eV (in 5TiN-SBA-15) to 464.6 eV (in 10Ni/5TiN-SBA-15). An increasing of binding energy after the incorporation of Ni suggests a strong interaction of Ni-TiN. It can be also seen that, the 10Ni/5TiN-SBA-15 has higher binding energy than 7.5Ni/10TiN-SBA-15. Thus, the composition of Ni and TiN has impact on surface binding energy.

The main peak $Ni2p_{3/2}$ of Ni-based catalysts both with and without TiN loading is presented at 855.5 eV with satellite peak at 864.1 eV. The peak position of $Ni2p_{1/2}$ was shifted from 872.7 and 880.2 eV (10Ni/SBA-15) to 873.7 and 880.7 eV (7.5Ni/10TiN-SBA-15) and 873.5 and 880.4 eV (10Ni/5TiN-SBA-15). The higher binding energy may associated with an increasing of metal–support interaction that improved by TiN promoter. Thus, these catalysts can manifest in high catalytic performance and stability along with low carbonaceous deposition and metal sintering [85].

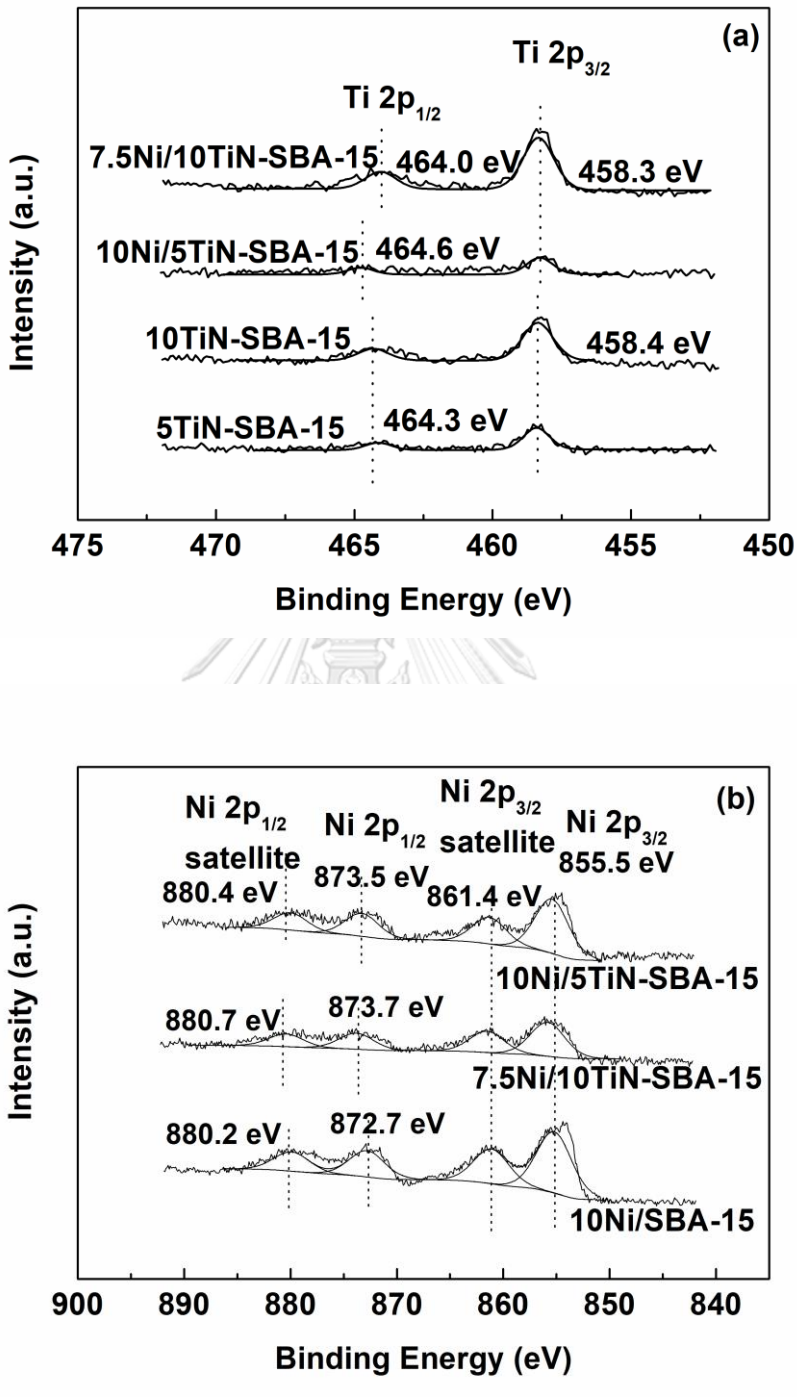

Figure 4.4 XPS spectra (a) Ti2p and (b) Ni2p of fresh catalysts.

4.1.4 Fourier transform infrared spectroscopy (FTIR)

The FTIR spectra of SBA-15 and TiN-SBA-15 are shown in Fig. 4.5. All samples demonstrated three characteristics peaks of SBA-15 at 1089, 806, and 470 cm^{-1}, respectively. These peaks were identified as condensed silica (Si–O–Si and O–Si–O bending vibration). The peak shoulder around 970 cm^{-1} was indicated as the stretching vibration of the silanol group (Si–OH) [86, 87]. Moreover, the O–H bending and stretching vibrations of the adsorbed water were indexed at 1640 cm^{-1} and 3400 cm^{-1}, respectively [87]. Nonetheless, the exhibited peak at *ca.* 1400 cm^{-1} was used as a fingerprint of the existing incorporated TiN in the SBA-15 matrix, which could not be found in the spectrum of conventional SBA-15. It was assigned to the bending vibrations of O–H which formed by the N–H groups and the adsorbed water as reported in the literatures [88, 89]. This is also another proved evidence of TiN containing in SBA-15 framework.

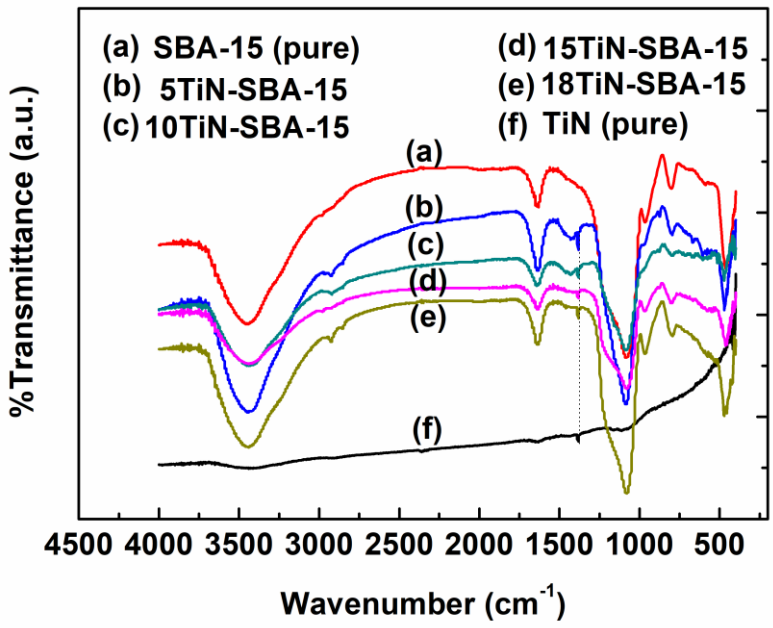

Figure 4.5 FT-IR spectra of (a) pure SBA-15, (b) 5TiN-SBA-15, (c) 10TiN-SBA-15TiN, (d) 15TiN-SBA-15, (e) 18TiN-SBA-15 and (f) TiN modified SBA-15.

4.1.5 Nitrogen adsorption measurements

The nitrogen adsorption–desorption isotherms of the synthesized SBA-15 and TiN-SBA-15 are shown in Fig. 4.6. The results represented a type IV isotherm with an H_1-hysteresis loop, indicating that the incorporation of TiN preserved the mesoporous structure of SBA-15. However, loading TiN into siliceous SBA-15 resulted in a reduction of the surface area and the pore volume and a slight change in the pore size of SBA-15, as shown in Table 4.2 and Fig. 4.7. The adsorption step of TiN-modified SBA-15 also occurred at lower P/P_0 than that of normal SBA-15. This means the increasing amount of TiN can influence the SBA-15 framework by partial pore blocking and contributed to more disordered structure. This result was in consistent with the low-angle XRD result.

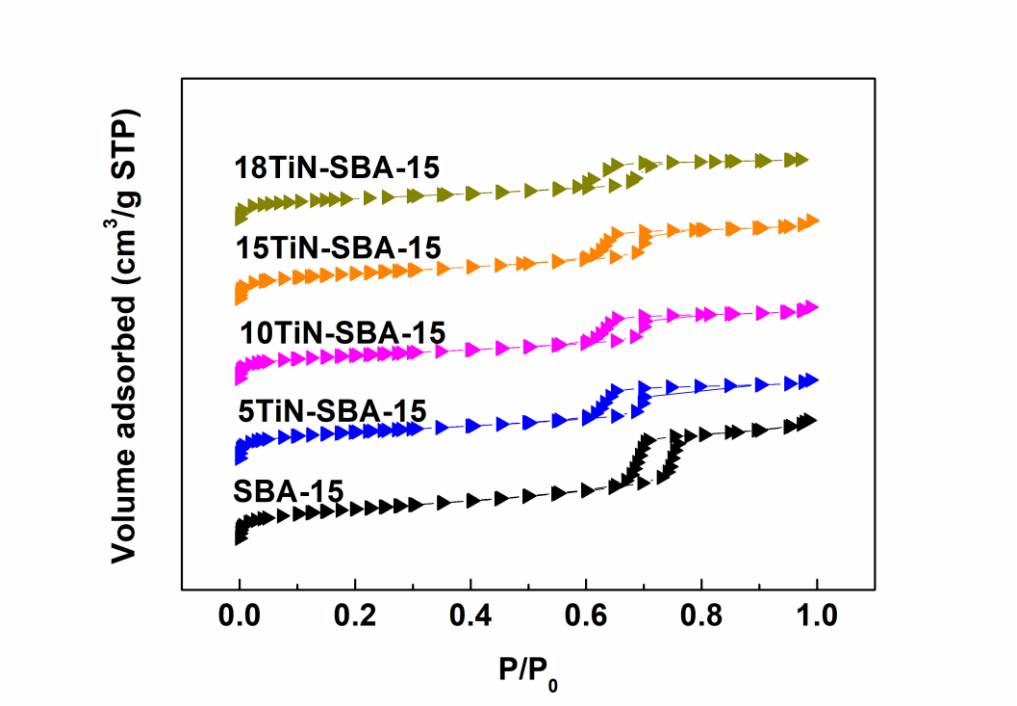

Figure 4.6 N_2 adsorption isotherms of SBA-15 and TiN-SBA-15 with different TiN contents.

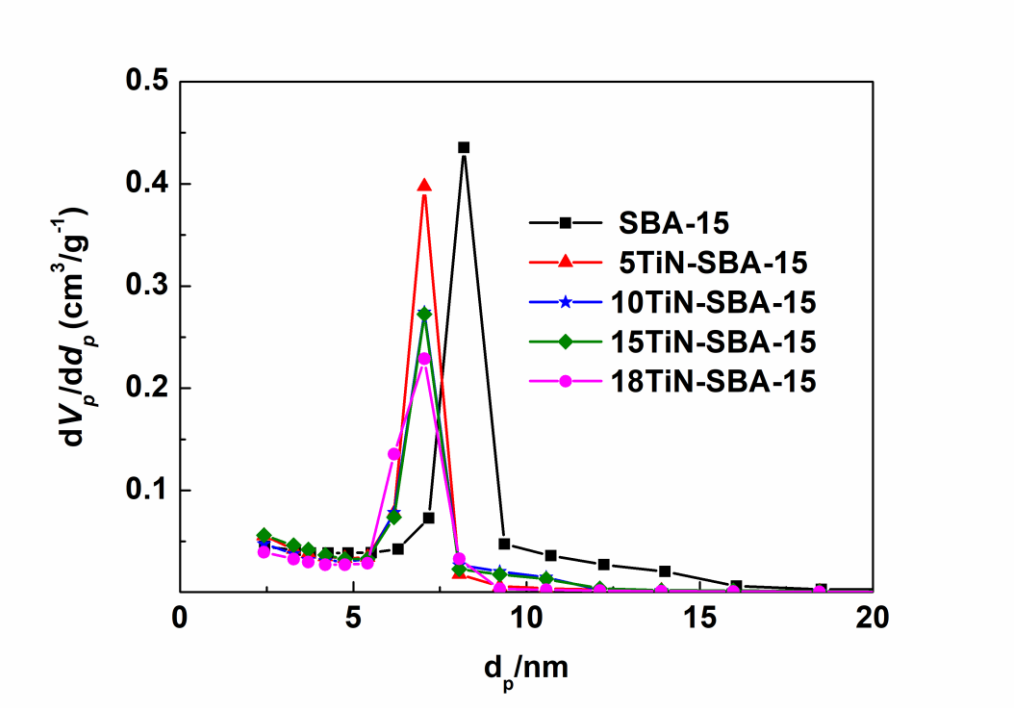

Figure 4.7 Pore size distribution curves of SBA-15 and TiN-SBA-15 with different TiN contents.

After Ni impregnation, the nitrogen adsorption-desorption isotherms of the synthesized samples still presented a type IV isotherm with H1-hysteresis loop between P/P_0 = 0.5–1.0, as seen in Fig. 4.8. This shows that having Ni incorporated into TiN-SBA-15 can still preserve the mesoporous structure of SBA-15. From Table 4.2, a decreasing in surface area was found in all samples due to Ni incorporation in the mesoscopic structure. The modified catalysts with TiN (10Ni/5TiN-SBA-15 and 7.5Ni/10TiN-SBA-15) also showed lower surface area and pore volume than non-modified catalyst (10Ni/SBA-15) that attributed to those blocked pores by TiN. The catalysts pore diameters of 8.20, 7.18 and 7.18 nm were measured from 10Ni/SBA-15, 10Ni/5TiN-SBA-15 and 7.5Ni/10TiN-SBA-15, respectively. It was also in agreement with the results measured from TEM micrographs.

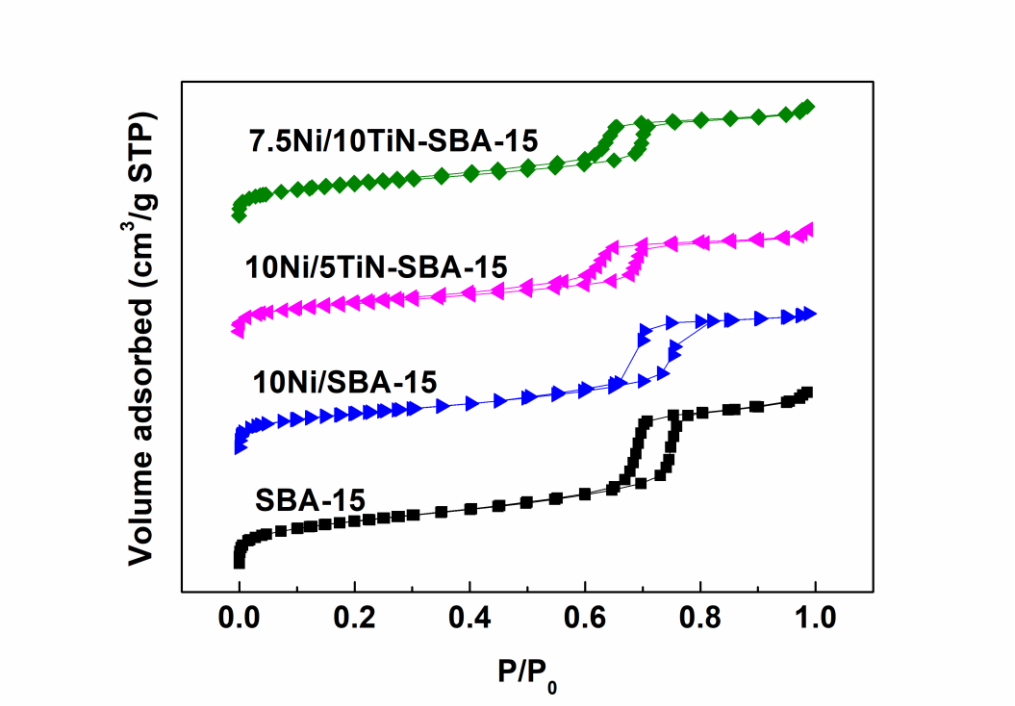

Figure 4.8 N_2 adsorption-desorption isotherms SBA-15 and Ni-based catalysts.

Table 4.2 Textural parameters of SBA-15 and TiN modified SBA-15.

Sample	Surface area S_{BET} (m^2g^{-1})	Pore volume $Vt_{(BJH)}$ (cm^3/g)	Pore diameter $D_{(BJH)}$ (nm)
SBA-15	703.74	1.10	8.20
5TiN-SBA-15	685.91	0.83	7.18
10TiN-SBA-15	592.02	0.62	7.05
15TiN-SBA-15	586.41	0.60	7.05
18TiN-SBA-15	532.11	0.52	7.05
10Ni/SBA-15	591.75	0.86	8.20
7.5Ni/10TiN-SBA-15	562.12	0.69	7.18
10Ni/5TiN-SBA-15	505.45	0.66	7.18

4.1.6 Temperature-programmed reduction (TPR)

The reduction temperature of the prepared catalysts was characterized by H_2-TPR. Fig. 4.9 shows the TPR spectra of the pure TiN and some prepared samples of Ni/TiN-SBA-15. It is obvious that there is no reduction profile of pure TiN while there are two reduction peaks of the Ni-based catalysts. All samples with Ni showed two sites of reduction signal around 400°C and 600°C. The first peak possesses the highest intensity at ca.400°C which is the reduction temperature of bulk NiO species or isolated NiO particles. This indicates the weak interaction with the support. The second broad peaks at higher temperature mostly attribute to the reduction of NiO species which had stronger interaction with the support [90, 91].

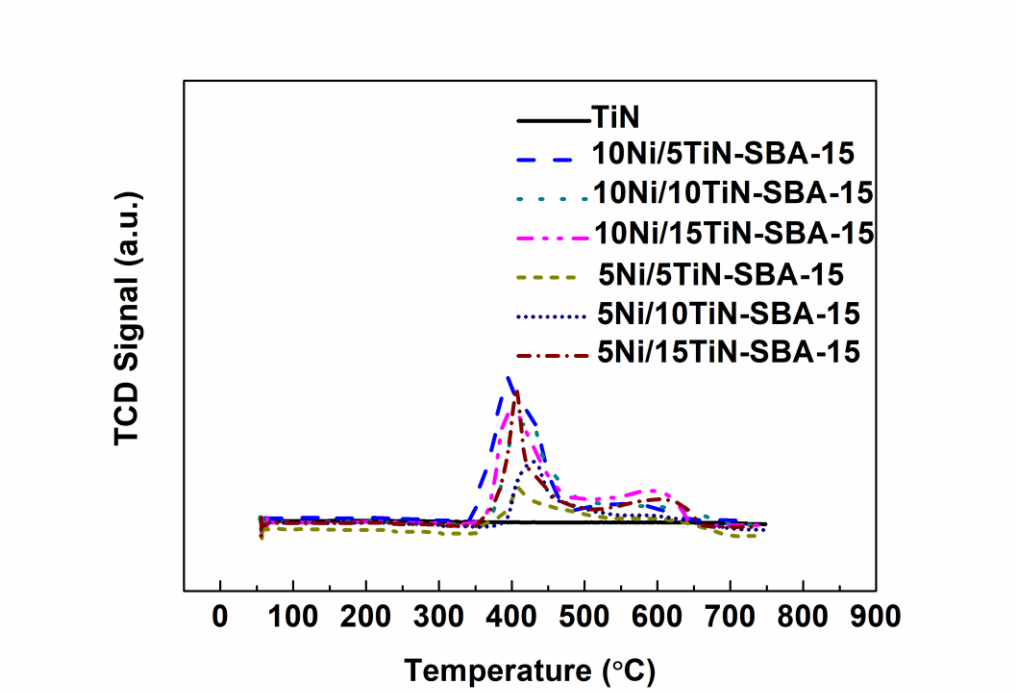

Figure 4.9 TPR profile of pure TiN and Ni-based catalyst at 5 and 10%Ni containing in 5TiN-SBA-15, 10TiN-SBA-15 and 15TiN-SBA-15**.**

4.1.7 Temperature Programmed Desorption (TPD)

The CO_2-TPD profiles of some Ni-based catalysts, 10Ni/SBA-15, 10Ni/5TiN-SBA-15 and 7.5Ni/10TiN-SBA-15, were compared with pure TiN and 10TiN-SBA-15, as shown in Fig 4.10. A desorption peak at around 460°C reflected the presence of medium basic sites which were found in ones contained Ni-loading. Another appeared adsorption peak was in temperature range around 800-950°C indicating the strong basicity of pure TiN and TiN containing in SBA-15.

In comparison between pure TiN and TiN-promoted SBA-15, the desorption temperature of 10Ni/5TiN-SBA-15 and 7.5Ni/10TiN-SBA-15 slightly shifted toward lower temperature due to the incorporation of Ni. However, the desorption temperature of 10Ni/5TiN-SBA-15 was higher than 7.5Ni/10TiN-SBA-15, indicating its stronger basicity which could be related to the catalyst activity. Noteworthy, the quantity of CO_2 adsorption on 10Ni/5TiN-SBA-15 and 7.5Ni/10TiN-SBA-15 catalysts was greatly higher than 10Ni/SBA-15 catalyst and 10TiN-SBA-15 (see Table 4.3). The increasing of the basic site concentration for the Ni-based catalysts could be an outcome of the higher electron density introduced by TiN. Therefore, the presence of medium and strong basicity on the catalysts increased the adsorption capacity of CO_2 on catalysts surface and urged to convert Boudouard reaction [24, 92]. This is important information to prove that TiN can promote the catalytic activity and reduce carbon formation of Ni catalysts.

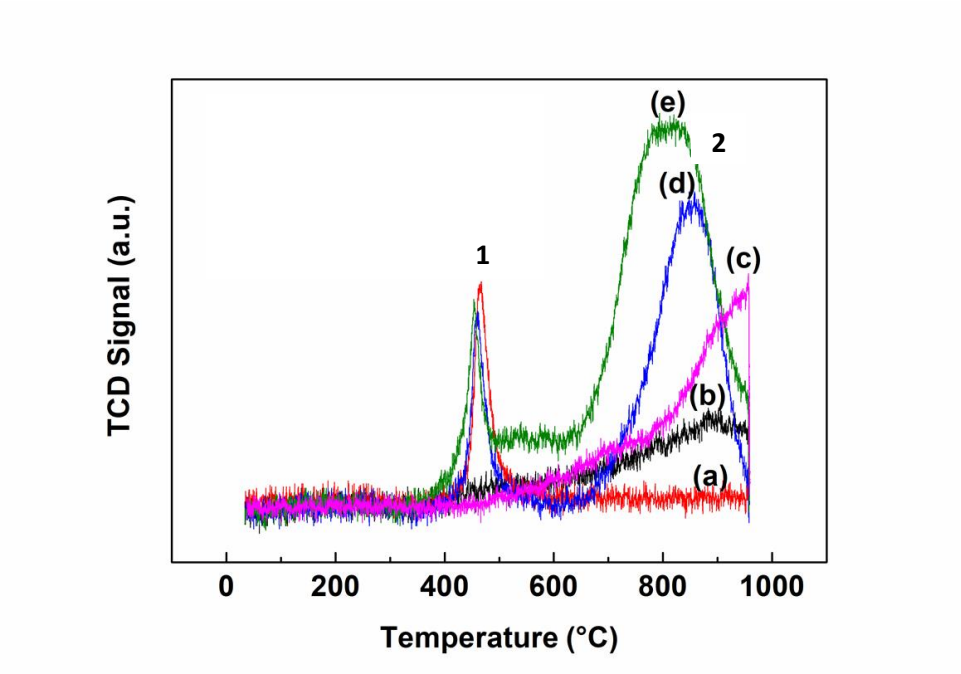

Figure 4.10 CO_2-TPD profile of (a) 10Ni/SBA-15, (b) pure TiN (c) 10TiN-SBA-15 (d) 10Ni/5TiN-SBA-15 and (e) 7.5Ni/10TiN-SBA-15.

Table 4.3 CO_2 adsorption properties of fresh catalysts.

Sample	Desorption temperature T(°C)		Amount gas adsorbed (µmol/g)	
	Peak 1	Peak 2	Peak 1	Peak 2
TiN (pure)	-	883	-	56.76
10TiN-SBA-15	-	957	-	83.60
10Ni/SBA-15	467	-	32.71	-
10Ni/5TiN-SBA-15	460	848	27.68	154.55
7.5Ni/10TiN-SBA-15	453	794	32.48	312.68

4.1.8 X-ray Electron Microscopy

- **Scanning electron microscope analysis (SEM)**

The scanning electron micrographs of the incorporation of TiN in SBA-15 mesoporous structure were shown in Fig.4.11. TiN modified SBA-15 revealed a rod-like structure with a short channel size of ca. 0.6 μm which is similar to the parent SBA-15 morphology. Thus, mesoporous structure of SBA-15 still preserved which corresponding to the results from XRD and N_2-adsorption analysis.

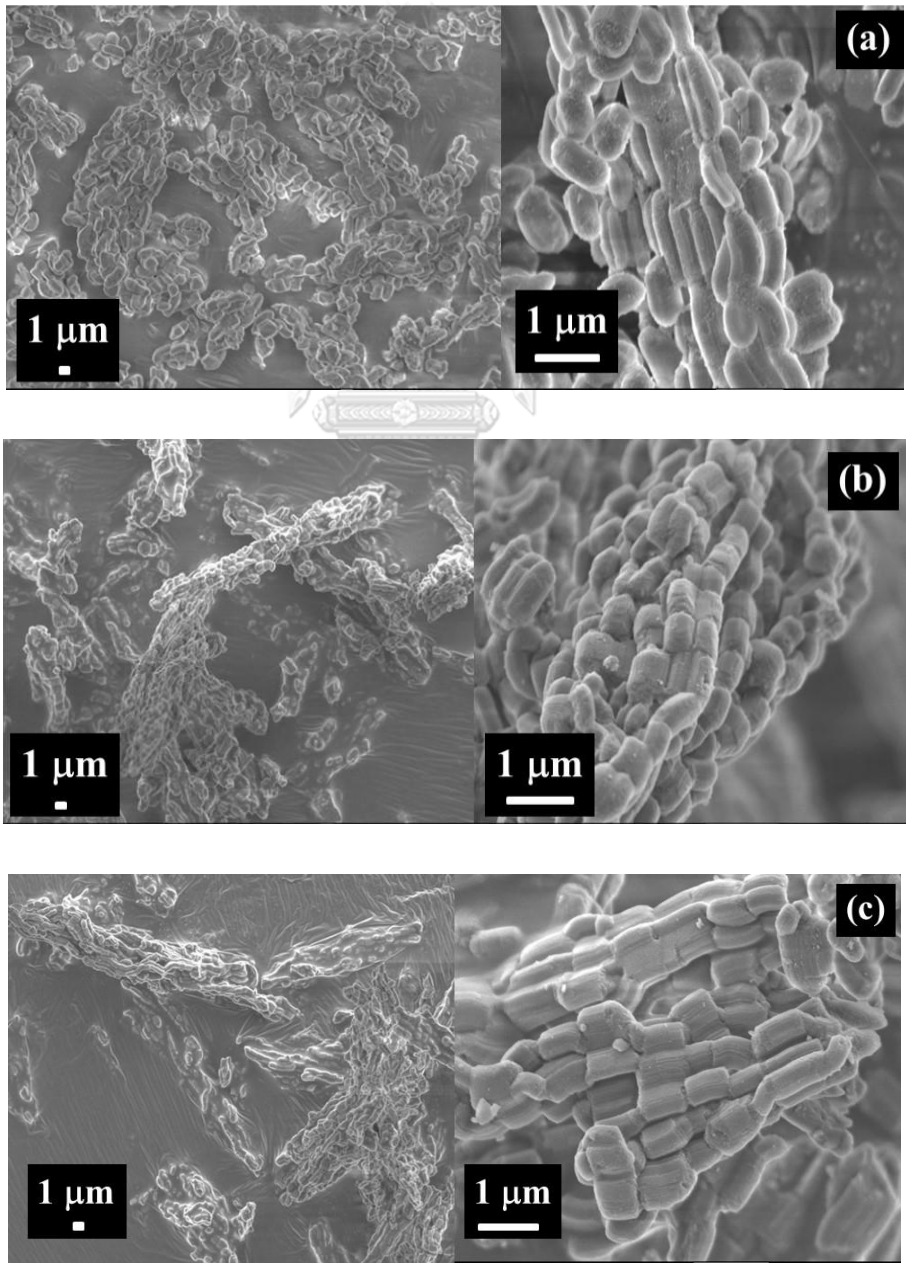

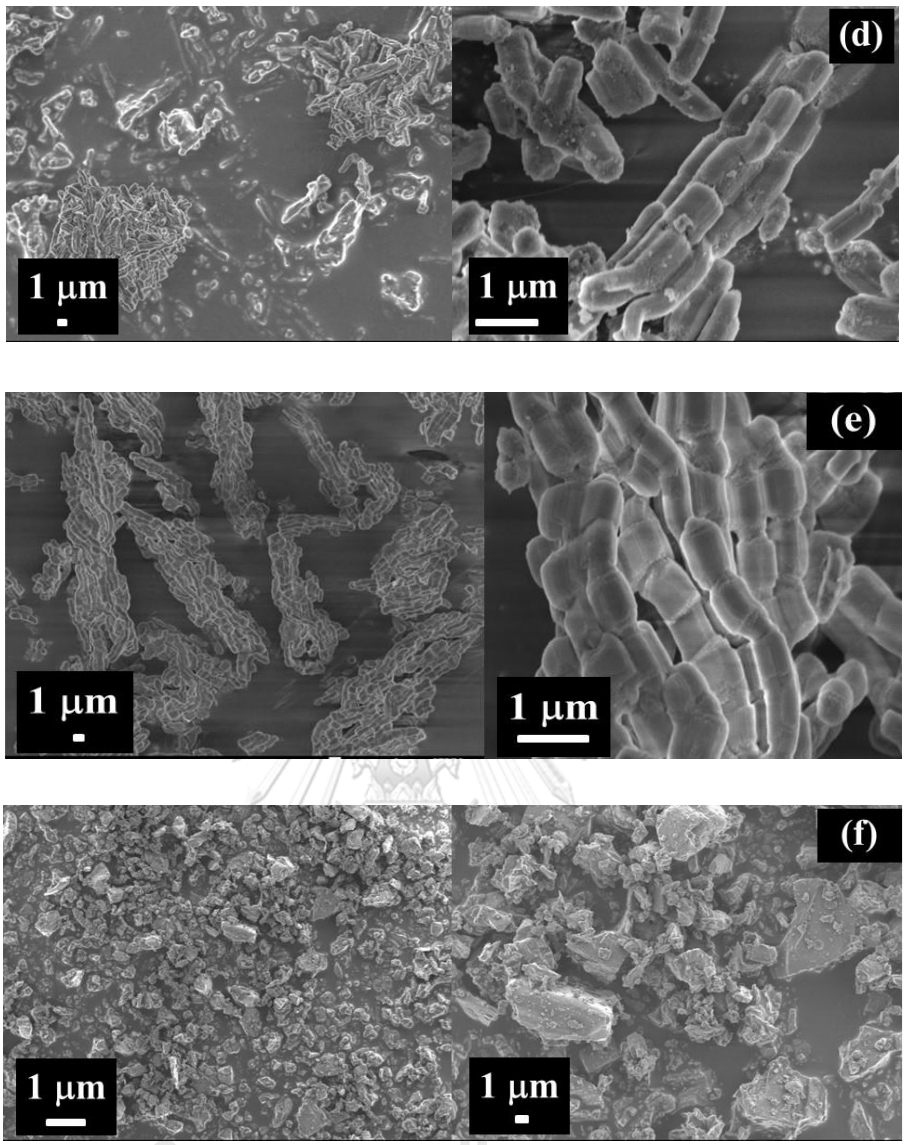

Figure 4.11 Scanning electron micrographs with ×3,000 and ×20,000 magnification of (a) SBA-15 (b) 5TiN-SBA-15 (c) 10TiN-SBA-15 (d) 15TiN-SBA-15 (e) 18TiN-SBA-15 and ×1,000 and ×3,000 magnification of (f) TiN-SBA-15.

- SEM-EDS elemental maps

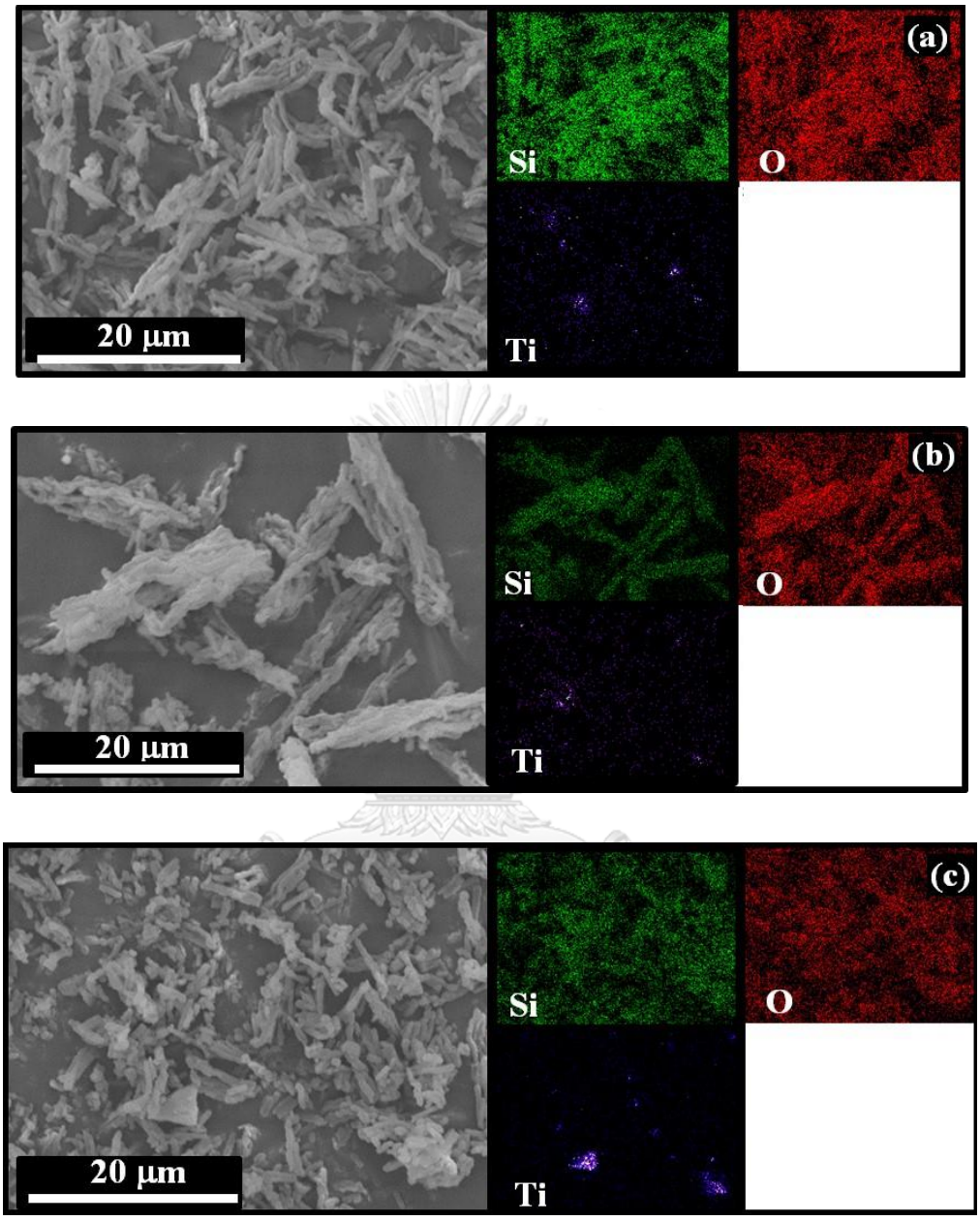

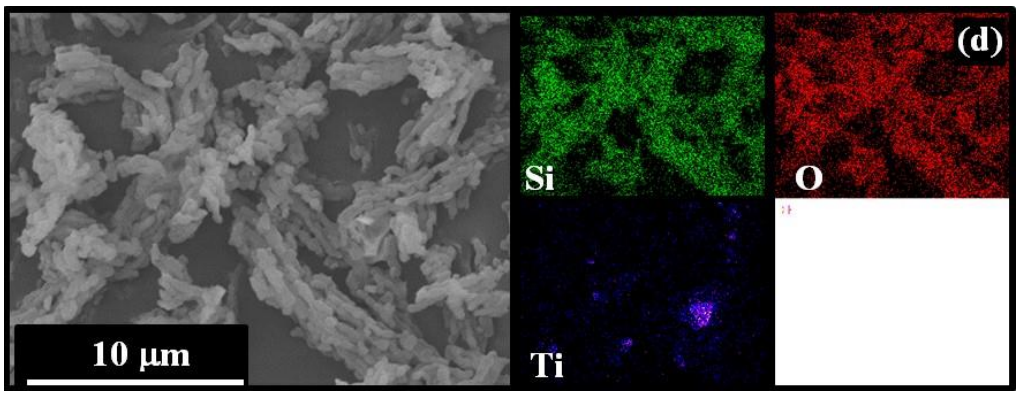

Figure 4.12 SEM-EDS elemental maps of TiN modified SBA-15 samples; (a) 5TiN-SBA-15 (b) 10TiN-SBA-15, (c) 15TiN-SBA-15 and (d) 18TiN-SBA-15.

The SEM images and EDS elemental maps of Ni-based catalysts were shown in Fig. 4.13 and 4.14, respectively. This also confirmed the existence of Ni and TiN containing in SBA-15 structure.

- **Fresh catalysts**

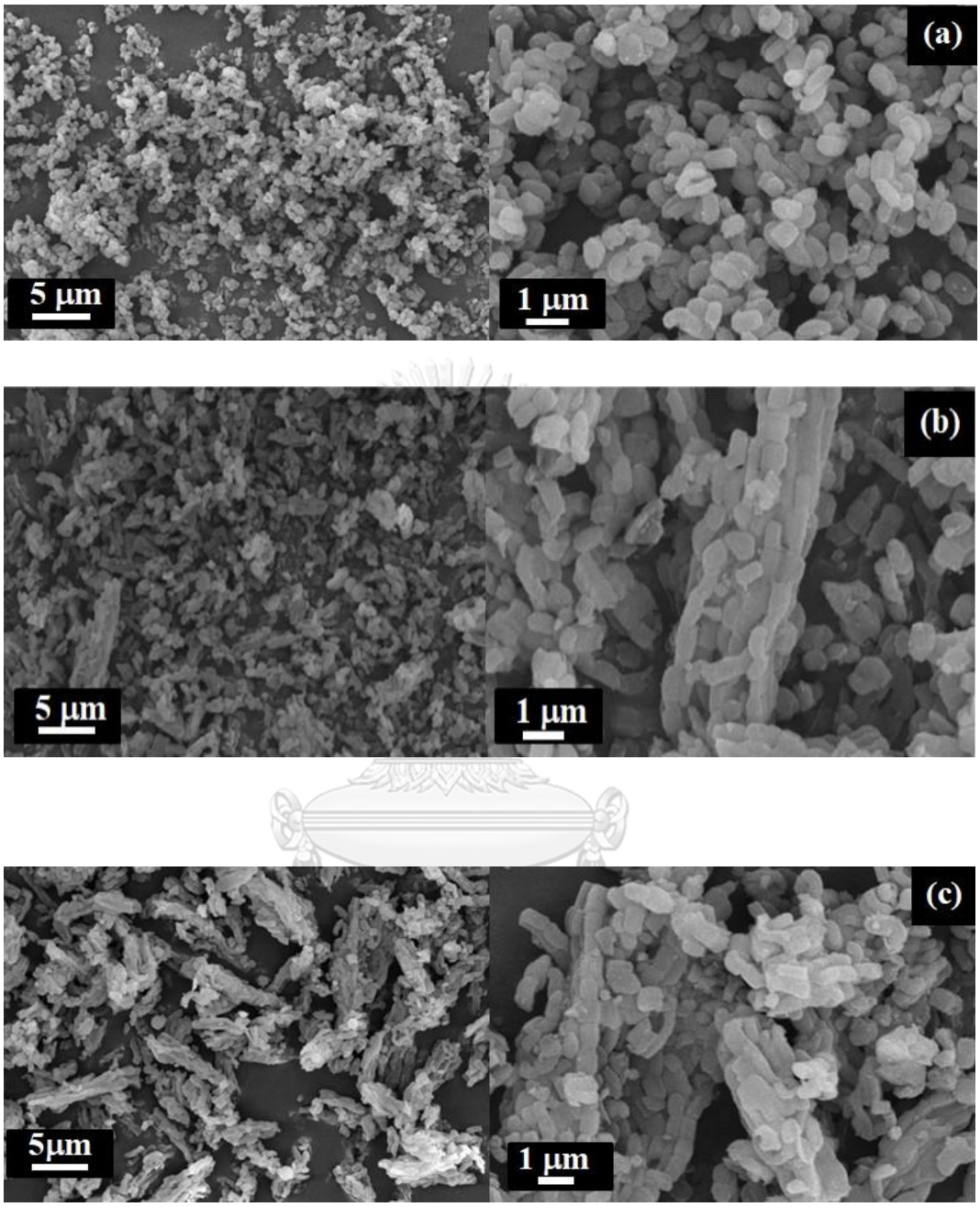

Figure 4.13 SEM photographs of fresh catalysts with ×3,000 and ×10,000 magnifications; (a)10Ni/SBA-15, (b) 10Ni/5TiN-SBA-15 and (c) 7.5Ni/10TiN-SBA-15.

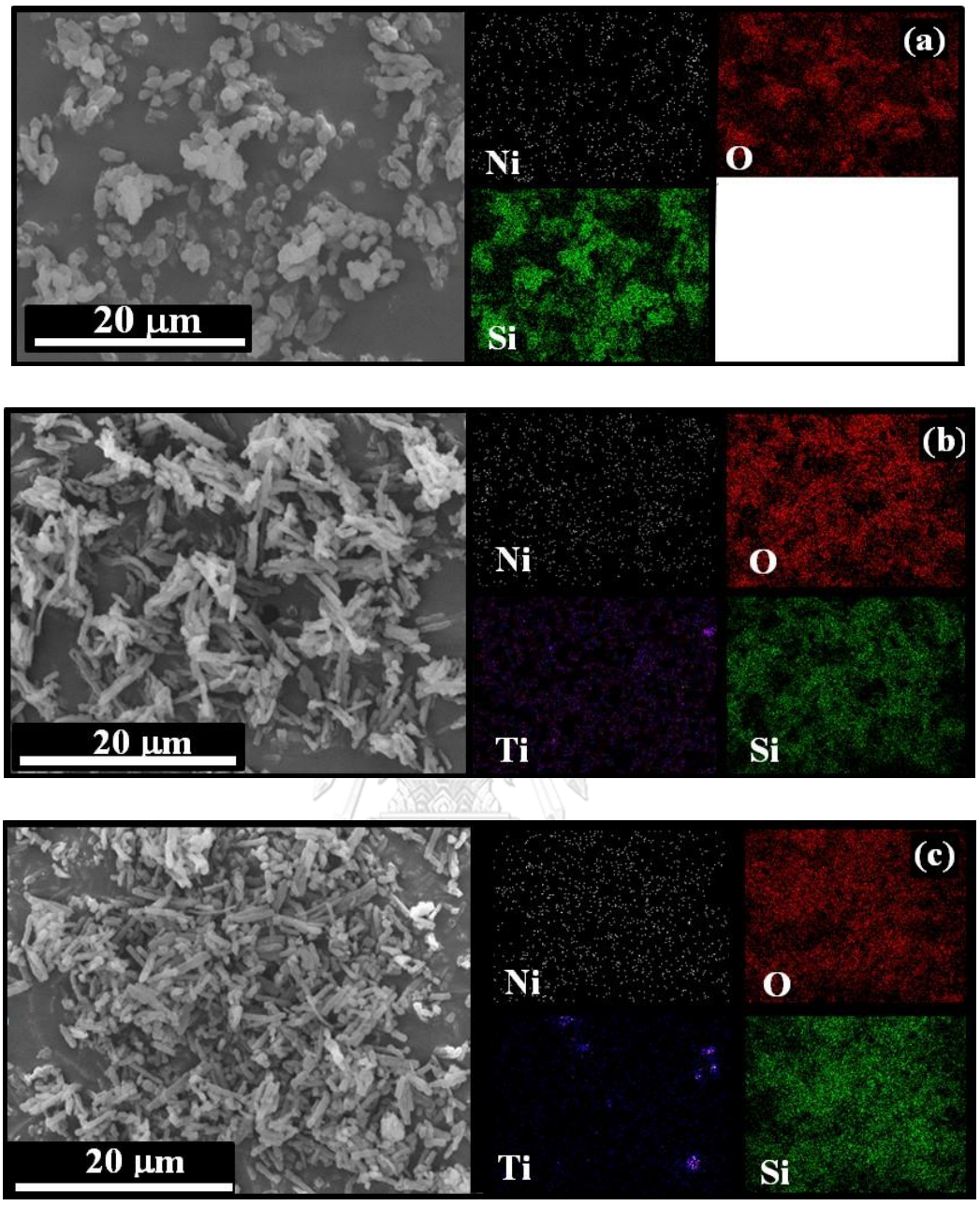

Figure 4.14 SEM-EDS mapping of fresh catalysts; (a) 10Ni/SBA-15, (b) 10Ni/5TiN-SBA-15 and (c) 7.5Ni/10TiN-SBA-15.

- **Transmission electron microscopy (TEM)**

The long-range ordered with two dimensional of original SBA-15 structure can be seen from transmission electron micrographs, shown in Fig.4.15. The micrograph, show highly ordered hexagonal structure as a typical characteristic of mesoporous SBA-15. They also shows an evidence of bulk TiN condensed on the external surface of SBA-15 with the interference fringes which were investigate by TEM-EDS analysis later. Thus, these particles may cause the partial pore blockage in the mesoporous structure which was reflected in the N_2 adsorption results. Nonetheless, TiN particles could not be observed on some parts of the external surface from the micrographs. Summarized all the results from XRD, SEM-EDS, XPS, FTIR and N_2 adsorption-desorption analysis, we can confirm that adding an appropriate amount of TiN did not change or disrupt the morphology and structure of the pristine SBA-15.

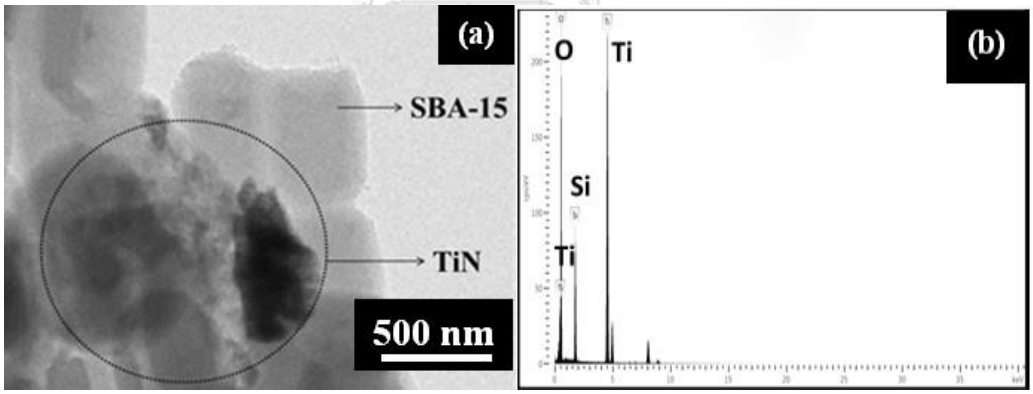

Figure 4.15 (a) Transmission electron micrographs and (b) EDS spectrum of 15TiN-SBA-15.

The TEM micrographs of Ni incorporated catalysts were presented in Fig 4.16.The pore diameter was measured from the distance of two bright strips of fresh catalysts in the micrographs. The pore sizes were at 8.25, and 7.17 and 7.18 nm for the 10Ni/SBA-15, 10Ni/5TiN-SBA-15 and 7.5Ni/10TiN-SBA-15, respectively. The

measurement was also in agreement with the results from BET analysis (8.20, 7.18 and 7.18, respectively). It can be seen that the average crystallite sizes of Ni particles of Ni/TiN-SBA-15 is smaller than Ni/SBA-15, according to results from the measurement from transmission electron micrographs, as summarized in Table 4.4. The random distribution of Ni particles was clearly seen throughout inside the pore and on the external surface. However, the occurrence of Ni particles on the external surface of SBA-15 is easily to reduce and sinter owning to their week interaction of the support [91]. Thus, the larger of nickel particle could promote coke deposited on the catalyst surface.

Table 4.4 Particle sizes of Ni determined from TEM.

Sample	TEM (nm)
10Ni/SBA-15	11.84
10Ni/5TiN-SBA-15	11.30
7.5Ni/10TiN-SBA-15	8.05

- **Fresh catalysts**

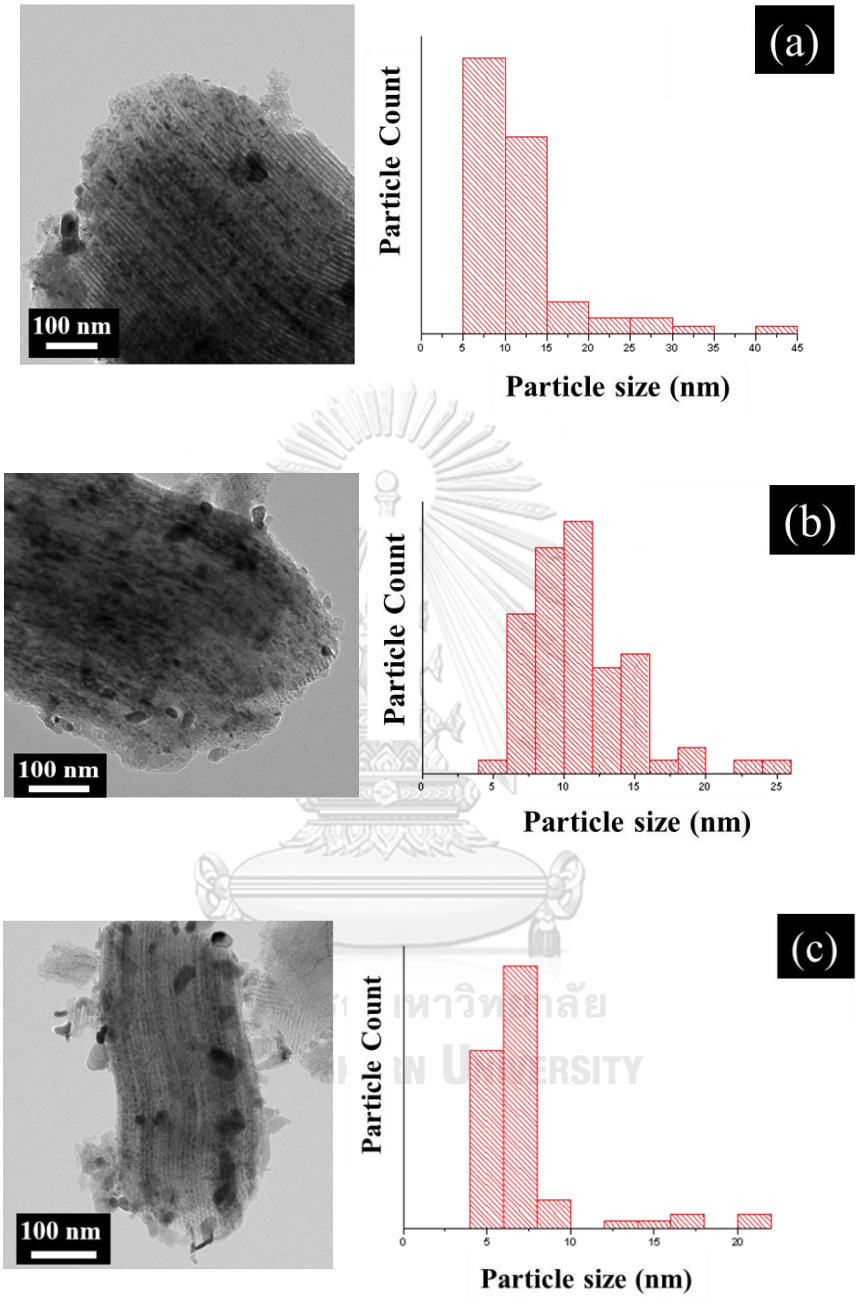

Figure 4.16 TEM micrographs and Ni particle sizes of fresh catalysts; (a) 10Ni/SBA-15, (b) 10Ni/5TiN-SBA-15 and (c) 7.5Ni/10TiN-SBA-15.

4.2 Catalytic activity

4.2.1 Influence of Ni and TiN loading

- **Reaction time of 4 h**

For the catalyst performance test, a correlation between Ni and TiN contents on the catalytic performance in dry reforming reaction at $700^{O}C$ was investigated. The study in catalytic activity both with and without catalysts in dry reforming reactions was shown in Table A2 of Appendix. The influence of Ni and TiN loading on the catalyst performance, tested at 700°C was shown in Fig. 4.17–4.19.

The increase in the conversion of both CH_4 and CO_2 was clearly observed with an increasing of Ni content. The results indicated that the high conversions were obtained as the catalysts contained at least 5 wt% Ni loading ($x \geq 5\%$), whereas the reaction on SBA-15, without Ni and TiN, showed almost no activity at all. Moreover, Ni-based catalyst with a TiN promoter showed a significant improvement in the catalytic activity comparing to non-promoted conventional Ni-based catalyst, although a minimal difference was exhibited at 10 wt% loading of Ni. Evidently, the small amount of TiN (5TiN-SBA-15 and 10TiN-SBA-15) was sufficient to promote 5–10 wt% Ni-based catalysts in the reaction to achieve high CH_4 and CO_2 conversions. It was found that the conversion of CO_2 was slightly higher than CH_4 in most reactions by using TiN-promoted Ni catalysts while H_2/CO was lower than unity for all reactions. This can be due to the effects of reverse water gas shift reaction (RWGS), ($CO_2 + H_2 \rightarrow CO + H_2O$). A side reaction which is partially depleted H_2 to produce H_2O and CO then resulted in low H_2 yield, high CO_2 conversion and H_2/CO less than 1 [24, 26, 91].

There are some superior catalytic performance among 25 catalysts for the reactions at 4 h, 5Ni/5TiN-SBA-15, 7.5Ni/5TiN-SBA-15, 7.5Ni/10TiN-SBA-15, 7.5Ni/18TiN-SBA-15 and 10Ni/5TiN-SBA-15, 10Ni/10TiN-SBA-15, 10Ni/15TiN-SBA-15, and 10Ni/18TiN-SBA-15. These catalyst gave high CO_2 and CH_4

conversions (~70%) and high H_2 and CO yields (>30%). However, the H_2/CO ratio between the initial and final hour of the reaction were quite varied and different, reflecting the stability of the catalysts. In particular, high H_2/CO ratio in the range 0.80–0.85 through the reaction period was found on 7.5Ni/10TiN-SBA-15, 7.5Ni/18TiN-SBA-15 and 10Ni/5TiN-SBA-15. This indicates a good stability of our new catalyst. The best catalytic performance typically demonstrated toward high-yield H_2 and CO production, high CH_4 and CO_2 conversions and H_2/CO ratio close to 1. For 7.5Ni/10TiN-SBA-15 and 10Ni/5TiN-SBA-15, the maximal H_2 production (~33%), high CO production (~40%), high CH_4 and CO_2 conversions (>70%), were selected as a suitable catalyst for the stability test compared to non-promoted 10Ni/SBA-15 catalyst in the 12 h reaction test.

- CH_4 conversion

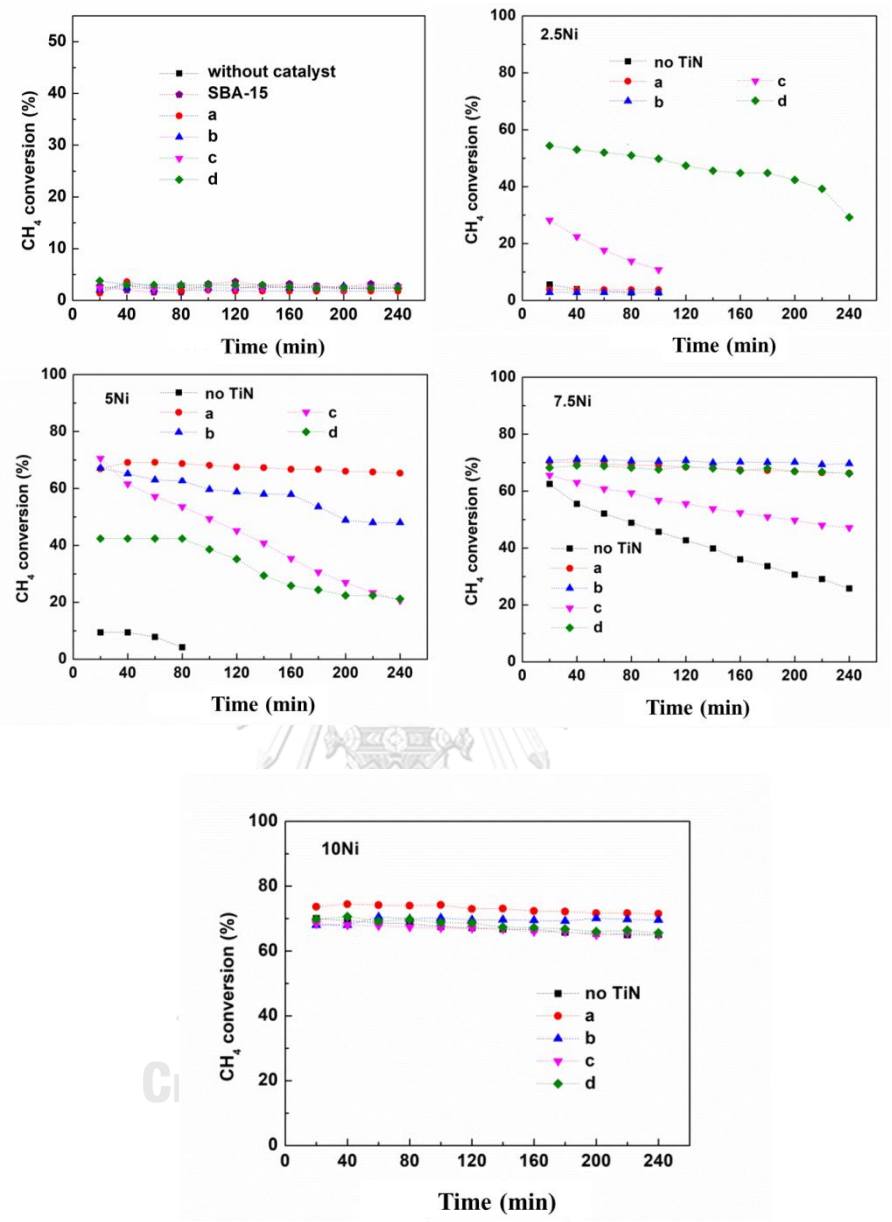

Figure 4.17 CH_4 conversion at 4 h reaction of 2.5-10 wt% of Ni loading in different TiN containing in SBA-15; (a) 5TiN-SBA-15 (b) 10TiN-SBA-15, (c) 15TiN-SBA-15 and (d) 18TiN-SBA-15.

- CO_2 conversion

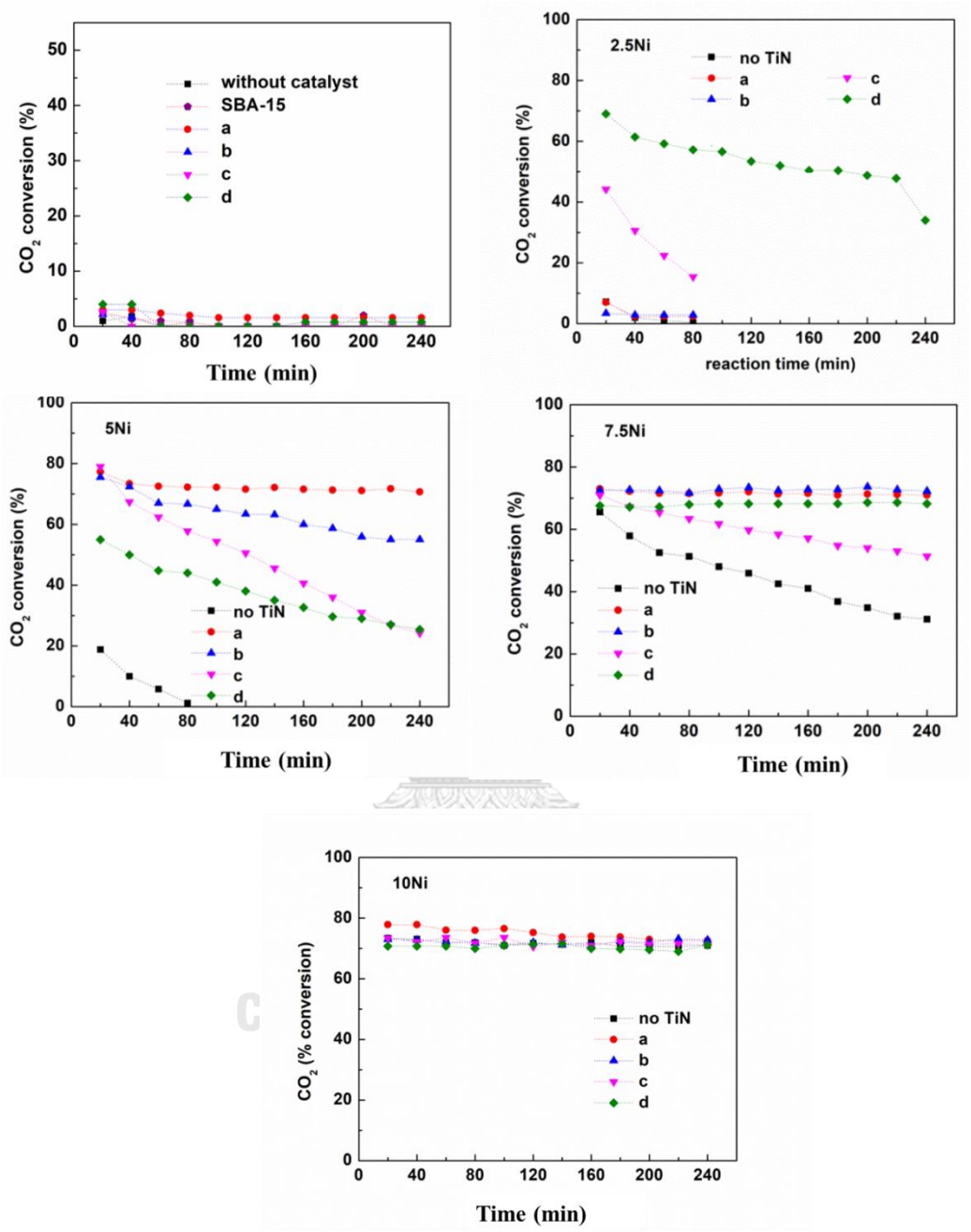

Figure 4.18 CO_2 conversion at 4 h reaction of 2.5-10 wt% of Ni loading in different TiN containing in SBA-15; (a) 5TiN-SBA-15 (b) 10TiN-SBA-15, (c) 15TiN-SBA-15 and (d) 18TiN-SBA-15.

- H_2/CO ratio

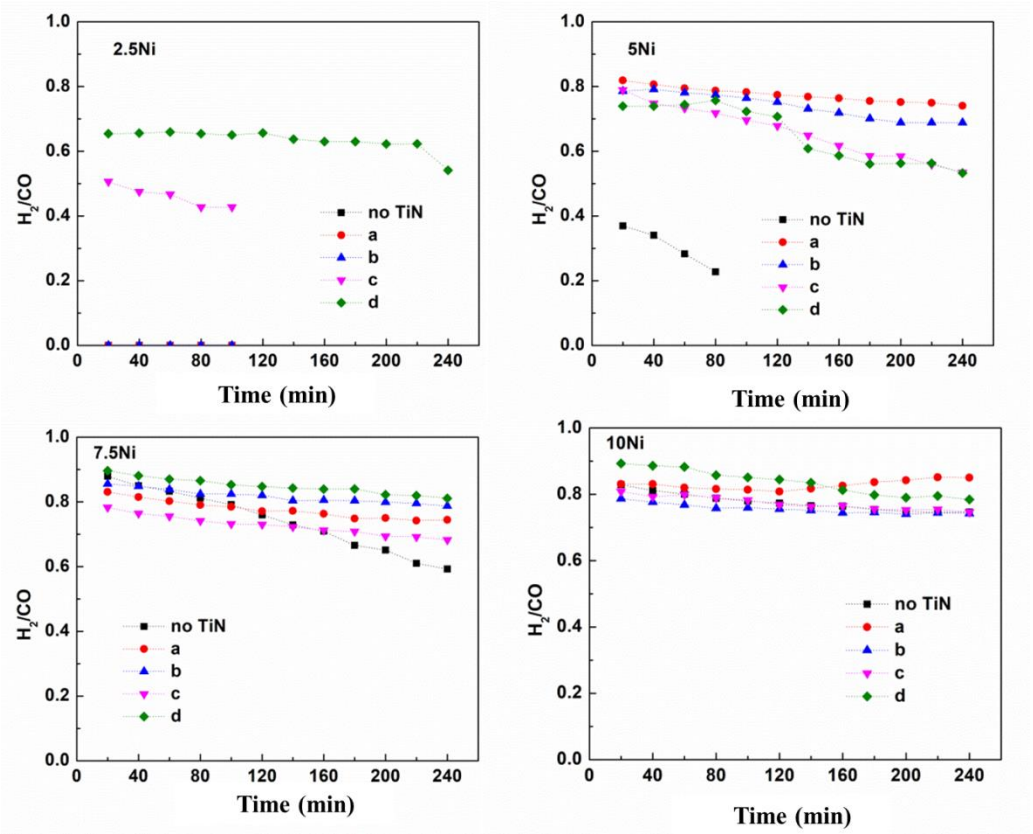

Figure 4.19 H_2/CO ratio at 4 h reaction of 2.5-10 wt% of Ni loading in different TiN containing in SBA-15 ; (a) 5TiN-SBA-15 (b) 10TiN-SBA-15, (c) 15TiN-SBA-15 and (d) 18TiN-SBA-15.

4.2.2 Effect of catalyst amount

From the study of DRM reaction with different amount of the high performance catalyst (10Ni/5TiN-SBA-15) in Table 4.5, the results does not show a significant different in catalytic activity over the reaction period of 4 h. However, the carbon removal by TGA analysis was the highest in catalyst usage of 25 mg following by 50 mg and 100 mg, respectively. Normally, the increasing of catalyst amount will increase the reaction activity. High mass of catalyst usage could provide more active sites for the reaction. However, catalyst amount also affects gas flow or mass transport inside the packed-bed reactor such as a pressure drop [16]. Thus, an optimum catalyst amount is required to achieve the effective catalytic activity. In order to obtain high catalyst performance and utilize low catalyst amount, we found that the appropriate catalyst quantity for the reaction for the 12 h reaction is about 50 mg.

Table 4.5 Catalytic activity of 10Ni/5TiN-SBA-15 with 0.025-0.1 g.

Catalyst (g)	Conversion (%)		Yield (%)		Carbon deposition
	CH_4	CO_2	H_2	CO	TGA analysis Mass change (%)
0.025	69	72	64	78	39.20
0.05	71	74	66	80	40.84
0.1	73	73	68	78	45.76

4.2.3 Influence of temperature

The activity investigation as a function of reaction temperature was conducted in the range of 450°C–800°C. Fig. 4.20 showed the conversions of CH_4 and CO_2 for all samples increased with temperature as the characteristic of endothermic reactions [18, 22]. The TiN promoted Ni-based catalysts reached 100% for both CH_4 and CO_2 conversions at 800°C while 10Ni/SBA-15 acquired 83.2% and 100%, respectively. This might be due to a contribution of RWGS. A similar trend of the catalytic activity was shown at 700° and 750°C. Therefore, the stability test of the catalysts was performed at 700°C in order to reduce energy consumption and expedient observation the capacity of the TiN promoter.

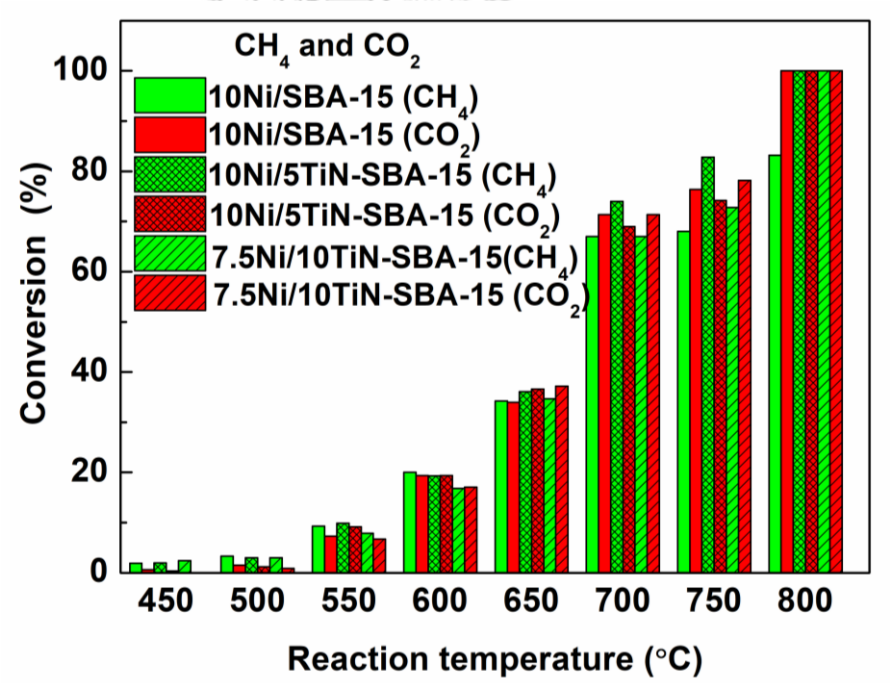

Figure 4.20 Influence of temperature on catalytic activity of 10Ni/SBA-15 and 10Ni/5TiN-SBA-15 and 7.5Ni/10TiN-SBA-15 catalysts.

4.2.4 Catalyst stability test

In Fig. 4.21, all catalysts showed their highest catalytic activity in the initial stage of the reaction with the conversions about 70% for both CH_4 and CO_2 and the product yields over 30% mol for H_2 and CO. In most cases, 10Ni/5TiN-SBA-15 catalyst possessed excellent catalytic performance and the second best was 7.5Ni/10TiN-SBA-15 catalyst. A significant improvement of catalytic activity and catalyst stability were obviously noticed for the catalysts containing of both Ni and TiN. This could ascribe that their great performance is due to both electronic and geometrics effect of these two active metals [93, 94]. Bimetallic catalyst has different chemical and electronic properties from the original metals which can enhance their catalytic activity [57]. Especially an oxidative stability of Ni and a partial oxidation of TiN, this composite was explained by electron transfer from the Ni (less noble) to the TiN (more noble) in order to achieve a balance of state in the Fermi levels. The Ni electron-deficient species could be highly reactive to CH_4 and CO_2 in the chemisorption step occurring on the catalyst surface which led to the increase in the catalytic activity [13, 33, 94]. In addition, the SBA-15 support also plays an important role in which mesoporous silica could favor the formation of both Ni and TiN particles with proper morphology and site density to delocalize electron [13, 33]. In order to gain more understanding of this reaction mechanism, a further study has now been in process. The similar catalytic activity of metal nitride promoter in DRM reaction was reported by Yang et. Al [8]. They synthesized h-BN supported mesoSiO_2-confined Ni catalysts which exhibited high coke- and sintering-resistance.

The H_2 and CO selectivity and H_2/CO ratio during the stability test were shown in Fig. 4.22. During the course of dry reforming reaction, the decrease of H_2/CO ratio was accelerated in the first 6 h then gradually declined for 10Ni/SBA-15 catalyst. In case of 7.5Ni/10TiN-SBA-15 and 10Ni/5TiN-SBA-15 catalysts, a similar decrease of H_2/CO ratio was obtained only in the first three hours, and then it became rather constant after 6 hours of reaction. It has been reported by Arbag et al. [95] and Yasyerli et al. [69] that the selectivity to CO against that to H_2 was higher for Ni-MCM-41 catalysts than the promoted catalysts with Rh and Ru due to a consequence

of the side effects of RWGS reaction. In this study, the promoted catalysts also showed better activity and stability for the reaction times longer than 6 h with lower selectivity to CO when compared to non-promoted catalyst. Although CO was produced by the promoted catalyst greater than non-promoted catalyst, suggesting that TiN promoter facilitate to enhance the catalytic activity of DRM reaction better than side reactions. This was also in agreement with the previous report that the contribution of RWGS reaction was decreased by the addition of Rh into the Ni-MCM-41 catalyst [95].

Regarding several catalysts for DRM reaction, variety of design catalysts were prepared and tested with varying condition. The similar experimental condition were selected and summarized in Table 4.6. It is notable that the desired conversion depends on many factors such as GHSV, catalyst amount and reaction temperature. Nonetheless, the synthesized catalyst in this study was the ones with great performance in catalytic activity although the conversions were not as high as others. It was effective to keep the constant activity with $H_2/CO \sim 0.8$ and reduce coke formation that could inhibit catalyst deactivation and prolong the catalyst life time.

- **The stability test over 12 h**

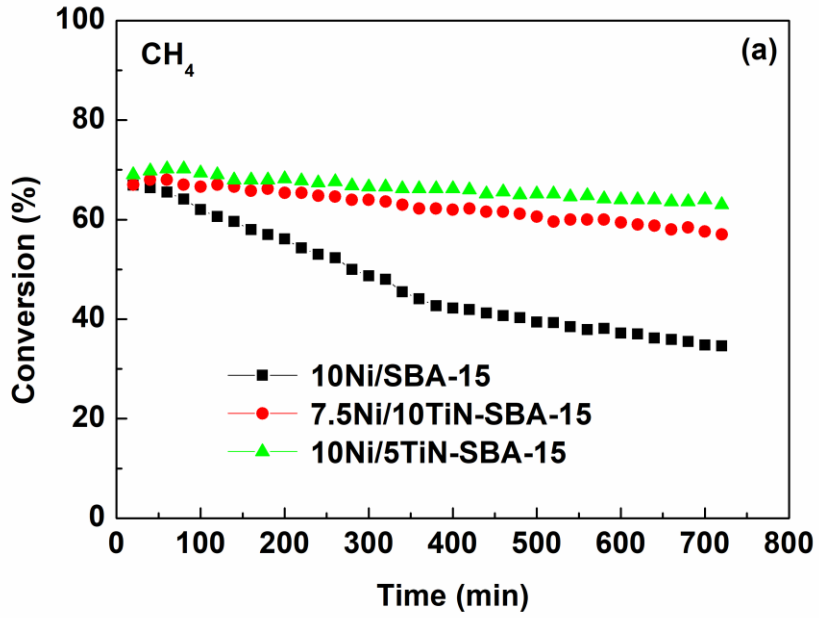

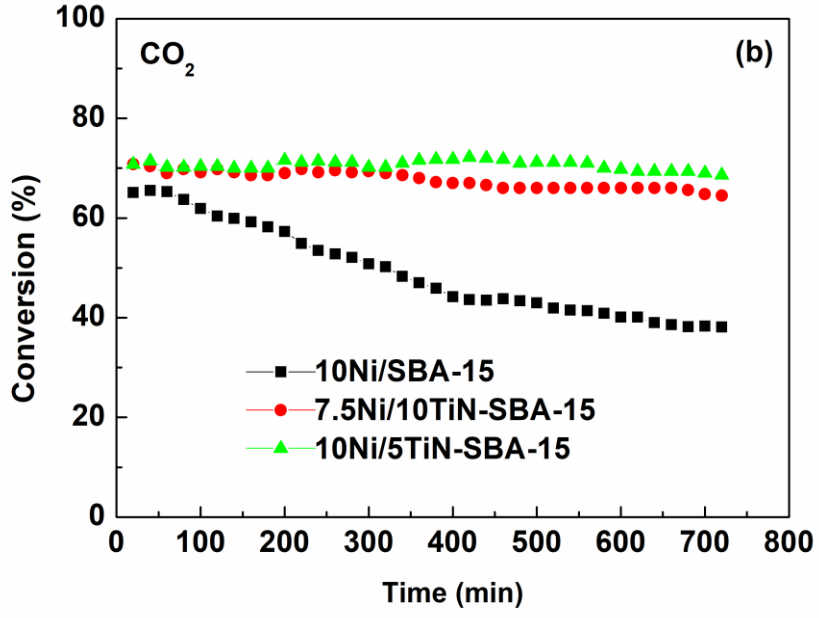

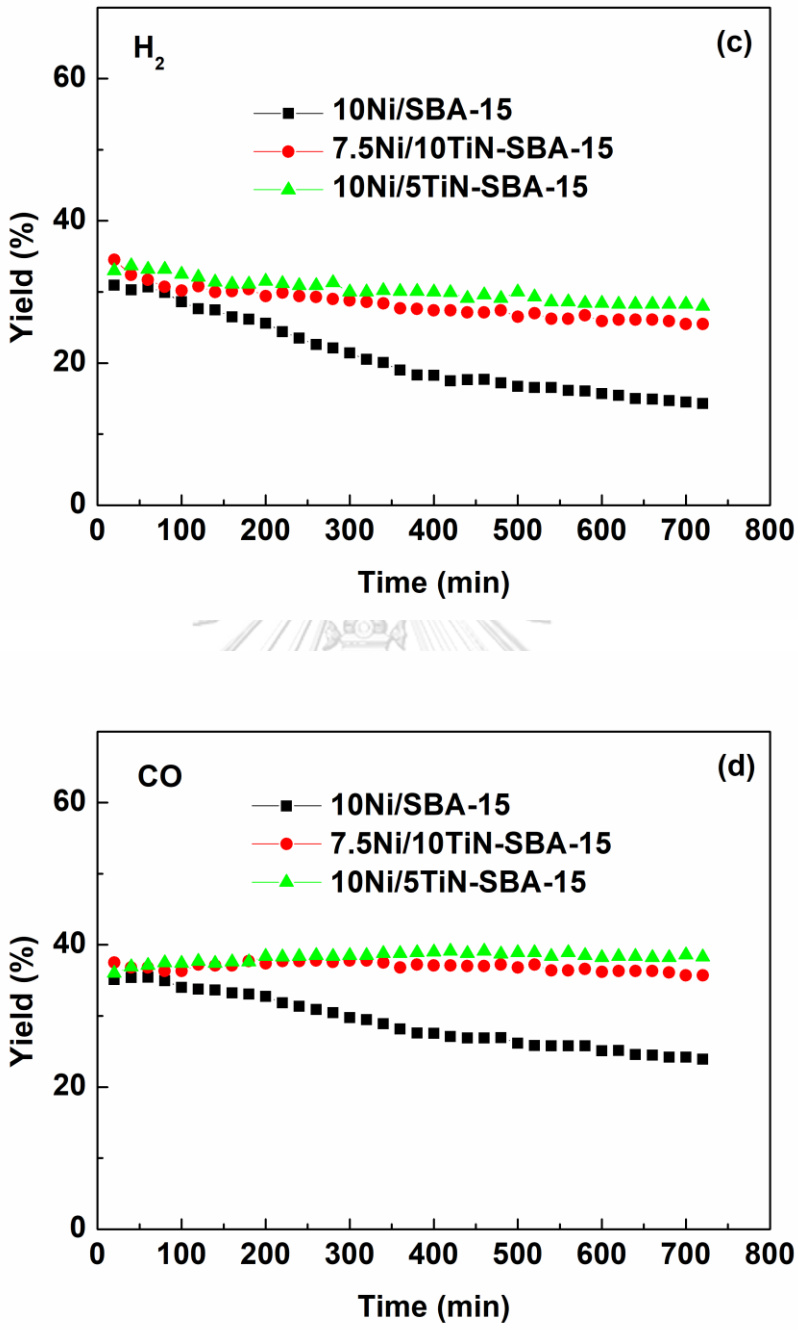

Figure 4.21 Conversion of (a) CH_4 and (b) CO_2 and % yield of (c) H_2 and (d) CO at 12 h of dry reforming reaction using 10Ni/SBA-15, 10Ni/5TiN-SBA-15 and 7.5Ni/10TiN-SBA-15 catalysts.

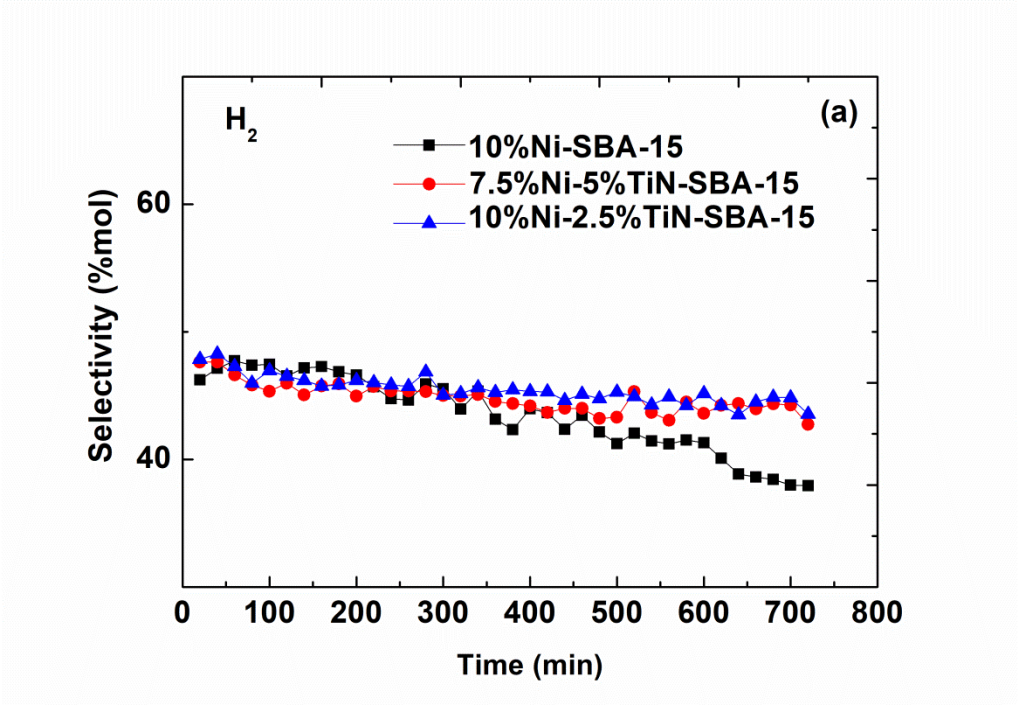
H2
(a)
10%Ni-SBA-15
7.5%Ni-5%TiN-SBA-15
10%Ni-2.5%TiN-SBA-15
Selectivity (%mol)
60
40
0
100
200
300
400
500
600
700
800
Time (min)

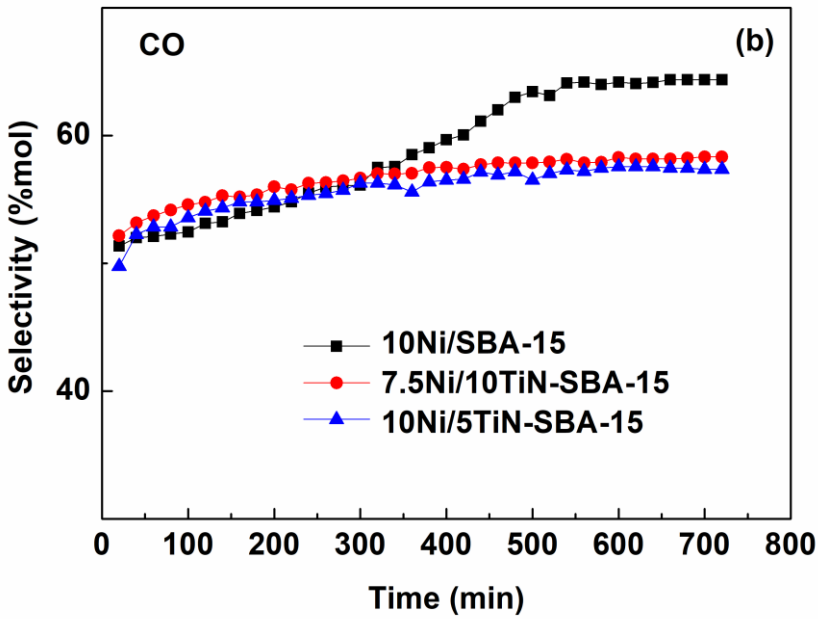
CO
(b)
10Ni/SBA-15
7.5Ni/10TiN-SBA-15
10Ni/5TiN-SBA-15
Selectivity (%mol)
60
40
0
100
200
300
400
500
600
700
800
Time (min)

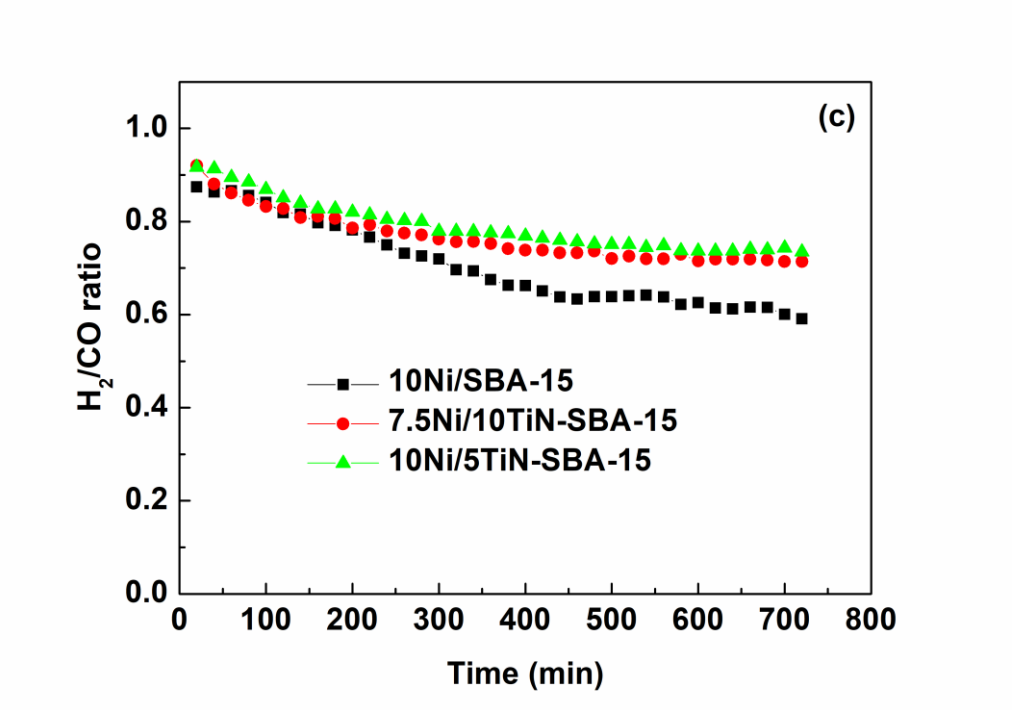

Figure 4.22 Selectivity of (a) H_2 and (b) CO and (c) H_2/CO ratio at 12 h of dry reforming reaction using 10Ni/SBA-15, 10Ni/5TiN-SBA-15 and 7.5Ni/10TiN-SBA-15 catalysts.

Table 4.6 Performance of different catalysts in similar experimental conditions.

Catalyst	g	GHSV $ml/g_{(cat)}h$	Temperature (°C)	Reaction time (h)	Conversion (%) (CO_2:CH_4 = 1:1)		H_2/CO	Ref.
					CO_2	CH_4		
7%Ni/Si_3N_4	0.15	8000	800	12	91	95	-	[7]
Co_3Mo_3N	-	6000	800	50	91	96	~0.9	[93]
Ni/WC	-	6000	800	12	~90	~80	-	[5]
10%Ni/8%MgO-SBA-15	0.10	36000	700	40	65	67	0.9-1.1	[24]
7%La/6%Ni–SBA-15	0.045	20000	750	1	80	73	0.8	[20]
5%Ni/SiO_2	0.10	36000	750	3	89	73	0.8	[96]
20wt%Co/80wt%La_2O_3	0.20	30000	750	-	60	50	0.78	[97]
3%Gd/10%Ni/Y_2O_3	0.30	8000	700	6	80	80	0.9<x<1.1	[98]
$3Sm_2O_3$/10Ni/SBA-15	0.2	12000	700	5	~75	~72	0.8	[28]
25%Ni-Al_2O_3	0.20	12000	700	5	80	70	0.9	[99]
10%Ni/6%MgO-$MgSiO_3$	0.10	18000	700	12	~80	75	0.6	[60]
10%Ni/45%TiO_2SiO_2	0.1	36000	700	10	78	65	-	[59]
0.1Rh10Ni/BN	0.06	WHSV = 60 $l/g_{(cat)}h$	700	6	81	72	~0.7	[66]
Cu-Ni/SBA-15	-	10000 (space velocity)	650	6	77	75	-	[93]
10Ni/5TiN-SBA-15	0.05	1558	700	12	71	66	0.80	this work

4.2.5 Spent samples characterization

After the long term reaction, all of the spent samples in Fig 4.23 showed the appearance of the graphitic carbon with the intense diffraction peak at 2θ values of 26° [2]. The reflection peaks of Ni were obviously attenuant, evidencing the catalysts suffered from carbon deposition after the stability test. The elemental composition can be verified by SEM-EDS including metals; Ni, Ti, Si, O and C as shown in Fig (4.26). Confirming the well dispersion of Ni within SBA-15 pore structure still maintain the active site which can restrain the segregation of nickel oxide and lead to the elimination of accumulated carbon and prolongation the catalysts performance.

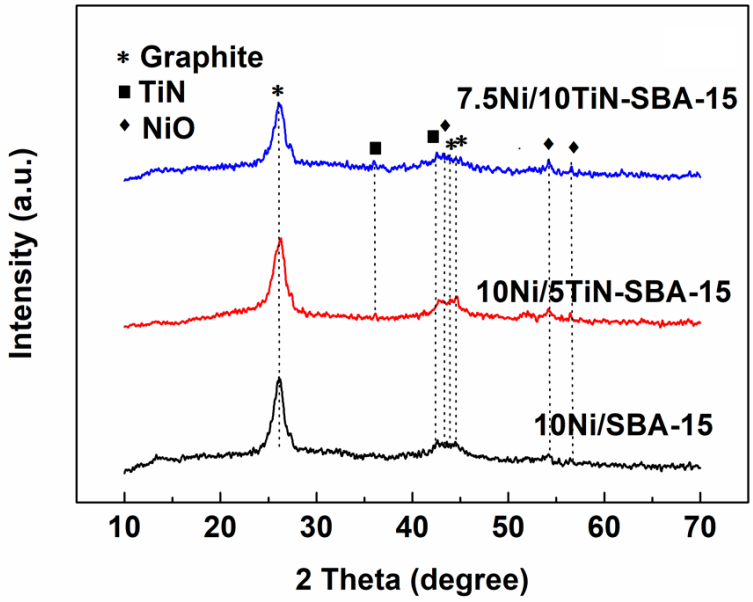

Figure 4.23 XRD pattern of spent catalyst 10Ni/SBA-15, 10Ni/5TiN-SBA-15 and 7.5Ni/10TiN-SBA-15 catalysts.

The amount of carbon deposition of the spent 10Ni/SBA-15, 10Ni/5TiN-SBA-15 and 7.5Ni/10TiN-SBA-15 catalysts after 12 h reaction was measured by TGA analysis in the temperature range of 50–800°C Fig.4.24. All three catalysts exhibited

their weight loss of carbon removal gradually happened during 100–400°C and more rapid at higher temperature than 500°C. This phenomenon can be explained that carbon on the surface was mostly the graphitic carbon that oxidized at temperature above 500°C [100, 101]. The amount of carbon removal followed the order of 10Ni/5TiN-SBA-15 (62.48%) < 7.5Ni/10TiN-SBA-15 (74.88%) < 10Ni/SBA-15 (83.28%). It was clear that 10Ni/SBA-15 (non-promoted catalyst) showed higher weight loss than the TiN incorporated-catalysts. As described before, 10Ni/SBA-15 has the largest Ni particle size which could be sintered easily. Therefore, the sintering of Ni metals during dry reforming reaction can provoke the deposited carbon on the catalyst surface and cause the most rapid deactivation [102]. Furthermore, the TGA results also support the carbon conversion in Boudouard reaction which resulted in low amount of carbonaceous species and CO-rich production in the promoted catalyst. Thus, the promoted catalyst can reduce carbon accumulation, resist to Ni sintering and maintain the catalyst stability.

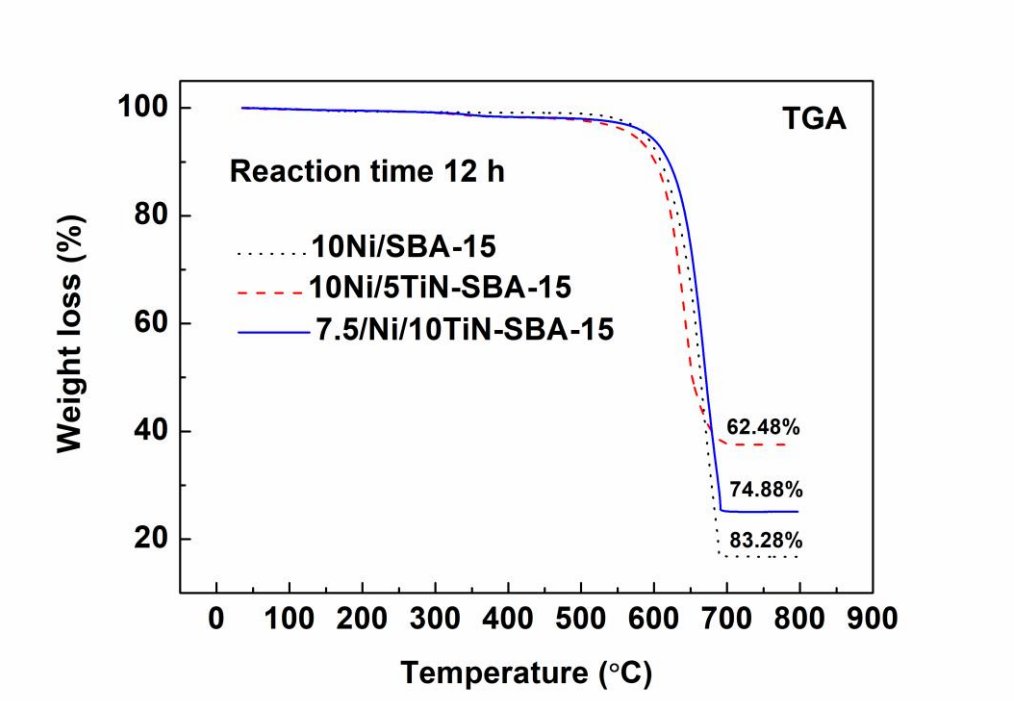

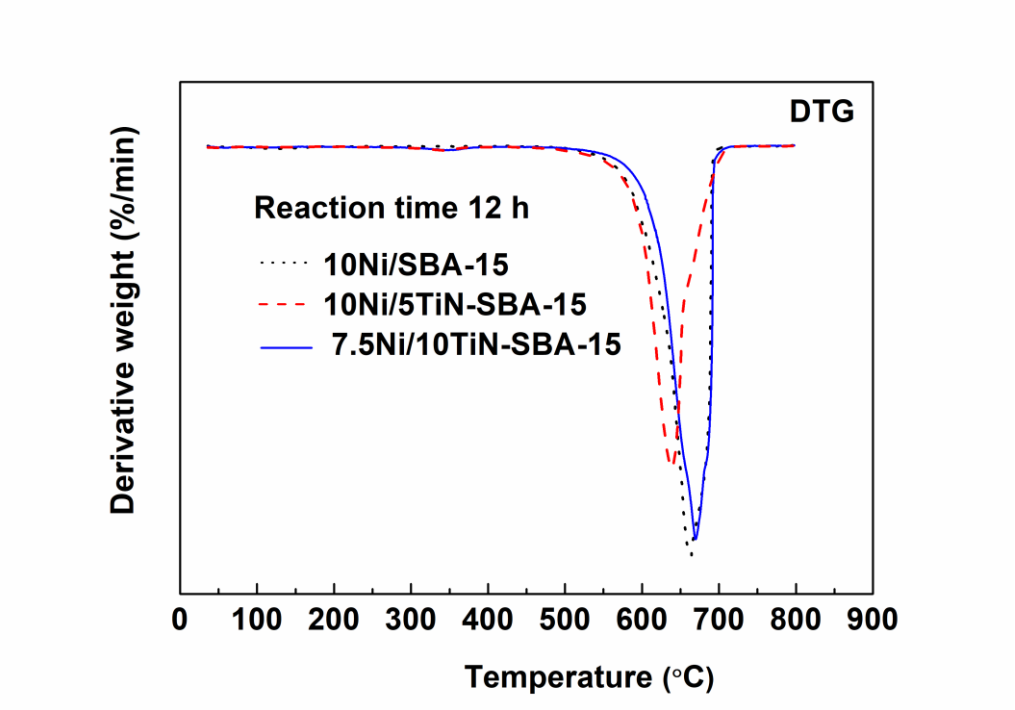

Figure 4.24 TGA and DTG profiles of the catalysts after 12 h reaction.

The SEM images and SEM-EDS mapping of the spent catalysts after 12 h DRM reaction were shown in Fig. 4.25 and 4.26, respectively. The morphology of the spent catalysts was changed and aggregated. The elemental compositions from EDS analysis confirmed the existence of Ni and TiN after the reaction which is not clear in the XRD results. The carbon deposition covered on the catalyst surface was also obviously observed and more apparent in EDS mapping images**.**

- **Spent catalysts**

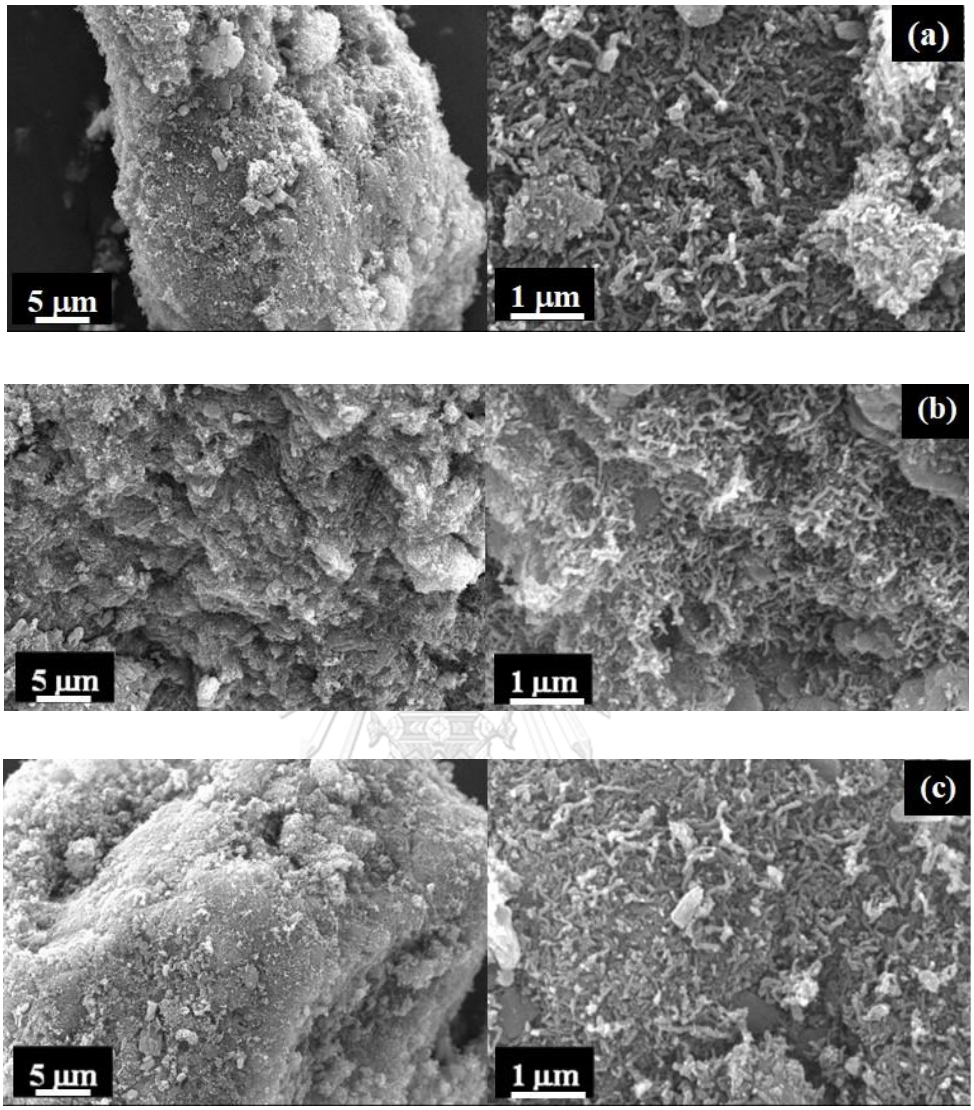

Figure 4.25 SEM photographs of spent catalysts with ×3,000 and ×20,000 magnifications: (a) 10Ni/SBA-15, (b) 10Ni/5TiN-SBA-15 and (c) 7.5Ni/10TiN-SBA-15.

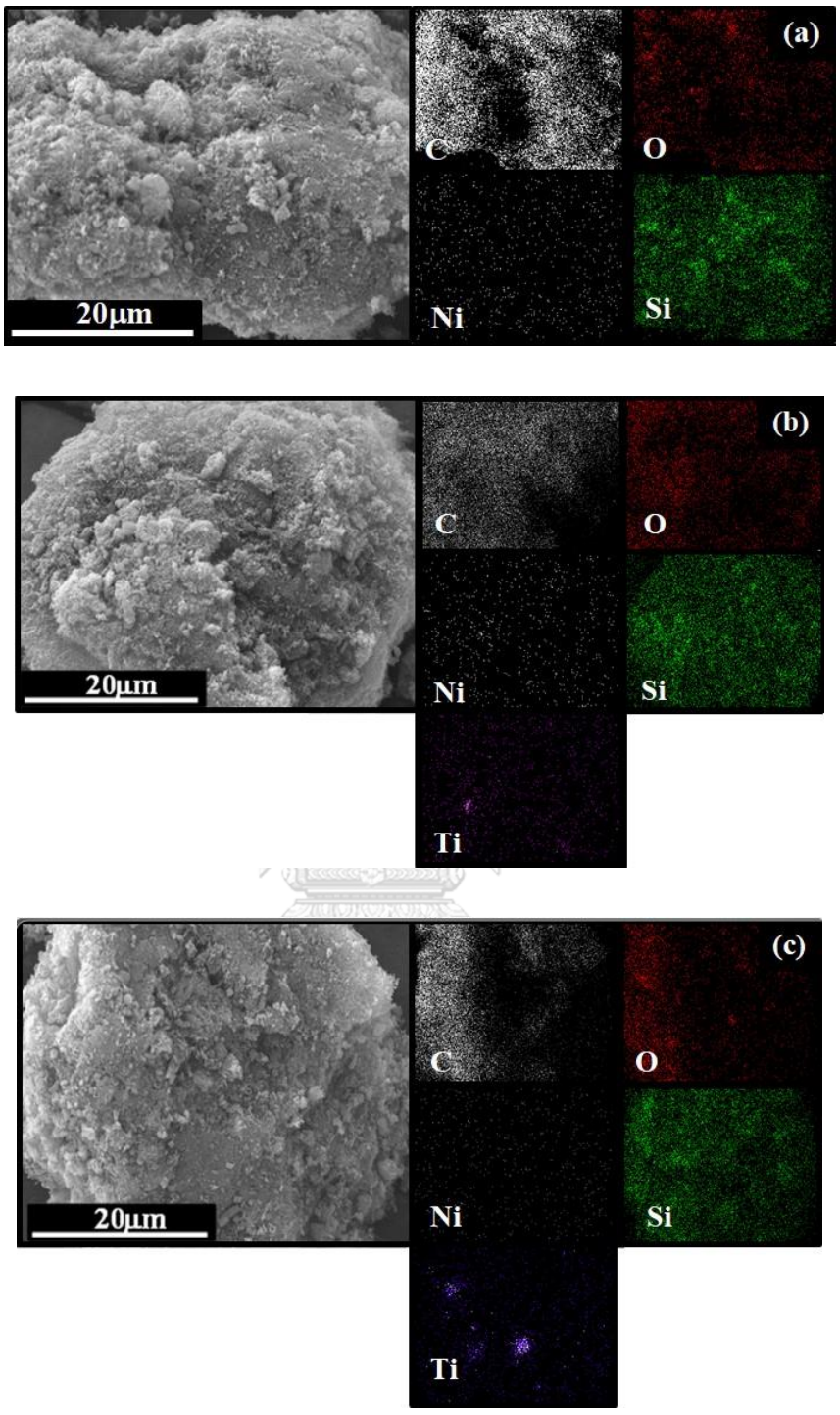

Figure 4.26 SEM-EDS mapping of the spent catalysts; (a) 10Ni/SBA-15, (b) 10Ni/5TiN-SBA-15 and (c) 7.5Ni/10TiN-SBA-15.

The TEM micrographs of spent catalysts were recorded after 12 h of the stability test on the selected catalysts, displayed in Fig. 4.27. It can be seen the aspect of carbonaceous species formation which was consistent with the graphite reflection peaks in the XRD patterns. Moreover, all samples still preserved the ordered mesoporous structure of SBA-15 although undergoing the coke deposition. Interestingly, the resident nickel particles on the outer surface, with weak interaction with the support, were apart from the surface of SBA-15 so the reaction could still continue on these particles [24, 103] . In addition, the larger particles sized due to Ni sintering were observed with the encapsulated carbon.

Noted, two types of carbons were found on the spent catalyst; filamentous carbon and encapsulating carbon as shown in Fig. 4.28 carbon [24, 91]. The filamentous structure is the long tube carbon, when the carbon was dissolved and located through the active sites of nickel particles then dark pear-shaped of nickel (in Figure 4.28a) was formed as the encapsulating carbon [24, 63, 103]. The filamentous carbon has minor influence on the catalyst efficiency [24, 91, 103], noticed in TiN-coated samples, but a high volume of the filaments, found in 10Ni/SBA-15 could impact the catalyst structure, plug the reactor and suppress the catalytic activity. Therefore, the coating TiN-catalysts posed high %conversion and %yield during the reaction over 12 h whilst both %conversion and %yield were gradually reduced for 10Ni/SBA-15.

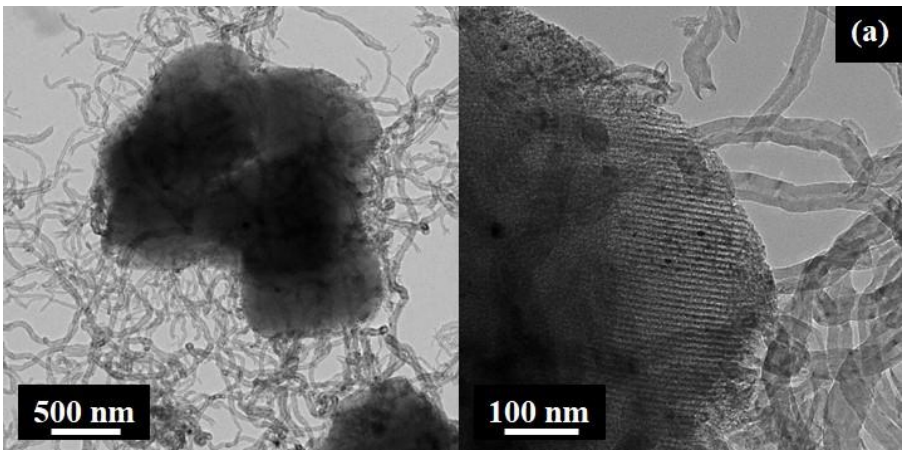

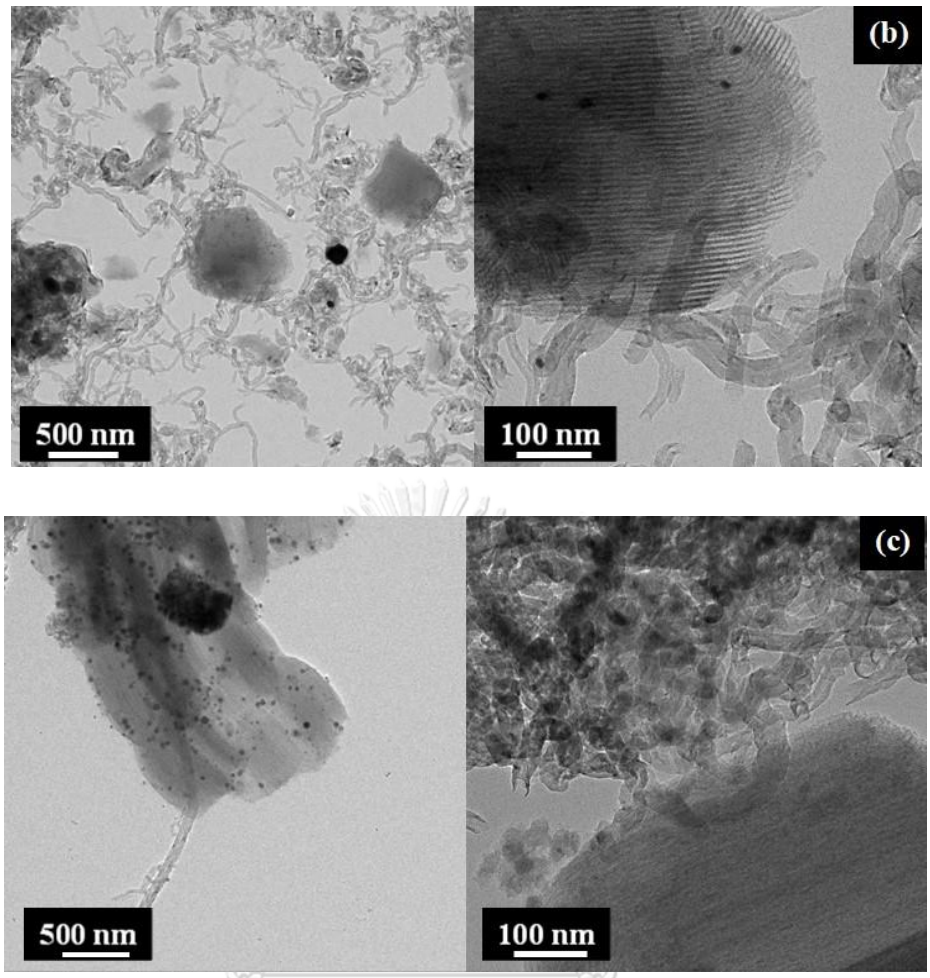

Figure 4.27 TEM micrographs of spent catalysts: (a) 10Ni/SBA-15, (b) 10Ni/5TiN-SBA-15 and (c) 7.5Ni/10TiN-SBA-15.

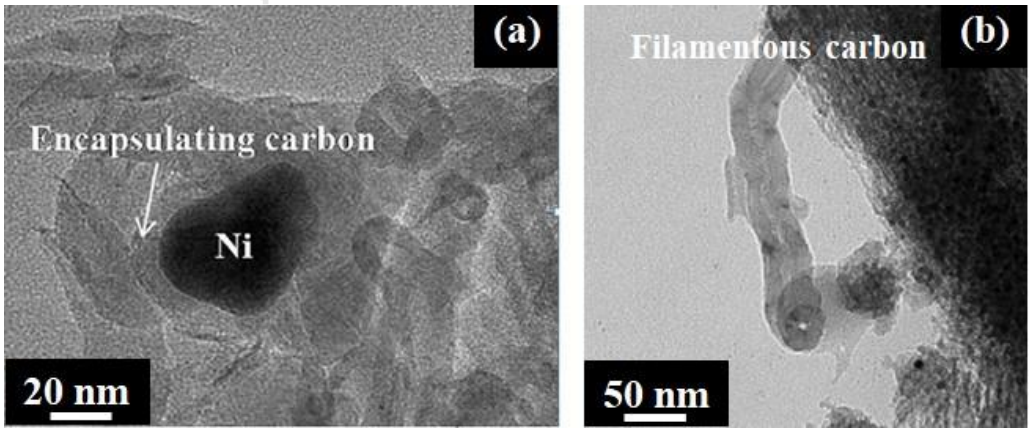

Figure 4.28 Example of TEM images of (a) encapsulating carbon and (b) filamentous carbon [24, 91].

Further investigation of catalyst stability was investigated on the catalytic performance of the regenerated catalysts. The performance of the reused catalysts (10Ni/SBA-15 and 10Ni/5TiN-SBA-15) in terms of CH_4 and CO_2 conversions, H_2 and CO selectivity and H_2/CO ratio were shown in Fig.4.29. The used catalysts were reduced in H_2 at 600°C after the 12 h on stream reaction. As can be observed, the promoted catalyst showed almost sustained catalytic performance whereas it gradually declined in unpromoted catalyst. Indicating that TiN promoted catalyst is productive after the regeneration process as well as prolonged the catalyst stability.

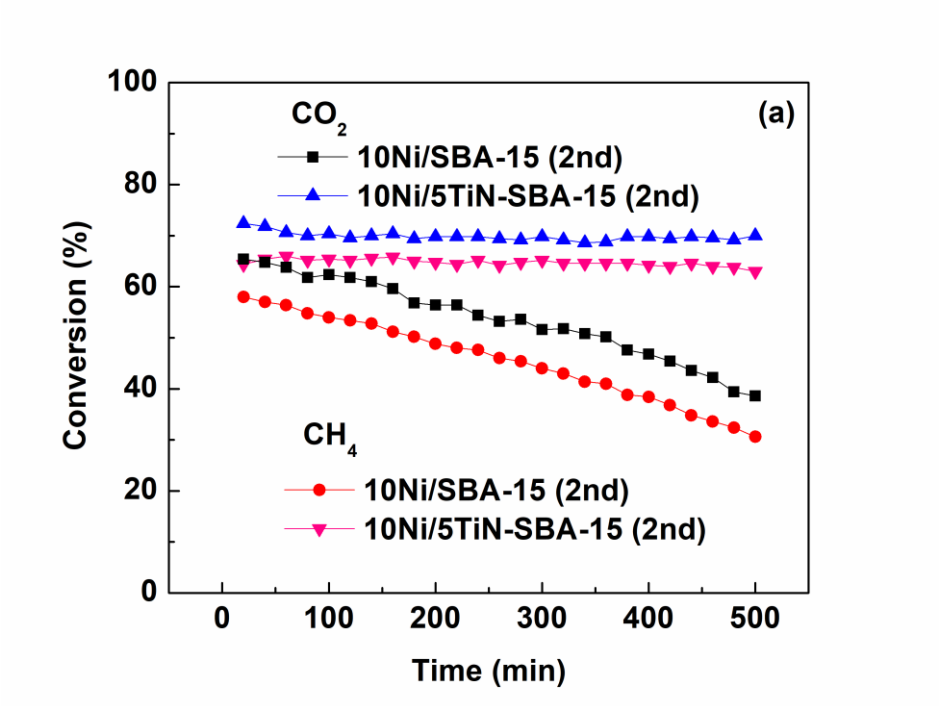

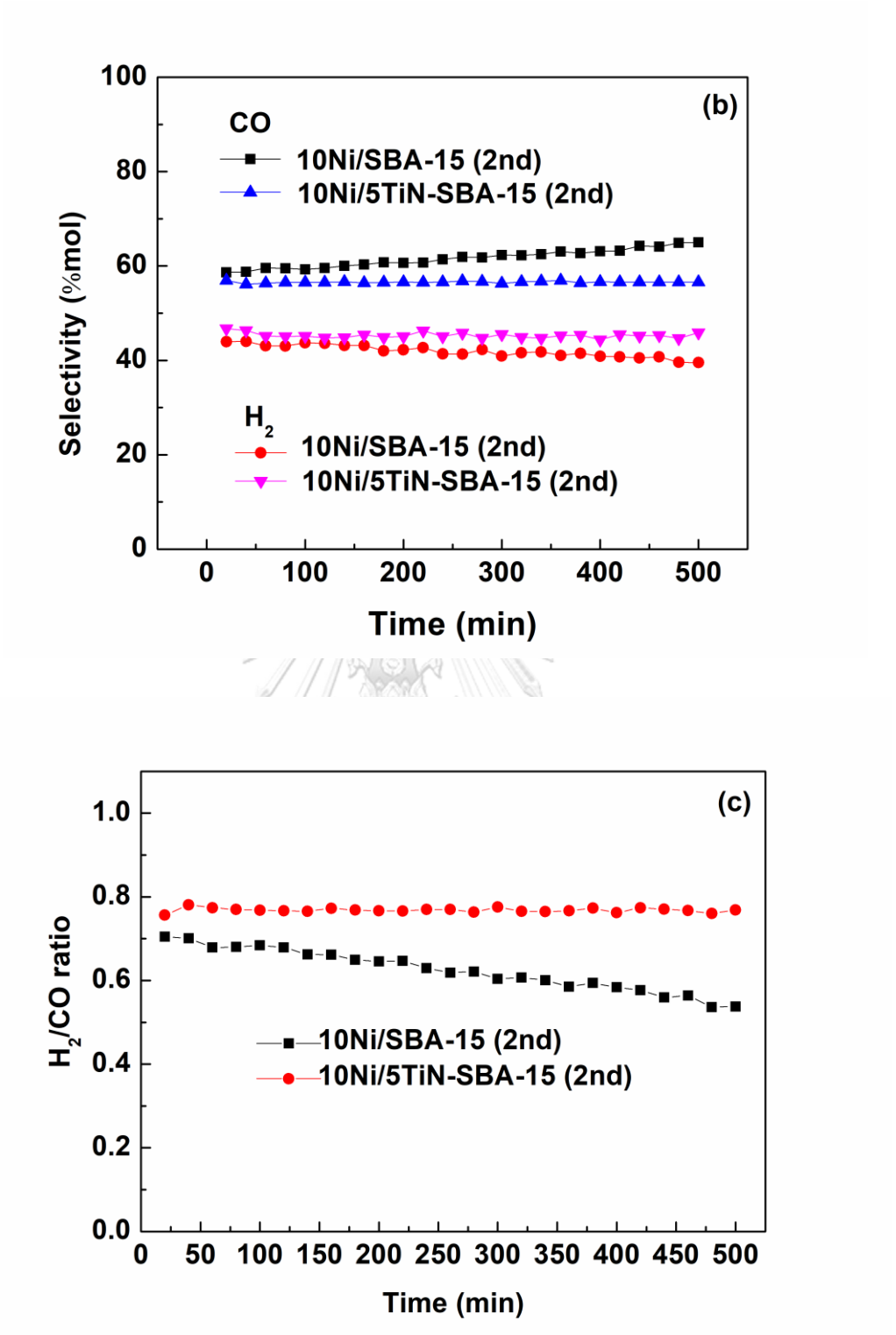

Figure 4.29 (a) Conversion of CH_4 and CO_2 (b) Selectivity of H_2 and CO and (c) H_2/CO ratio at 12 h of dry reforming reaction using regenerated 10Ni/SBA-15 and 10Ni/5TiN-SBA-15 catalysts.

4.3 Zeolite Y support

There are some literatures about the catalytic effectiveness of zeolite Y in DRM reaction [51, 52, 58]. Thus, Zeolite Y was selected to use as a microporous support for TiN promoted Ni-based catalyst in DRM reaction. Ni/TiN-HY catalyst was prepared by impregnation of TiN follow by Ni into HY before calcination.

Elemental composition of TiN incorporated in Zeolite Y materials was investigated by WDXRF technique in Table 4.7. In case of SBA-15 mesoporous support, the effective catalyst is 10Ni/5TiN-SBA-15 which contains 10 wt% of Ni and 4.9% of TiN. Therefore, sample 5TiN-ZY which has 4.8% of TiN is selected to study the catalytic activity in order to use the same quantity of TiN.

Table 4.7 Chemical composition of TiN-SBA-15 and TiN-HY.

Sample	Composition by WDXRF (wt%)		
	Ti	TiN (calculation)	Ni
5TiN-SBA-15	3.8	4.9	-
10TiN-SBA-15	7.2	9.3	-
2.5TiN-HY	1.9	2.4	-
5TiN-HY	3.7	4.8	-
7.5TiN-HY	5.9	7.6	-
10TiN-HY	7.3	9.5	-
5Ni/5TiN-HY	3.5	5.3	5.6
7.5Ni/2.5TiN-HY	2.04	2.6	8.7
10Ni/2.5TiN-HY	1.55	2.0	9.4

The results in Fig.4.30 obviously indicated high catalytic activity was obtained in the first hour and then it was gradually decline, especially H_2 yield was less than 10%mol so the reaction was observed of about 2 h. Nonetheless, TiN-promoted catalysts (10Ni/5TiN-HY) showed the improvement of catalytic activity better than non-promoted catalyst (10Ni/HY) with slightly higher for both conversions (CH_4 and CO_2) and yields of H_2 and CO.

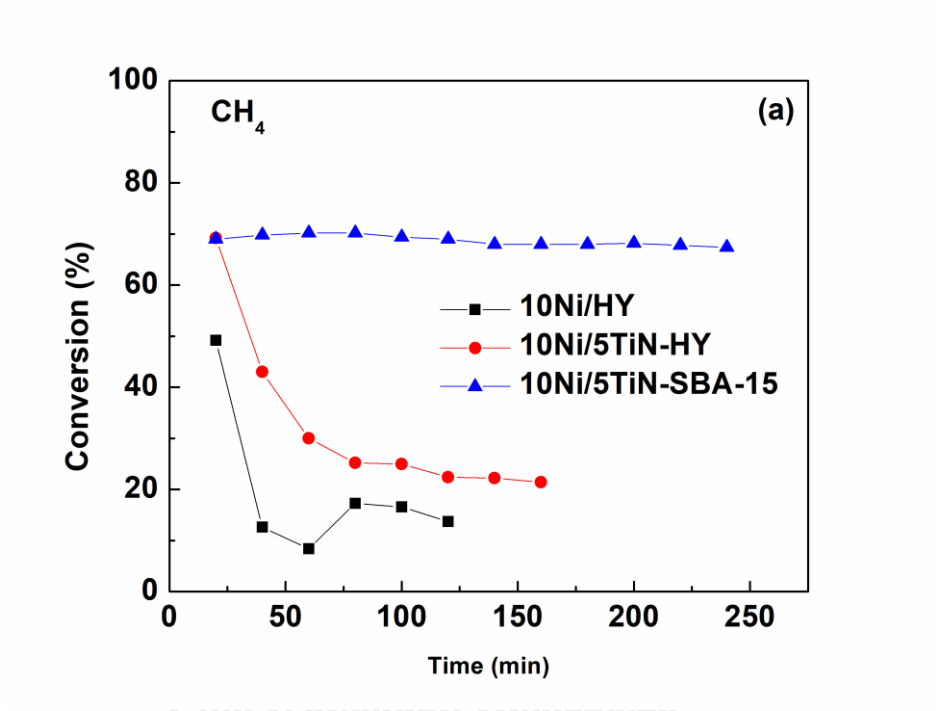

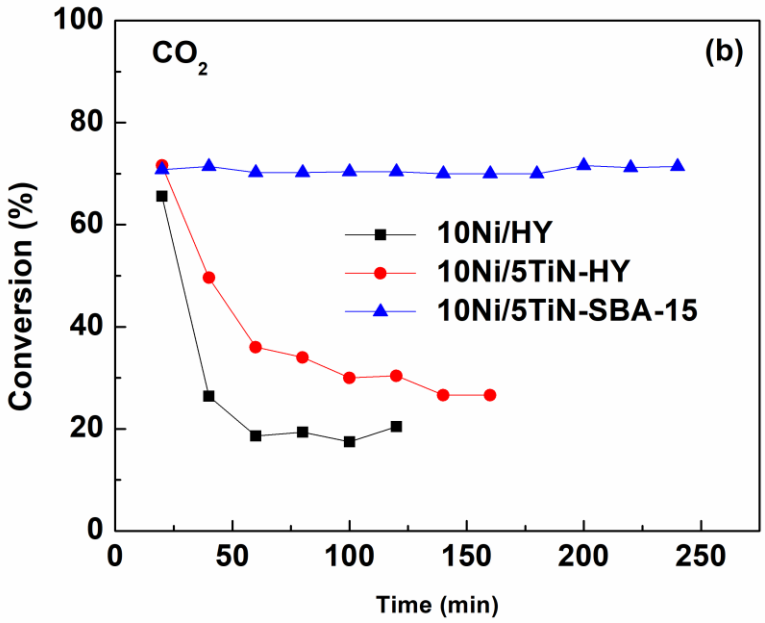
CO2
(b)
Conversion (%)
Time (min)
10Ni/HY
10Ni/5TiN-HY
10Ni/5TiN-SBA-15
0
20
40
60
80
100
0
50
100
150
200
250

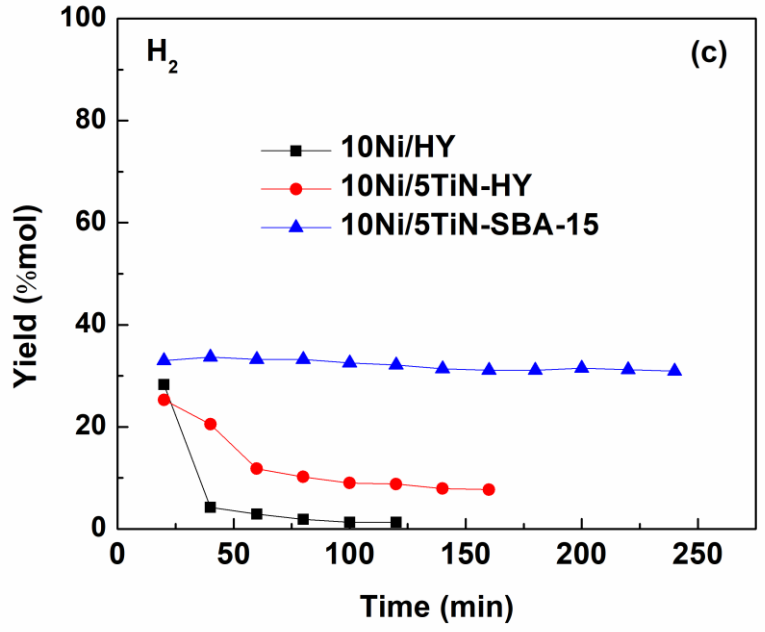
H2
(c)
Yield (%mol)
Time (min)
10Ni/HY
10Ni/5TiN-HY
10Ni/5TiN-SBA-15
0
20
40
60
80
100
0
50
100
150
200
250

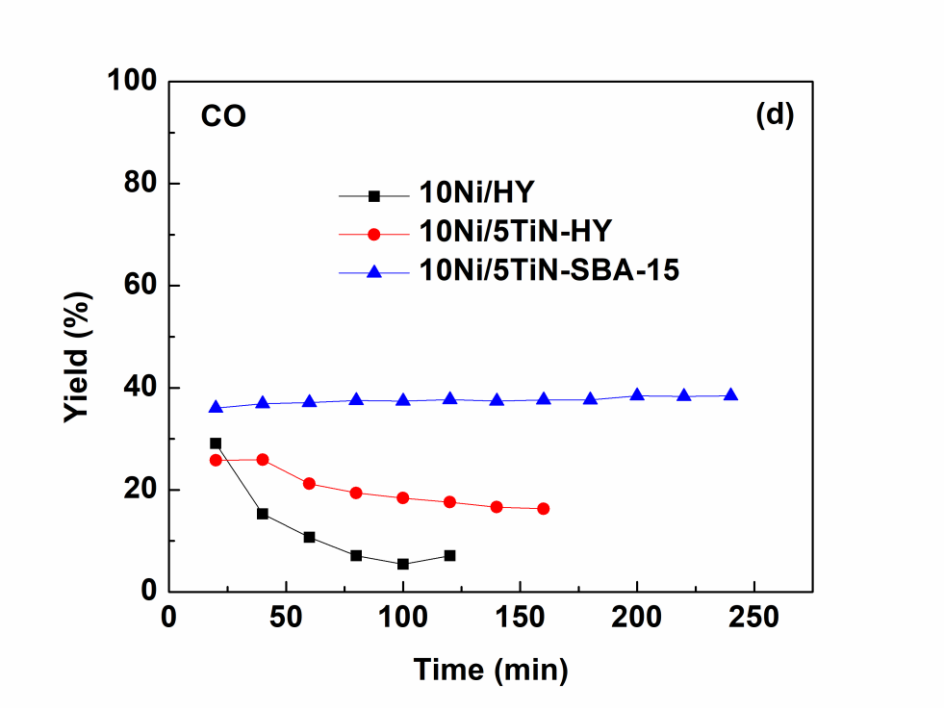

Figure 4.30 Conversion of (a) CH_4 and (b) CO_2 and % yield of (c) H_2 and (d) CO in dry reforming reaction using 10Ni/HY, 10Ni/5TiN-HY and 10Ni/5TiN-SBA-15 catalysts.

H_2 and CO selectivity and H_2/CO ratio of 10Ni/HY and 10Ni/5TiN-HY were shown in Fig.4.31. It was found that H_2 selectivity of the promoted catalysts maintained of about 40%mol approximately 2 h on stream whereas CO selectivity gradually increased to ~60%mol. H_2 and CO selectivity of non-promoted catalyst was lower than the promoted catalyst and it was gradually declined after first hour of reaction. The H_2/CO ratio of non-promoted catalyst was also less than the promoted catalyst. Thus, this is also evidenced that TiN can promote the catalytic activity of Ni-based catalyst.

Noted, type of support has much influenced on the catalytic activity. It can be concluded that SBA-15 is favor to DRM reaction more than zeolite Y. The result was also reported by some literatures about the effect of the acidity of the support, CO_2 is an acidic gas so it prone to adsorb on the basic alkaline or alkaline oxide modified support or the neutral support than the pristine zeolite [15, 51, 58, 104]. The proposed

reaction on the support in Table 2.2 (Chapter 2, page 13) indicates that the basic support plays bigger role than the acidic support. The activation of CO_2 also takes place on the basic support whereas only CO_2 adsorption occurs on the acidic surface [54]. This influences the deposition and polymerization of carbonaceous on the active metals which leads to pore blockage or destroy the zeolites' pore as shown in Fig 4.31 [104]. TGA analysis was used to determine the coke content as shown in Table 4.8. It was found that the deposited coke on 10Ni/5TiN-HY for 2 h reaction (47.26%) was higher than 10Ni/5TiN-SBA-15 (41.35%) for 4 h reaction. Confirming the growth of carbonaceous on the zeolite Y support was larger than SBA-15 support. Therefore, no additional investigation was performed on the zeolite Y supported Ni catalysts.

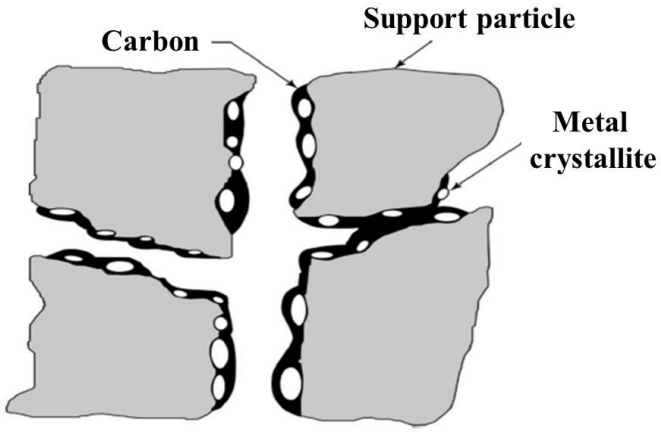

Figure 4.31 A supported metal catalyst with pore plugging due to carbon deposition [105].

Table 4.8 Mass change (%) of catalysts by TGA analysis over different supports.

Catalyst	Reaction Time (h)	TGA analysis Mass change (%)
10Ni/5TiN-HY	2	47.26
10Ni/5TiN-SBA-15	4	41.35

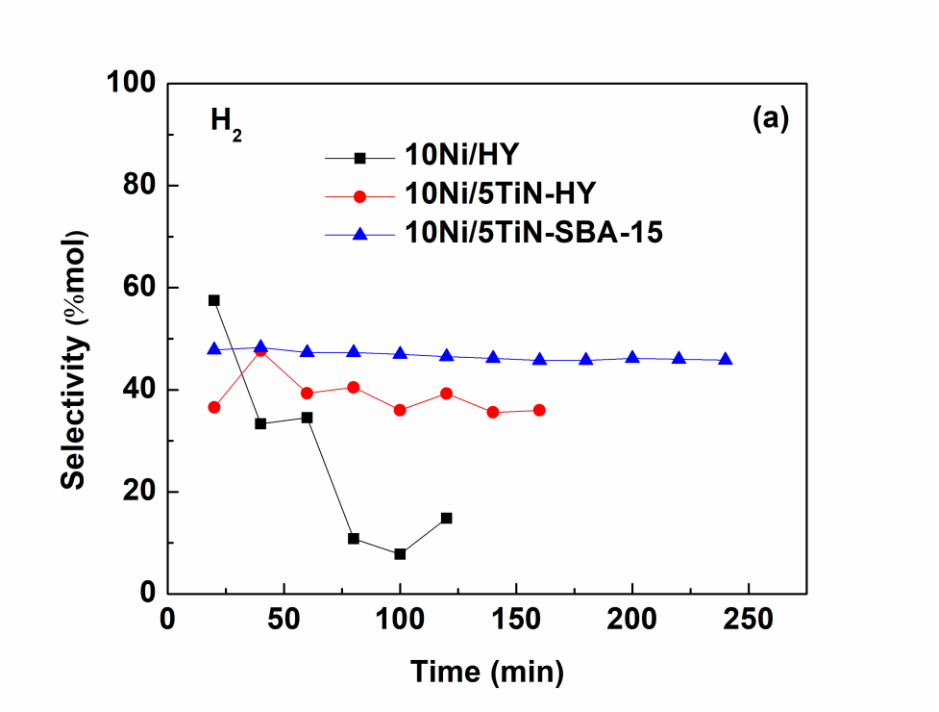
H2
(a)
10Ni/HY
10Ni/5TiN-HY
10Ni/5TiN-SBA-15
Selectivity (%mol)
Time (min)
0
20
40
60
80
100
0
50
100
150
200
250

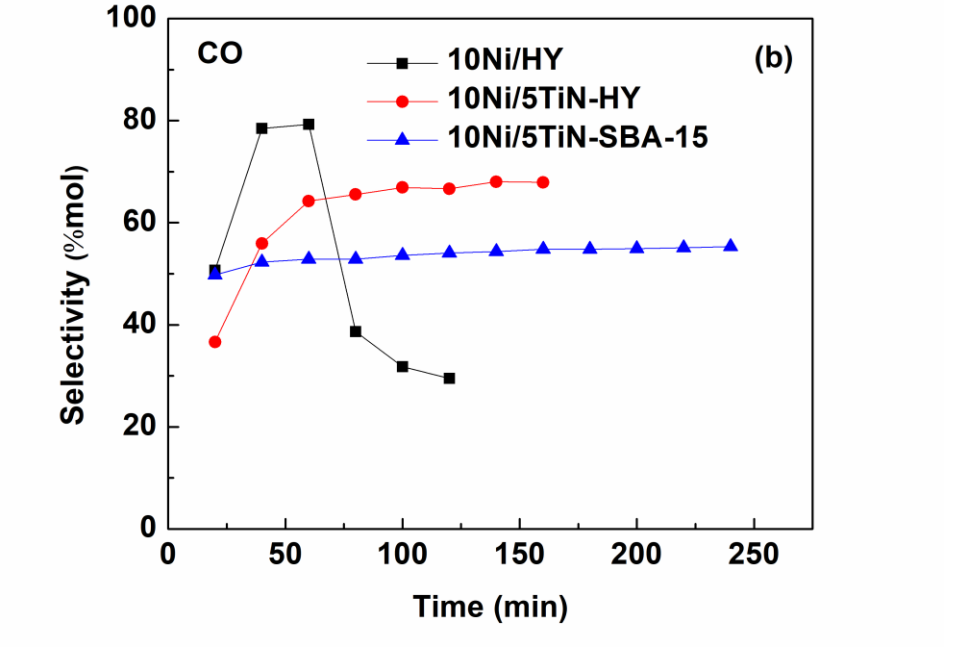
CO
(b)
10Ni/HY
10Ni/5TiN-HY
10Ni/5TiN-SBA-15
Selectivity (%mol)
Time (min)
0
20
40
60
80
100
0
50
100
150
200
250

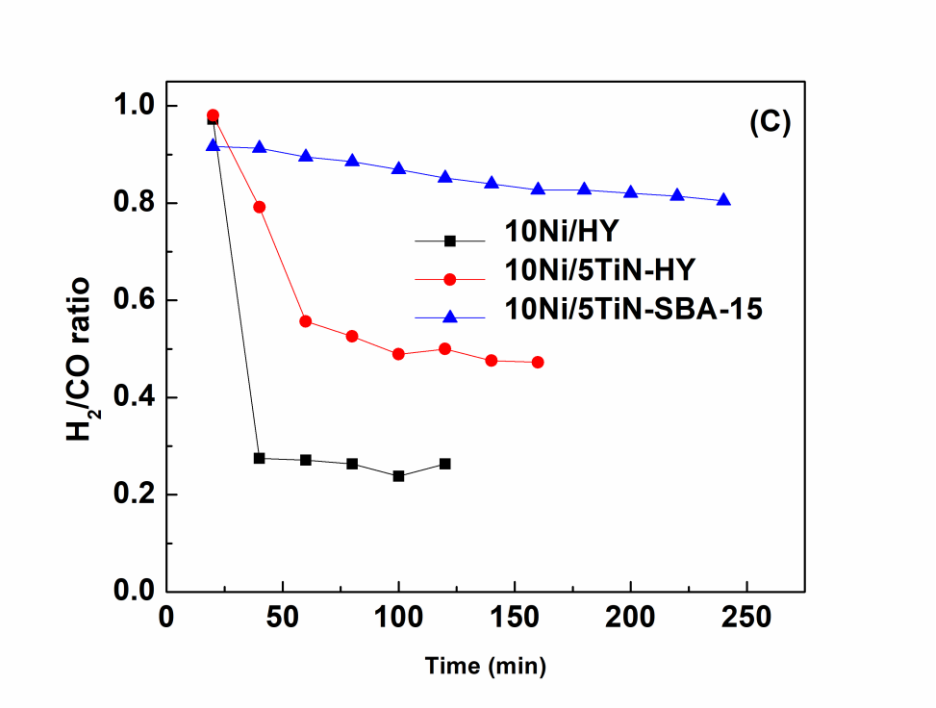

Figure 4.32 Selectivity of (a) H_2 and (b) CO and (c) H_2/CO ratio in dry reforming reaction using 10Ni/HY, 10Ni/5TiN-HY and 10Ni/5TiN-SBA-15 catalysts.

CHAPTER V
CONCLUSIONS AND OUTLOOKS

In this dissertation, the variations of Ni and TiN loading have been successfully prepared by a one-step hydrothermal route together with a facile impregnation method. The intrinsic properties of metals and support, such as the basicity of TiN and mesoporous framework of SBA-15, were still persisted. A difference of catalysts composition affects the catalytic performance and stability of the catalysts. This is the outcomes of the interaction and synergistic catalysis with respect to catalysts constituents: active component, support and promoter. The optimize quantity among Ni, TiN and silica support relates to the catalyst basicity which can enhance CO_2 adsorption, reduce carbon formation and prolong catalyst stability. Therefore, the catalytic performance of the promoted catalysts was greater than conventional catalyst.

In addition, the presence of TiN also reduced relative side reactions, particularly reverse water gas shift reaction with lower CO selectivity than just Ni-base catalyst without TiN promoter. The reaction test for 12 h revealed that the conversion of 66% CH_4 and 71% CO_2 and selectivity of about 45% H_2 and 55% CO were obtained from this new modified catalyst containing 10 wt% Ni and 5 wt% TiN supported on SBA-15. Moreover, supporting material has a strong effect on the catalytic activity. It can conclude that SBA-15 is more appropriate for DRM reaction than zeolite Y. Thus, acidic support is not well-suited to adsorption and dissociation of acidic CO_2. However, TiN is an efficient promoter for Ni-based catalyst with higher catalytic activity than non-promoted conventional catalyst for both silica supports. Therefore, Ni-TiN supported SBA-15 is a promising candidate to apply as a catalyst in DRM reaction.

Outlooks

From this study, it can prove that 10Ni/5TiN-SBA-15 is the promising catalyst for dry reforming of methane with high catalytic activity and stability at 700°C and CH_4:CO_2 =1:1. The reaction productivity could be improved by additional study as follow;

1. Adjust gas reactants ratio (CH_4 and CO_2) altered by the desired products i.e. H_2 or CO-rich syngas in order to find the capacity of catalyst, varying CH_4:CO_2 ratio such as high CO_2 may reduce side reaction by H_2 consumption for reverse water gas shift.

2. Prepare TiN into SBA-15 by post synthesis before Ni impregnation and compare its catalytic efficacy with this study in order to compare the catalyst performance from different preparation method with the same mesoporous structure.

3. Use dealumination of zeolite Y or silicalite-1 as a microporous support to avoid acidic property of the support in order to compare the impact on pore size and structure of SiO_2

4. Test long-term efficiency, stability, and selectivity of the prepared catalysts ~100 h of reaction time

Moreover, Ni/TiN-SBA-15 has a potential to apply in other reactions especially, for the basicity property requirement such as a catalyst, adsorbent or use in the reaction involving CO_2 in favor to make CO_2 utilization cost effective.

REFERENCES

[1] Gao, Q., Liu, N., Wang, S., and Tang, Y. Metal non-oxide nanostructures developed from organic-inorganic hybrids and their catalytic application. Nanoscale 6(23) (2014): 14106-14120.

[2] Ramanathan, S. and Oyama, S.T. New Catalysts for Hydroprocessing: Transition Metal Carbides and Nitrides. The Journal of Physical Chemistry 99(44) (1995): 16365-16372.

[3] Kaskel, S., Schlichte, K., and Kratzke, T. Catalytic properties of high surface area titanium nitride materials. Journal of Molecular Catalysis A: Chemical 208(1) (2004): 291-298.

[4] Duan, Y., Shang, R., Zhong, X., Xie, W., Wang, X., and Huang, L. In-situ synthesis of $NiMo_2C/Al_2O_3$ catalysts for dry reforming of methane. International Journal of Hydrogen Energy 41(47) (2016): 21955-21964.

[5] Yao, Z., et al. Insights into the deactivation mechanism of metal carbide catalysts for dry reforming of methane via comparison of nickel-modified molybdenum and tungsten carbides. RSC Advances 6(24) (2016): 19944-19951.

[6] Fu, X., Su, H., Yin, W., Huang, Y., and Gu, X. Bimetallic molybdenum nitride Co_3Mo_3N: a new promising catalyst for CO_2 reforming of methane. Catalysis Science & Technology 7(8) (2017): 1671-1678.

[7] Shang, R., et al. Carbon dioxide reforming of methane to synthesis gas over Ni/Si_3N_4 catalysts. International Journal of Hydrogen Energy 36(8) (2011): 4900-4907.

[8] Cao, Y., Lu, M., Fang, J., Shi, L., and Zhang, D. Hexagonal boron nitride supported mesoSiO_2-confined Ni catalysts for dry reforming of methane. Chemical Communications 53(54) (2017): 7549-7552.

[9] Avasarala, B. and Haldar, P. On the stability of TiN-based electrocatalysts for fuel cell applications. International Journal of Hydrogen Energy 36(6) (2011): 3965-3974.

[10] Yang, M., Allen, A.J., Nguyen, M.T., Ralston, W.T., MacLeod, M.J., and DiSalvo, F.J. Corrosion behavior of mesoporous transition metal nitrides. Journal of Solid State Chemistry 205 (2013): 49-56.

[11] Yao, W., Makowski, P., Giordano, C., and Goettmann, F. Synthesis of Early-Transition-Metal Carbide and Nitride Nanoparticles through the Urea Route and Their Use as Alkylation Catalysts. Chemistry – A European Journal 15(44) (2009): 11999-12004.

[12] Fischer, A., Makowski, P., Müller, J.-O., Antonietti, M., Thomas, A., and Goettmann, F. High-Surface-Area TiO_2 and TiN as Catalysts for the C-C Coupling of Alcohols and Ketones. ChemSusChem 1(5) (2008): 444-449.

[13] Molinari, V., Giordano, C., Antonietti, M., and Esposito, D. Titanium Nitride-Nickel Nanocomposite as Heterogeneous Catalyst for the Hydrogenolysis of Aryl Ethers. Journal of the American Chemical Society 136(5) (2014): 1758-1761.

[14] Kang, D., Lim, H.S., and Lee, J.W. Enhanced catalytic activity of methane dry reforming by the confinement of Ni nanoparticles into mesoporous silica. International Journal of Hydrogen Energy 42(16) (2017): 11270-11282.

[15] Albarazi, A., Beaunier, P., and Da Costa, P. Hydrogen and syngas production by methane dry reforming on SBA-15 supported nickel catalysts: On the effect of promotion by $Ce_{0.75}Zr_{0.25}O_2$ mixed oxide. International Journal of Hydrogen Energy 38(1) (2013): 127-139.

[16] Sumrunronnasak, S., Tantayanon, S., Kiatgamolchai, S., and Sukonket, T. Improved hydrogen production from dry reforming reaction using a catalytic packed-bed membrane reactor with Ni-based catalyst and dense PdAgCu alloy membrane. International Journal of Hydrogen Energy 41(4) (2016): 2621-2630.

[17] Pakhare, D. and Spivey, J. A review of dry (CO_2) reforming of methane over noble metal catalysts. Chemical Society Reviews 43(22) (2014): 7813-7837.

[18] Wang, N., Yu, X., Wang, Y., Chu, W., and Liu, M. A comparison study on methane dry reforming with carbon dioxide over $LaNiO_3$ perovskite catalysts supported on mesoporous SBA-15, MCM-41 and silica carrier. Catalysis Today 212 (2013): 98-107.

[19] Seo, H.O., Sim, J.K., Kim, K.-D., Kim, Y.D., Lim, D.C., and Kim, S.H. Carbon dioxide reforming of methane to synthesis gas over a TiO_2–Ni inverse catalyst. Applied Catalysis A: General 451 (2013): 43-49.

[20] Qian, L., et al. Investigation of La promotion mechanism on Ni/SBA-15 catalysts in CH_4 reforming with CO_2. Fuel 122 (2014): 47-53.

[21] Wang, Z., Cao, X.M., Zhu, J., and Hu, P. Activity and coke formation of nickel and nickel carbide in dry reforming: A deactivation scheme from density functional theory. Journal of Catalysis 311 (2014): 469-480.

[22] Lavoie, J.-M. Review on dry reforming of methane, a potentially more environmentally-friendly approach to the increasing natural gas exploitation. Frontiers in Chemistry 2(81) (2014).

[23] Zhang, G., Zhao, P., Xu, Y., and Qu, J. Characterization of Ca-promoted Co/AC catalyst for CO_2-CH_4 reforming to syngas production. Journal of CO_2 Utilization 18 (2017): 326-334.

[24] Wang, N., Yu, X., Shen, K., Chu, W., and Qian, W. Synthesis, characterization and catalytic performance of MgO-coated Ni/SBA-15 catalysts for methane dry reforming to syngas and hydrogen. International Journal of Hydrogen Energy 38(23) (2013): 9718-9731.

[25] Mette, K., et al. Redox dynamics of Ni catalysts in CO_2 reforming of methane. Catalysis Today 242 (2015): 101-110.

[26] Zhang, L., Wang, X., Chen, C., Zou, X., Ding, W., and Lu, X. Dry reforming of methane to syngas over lanthanum-modified mesoporous nickel aluminate/γ-alumina nanocomposites by one-pot synthesis. International Journal of Hydrogen Energy 42(16) (2017): 11333-11345.

[27] Zhang, Z.L. and Verykios, X.E. Carbon dioxide reforming of methane to synthesis gas over supported Ni catalysts. Catalysis Today 21(2) (1994): 589-595.

[28] Taherian, Z., Yousefpour, M., Tajally, M., and Khoshandam, B. A comparative study of ZrO_2, Y_2O_3 and Sm_2O_3 promoted Ni/SBA-15 catalysts for evaluation of CO_2/methane reforming performance. International Journal of Hydrogen Energy 42(26) (2017): 16408-16420.

[29] Yu, M., Zhu, Y.-A., Lu, Y., Tong, G., Zhu, K., and Zhou, X. The promoting role of Ag in Ni-CeO_2 catalyzed CH_4-CO_2 dry reforming reaction. Applied Catalysis B: Environmental 165 (2015): 43-56.

[30] Huirache-Acuña, R., et al. SBA-15 Mesoporous Silica as Catalytic Support for Hydrodesulfurization Catalysts—Review. Materials 6(9) (2013): 4139.

[31] Rahmat, N., Abdullah, A.Z., and Mohamed, A. A Review: Mesoporous Santa Barbara Amorphous-15, Types, Synthesis and Its Applications towards Biorefinery Production. Vol. 7, 2010.

[32] Zhao, D., et al. Triblock Copolymer Syntheses of Mesoporous Silica with Periodic 50 to 300 Angstrom Pores. Science 279(5350) (1998): 548-552.

[33] Li, X.-H. and Antonietti, M. Metal nanoparticles at mesoporous N-doped carbons and carbon nitrides: functional Mott-Schottky heterojunctions for catalysis. Chemical Society Reviews 42(16) (2013): 6593-6604.

[34] Sundgren, J.E., Johansson, B.O., Rockett, A., Barnett, S.A., and Greene, J.E. TiNx ($0.6<x<1.2$): Atomic arrangements, Electronic structure and recent results on crystal growth and physical properties of epitaxial layers. AIP Conference Proceedings 149(1) (1986): 95-115.

[35] Lee, T., Delley, B., Stampfl, C., and Soon, A. Environment-dependent nanomorphology of TiN: the influence of surface vacancies. Nanoscale 4(16) (2012): 5183-5188.

[36] Levy, R.B. and Boudart, M. Platinum-Like Behavior of Tungsten Carbide in Surface Catalysis. Science 181(4099) (1973): 547-549.

[37] Avasarala, B. and Haldar, P. Electrochemical oxidation behavior of titanium nitride based electrocatalysts under PEM fuel cell conditions. Electrochimica Acta 55(28) (2010): 9024-9034.

[38] ChemicalBook. [Online]. Available from: http://www.chemicalbook.com/ChemicalProductProperty_EN_CB0179816.htm [2 Novermber]

[39] Vinu, A., Mori, T., and Ariga, K. New families of mesoporous materials. Science and Technology of Advanced Materials 7(8) (2006): 753-771.

[40] Wan, M.M., Sun, X.D., Liu, S., Ma, J., and Zhu, J.H. Versatile drug releaser derived from the Ti-substituted mesoporous silica SBA-15. Microporous and Mesoporous Materials 199 (2014): 40-49.

[41] Huang, J., Yin, J., Chai, W., Liang, C., Shen, J., and Zhang, F. Multifunctional mesoporous silica supported palladium nanoparticles as efficient and reusable catalyst for water-medium Ullmann reaction. New Journal of Chemistry 36(6) (2012): 1378.

[42] Jeenpadiphat, S., Björk, E.M., Odén, M., and Tungasmita, D.N. Propylsulfonic acid functionalized mesoporous silica catalysts for esterification of fatty acids. Journal of Molecular Catalysis A: Chemical 410 (2015): 253-259.

[43] Li, Y., et al. Direct Synthesis of Al−SBA-15 Mesoporous Materials via Hydrolysis-Controlled Approach. The Journal of Physical Chemistry B 108(28) (2004): 9739-9744.

[44] Gómez-Cazalilla, M., Mérida-Robles, J.M., Gurbani, A., Rodríguez-Castellón, E., and Jiménez-López, A. Characterization and acidic properties of Al-SBA-15 materials prepared by post-synthesis alumination of a low-cost ordered

mesoporous silica. Journal of Solid State Chemistry 180(3) (2007): 1130-1140.

[45] Naik, B., Hazra, S., Prasad, V.S., and Ghosh, N.N. Synthesis of Ag nanoparticles within the pores of SBA-15: An efficient catalyst for reduction of 4-nitrophenol. Catalysis Communications 12(12) (2011): 1104-1108.

[46] Bonne, M., et al. Synthesis and characterization of high surface area TiO_2/SiO_2 mesostructured nanocomposite. Solid State Sciences 12(6) (2010): 1002-1012.

[47] Tomer, V.K., Jangra, S., Malik, R., and Duhan, S. Effect of in-situ loading of nano titania particles on structural ordering of mesoporous SBA-15 framework. Colloids and Surfaces A: Physicochemical and Engineering Aspects 466 (2015): 160-165.

[48] [Online]. Available from: http://www.iza-online.org/natural/Datasheets/Faujasite/faujasite.htm [2 Novermber]

[49] Sadeghi, M., Sharifi, S.L., and Hatami, H. Synthesis of nanocrystalline zeolite NaY by hydrothermal method and investigation of its structure and morphology. International Journal of Nano Dimension 5(1) (2014): 91-95.

[50] Fakeeha, A.H., Khan, W.U., Al-Fatesh, A.S., and Abasaeed, A.E. Stabilities of zeolite-supported Ni catalysts for dry reforming of methane. Chinese Journal of Catalysis 34(4) (2013): 764-768.

[51] Luengnaruemitchai, A. and Kaengsilalai, A. Activity of different zeolite-supported Ni catalysts for methane reforming with carbon dioxide. Chemical Engineering Journal 144(1) (2008): 96-102.

[52] Kwak, B.S., Lee, J.S., Lee, J.S., Choi, B.-H., Ji, M.J., and Kang, M. Hydrogen-rich gas production from ethanol steam reforming over Ni/Ga/Mg/Zeolite Y catalysts at mild temperature. Applied Energy 88(12) (2011): 4366-4375.

[53] Lutz, W. Zeolite Y: Synthesis, Modification, and Properties-A Case Revisited. Advances in Materials Science and Engineering 2014 (2014): 20.

[54] Fan, M.-S., Abdullah, A.Z., and Bhatia, S. Catalytic Technology for Carbon Dioxide Reforming of Methane to Synthesis Gas. ChemCatChem 1(2) (2009): 192-208.

[55] Wang, S., Lu, G.Q., and Millar, G.J. Carbon Dioxide Reforming of Methane To Produce Synthesis Gas over Metal-Supported Catalysts: State of the Art. Energy & Fuels 10(4) (1996): 896-904.

[56] Ling Qian, Z.Y. Studies on the Adsorption and Dissociation of Methane and Carbon Dioxide on Nickel. Journal of Energy Chemistry 11(3) (2002): 151-158.

[57] De, S., Zhang, J., Luque, R., and Yan, N. Ni-based bimetallic heterogeneous catalysts for energy and environmental applications. Energy & Environmental Science 9(11) (2016): 3314-3347.

[58] Frontera, P., et al. Catalytic dry-reforming on Ni–zeolite supported catalyst. Catalysis Today 179(1) (2012): 52-60.

[59] Zhang, S., Wang, J., and Wang, X. Effect of calcination temperature on structure and performance of Ni/TiO_2-SiO_2 catalyst for CO_2 reforming of methane. Journal of Natural Gas Chemistry 17(2) (2008): 179-183.

[60] Ghods, B., Meshkani, F., and Rezaei, M. Effects of alkaline earth promoters on the catalytic performance of the nickel catalysts supported on high surface area mesoporous magnesium silicate in dry reforming reaction. International Journal of Hydrogen Energy 41(48) (2016): 22913-22921.

[61] Usman, M., Wan Daud, W.M.A., and Abbas, H.F. Dry reforming of methane: Influence of process parameters—A review. Renewable and Sustainable Energy Reviews 45(C) (2015): 710-744.

[62] Baker, R.T.K. Catalytic growth of carbon filaments. Carbon 27(3) (1989): 315-323.

[63] Wang, G., Wang, H., Li, W., Ren, Z., Bai, J., and Bai, J. Efficient production of hydrogen and multi-walled carbon nanotubes from ethanol over Fe/Al_2O_3 catalysts. Fuel Processing Technology 92(3) (2011): 531-540.

[64] Wu, J., Helveg, S., Ullmann, S., Peng, Z., and Bell, A.T. Growth of encapsulating carbon on supported Pt nanoparticles studied by in situ TEM. Journal of Catalysis 338(Supplement C) (2016): 295-304.

[65] Ham, D. and Lee, J. Transition Metal Carbides and Nitrides as Electrode Materials for Low Temperature Fuel Cells. Energies 2(4) (2009): 873.

[66] Wu, J.C.S. and Chou, H.-C. Bimetallic Rh–Ni/BN catalyst for methane reforming with CO_2. Chemical Engineering Journal 148(2) (2009): 539-545.

[67] Cai, W.-J., Qian, L.-P., Yue, B., and He, H.-Y. Rh doping effect on coking resistance of Ni/SBA-15 catalysts in dry reforming of methane. Chinese Chemical Letters 25(11) (2014): 1411-1415.

[68] Amin, M.H.T., James and Bhargava, Suresh K. . A comparison study on carbon dioxide reforming of methane over Ni catalysts supported on mesoporous SBA-15, MCM-41, KIT-6 and gamma-Al_2O_3. Chemeca 2013 (2013): 543-548.

[69] Yasyerli, S., Filizgok, S., Arbag, H., Yasyerli, N., and Dogu, G. Ru incorporated Ni–MCM-41 mesoporous catalysts for dry reforming of methane: Effects of Mg addition, feed composition and temperature. International Journal of Hydrogen Energy 36(8) (2011): 4863-4874.

[70] Sing, K. The use of nitrogen adsorption for the characterisation of porous materials. Colloids and Surfaces A: Physicochemical and Engineering Aspects 187-188(Supplement C) (2001): 3-9.

[71] Zhao, D., et al. Triblock copolymer syntheses of mesoporous silica with periodic 50 to 300 angstrom pores. Science 279(5350) (1998): 548-52.

[72] Besançon, M., et al. Influence of the porous texture of SBA-15 mesoporous silica on the anatase formation in TiO_2–SiO_2 nanocomposites. New J. Chem. 40(5) (2016): 4386-4397.

[73] Molinari, V., Giordano, C., Antonietti, M., and Esposito, D. Titanium nitride-nickel nanocomposite as heterogeneous catalyst for the hydrogenolysis of aryl ethers. J Am Chem Soc 136(5) (2014): 1758-61.

[74] Jaeger, D. and Patscheider, J. A complete and self-consistent evaluation of XPS spectra of TiN. Journal of Electron Spectroscopy and Related Phenomena 185(11) (2012): 523-534.

[75] Saha, N.C. and Tompkins, H.G. Titanium nitride oxidation chemistry: An x-ray photoelectron spectroscopy study. Journal of Applied Physics 72(7) (1992): 3072-3079.

[76] Oja Acik, I., et al. Characterisation of samarium and nitrogen co-doped TiO_2 films prepared by chemical spray pyrolysis. Applied Surface Science 261 (2012): 735-741.

[77] Zhang, H., Tang, C., Lv, Y., Gao, F., and Dong, L. Direct synthesis of Ti-SBA-15 in the self-generated acidic environment and its photodegradation of Rhodamine B. Journal of Porous Materials 21(1) (2014): 63-70.

[78] Huang, D.G., et al. Synthesis of samarium- and nitrogen-co-doped TiO_2 by modified hydrothermal method and its photocatalytic performance for the degradation of 4-chlorophenol. Journal of Physics and Chemistry of Solids 70(5) (2009): 853-859.

[79] Wu, D., Long, M., Cai, W., Chen, C., and Wu, Y. Low temperature hydrothermal synthesis of N-doped TiO_2 photocatalyst with high visible-light activity. Journal of Alloys and Compounds 502(2) (2010): 289-294.

[80] Singh, U.G., Williams, R.T., Hallam, K.R., and Allen, G.C. Synthesis and characterisation of titanium and titanium nitride-functionalised MCM 41 materials. Solid State Sciences 7(9) (2005): 1104-1112.

[81] Yang, L., Jiang, Z., Lai, S., Jiang, C., and Zhong, H. Synthesis of Titanium Containing SBA-15 and Its Application for Photocatalytic Degradation of Phenol. International Journal of Chemical Engineering 2014 (2014): 7.

[82] Feng, J., et al. Post-Synthesis of Ti-SBA-15 in Supercritical CO_2-Ethanol Solution. CLEAN – Soil, Air, Water 37(7) (2009): 527-533.

[83] Pouilleau, J., Devilliers, D., Groult, H., and Marcus, P. Surface study of a titanium-based ceramic electrode material by X-ray photoelectron spectroscopy. Journal of Materials Science 32(21) (1997): 5645-5651.

[84] Cheng, G., Luo, J., Qian, J., and Miao, J. Surface modification of nano-TiN by using silane coupling agent. Materials Science-Poland 32(2) (2014).

[85] Wang, F., et al. Tuning the metal-support interaction in catalysts for highly efficient methane dry reforming reaction. Applied Catalysis B: Environmental 180 (2016): 511-520.

[86] Xu, J., Chen, T., Shang, J.-K., Long, K.-Z., and Li, Y.-X. Facile preparation of SBA-15-supported carbon nitride materials for high-performance base catalysis. Microporous and Mesoporous Materials 211 (2015): 105-112.

[87] Yang, C.-T. and Huang, M.H. Formation of Arrays of Gallium Nitride Nanorods within Mesoporous Silica SBA-15. The Journal of Physical Chemistry B 109(38) (2005): 17842-17847.

[88] Yao, P., Zhong, S., and Shen, Z. TiO_2/Halloysite Composites Codoped with Carbon and Nitrogen from Melamine and Their Enhanced Solar-Light-Driven Photocatalytic Performance. International Journal of Photoenergy 2015 (2015): 8.

[89] Wang, J., Zhu, W., Zhang, Y., and Liu, S. An Efficient Two-Step Technique for Nitrogen-Doped Titanium Dioxide Synthesizing: Visible-Light-Induced Photodecomposition of Methylene Blue. The Journal of Physical Chemistry C 111(2) (2007): 1010-1014.

[90] Dai, Q., Wang, X., Chen, G., Zheng, Y., and Lu, G. Direct synthesis of Cerium(III)-incorporated SBA-15 mesoporous molecular sieves by two-step synthesis method. Microporous and Mesoporous Materials 100(1) (2007): 268-275.

[91] Wang, N., Chu, W., Zhang, T., and Zhao, X.S. Synthesis, characterization and catalytic performances of Ce-SBA-15 supported nickel catalysts for methane dry reforming to hydrogen and syngas. International Journal of Hydrogen Energy 37(1) (2012): 19-30.

[92] Al-Fatesh, A.S., Naeem, M.A., Fakeeha, A.H., and Abasaeed, A.E. Role of La_2O_3 as Promoter and Support in Ni/γ-Al_2O_3 Catalysts for Dry Reforming of Methane. Chinese Journal of Chemical Engineering 22(1) (2014): 28-37.

[93] Dai, Y.-M., Lu, C.-Y., and Chang, C.-J. Catalytic activity of mesoporous Ni/CNT, Ni/SBA-15 and (Cu, Ca, Mg, Mn, Co)-Ni/SBA-15 catalysts for CO_2 reforming of CH_4. RSC Advances 6(77) (2016): 73887-73896.

[94] Coq, B. and Figueras, F. Bimetallic palladium catalysts: influence of the co-metal on the catalyst performance. Journal of Molecular Catalysis A: Chemical 173(1) (2001): 117-134.

[95] Arbag, H., Yasyerli, S., Yasyerli, N., and Dogu, G. Activity and stability enhancement of Ni-MCM-41 catalysts by Rh incorporation for hydrogen from dry reforming of methane. International Journal of Hydrogen Energy 35(6) (2010): 2296-2304.

[96] Gunduz Meric, G., Arbag, H., and Degirmenci, L. Coke minimization via SiC formation in dry reforming of methane conducted in the presence of Ni-based core–shell microsphere catalysts. International Journal of Hydrogen Energy 42(26) (2017): 16579-16588.

[97] Ayodele, B.V., Khan, M.R., Lam, S.S., and Cheng, C.K. Production of CO-rich hydrogen from methane dry reforming over lanthania-supported cobalt catalyst: Kinetic and mechanistic studies. International Journal of Hydrogen Energy 41(8) (2016): 4603-4615.

[98] Al-Fatesh, A.S. Promotional effect of Gd over Ni/Y_2O_3 catalyst used in dry reforming of CH_4 for H_2 production. International Journal of Hydrogen Energy 42(30) (2017): 18805-18816.

[99] Rahbar Shamskar, F., Rezaei, M., and Meshkani, F. The influence of Ni loading on the activity and coke formation of ultrasound-assisted co-precipitated Ni-Al_2O_3 nanocatalyst in dry reforming of methane. International Journal of Hydrogen Energy 42(7) (2017): 4155-4164.

[100] Liu, Z., et al. Highly dispersed nickel loaded on mesoporous silica: One-spot synthesis strategy and high performance as catalysts for methane reforming with carbon dioxide. Applied Catalysis B: Environmental 125 (2012): 324-330.

[101] Amin, R., Liu, B., Ullah, S., and Biao, H.Z. Study of coking and catalyst stability over CaO promoted Ni-based MCF synthesized by different methods for CH_4/CO_2 reforming reaction. International Journal of Hydrogen Energy 42(34) (2017): 21607-21616.

[102] Dębek, R., Motak, M., Galvez, M.E., Grzybek, T., and Da Costa, P. Influence of Ce/Zr molar ratio on catalytic performance of hydrotalcite-derived catalysts at low temperature CO_2 methane reforming. International Journal of Hydrogen Energy (2017).

[103] Li, D., et al. Ceria-promoted Ni/SBA-15 catalysts for ethanol steam reforming with enhanced activity and resistance to deactivation. Applied Catalysis B: Environmental 176 (2015): 532-541.

[104] Muraza, O. and Galadima, A. A review on coke management during dry reforming of methane. International Journal of Energy Research 39(9) (2015): 1196-1216.
[105] Argyle, M. and Bartholomew, C. Heterogeneous Catalyst Deactivation and Regeneration: A Review. Catalysts 5(1) (2015): 145.

APPENDIX

APPENDIX A

Catalyst preparation

1. Preparation of TiN-SBA-15 by direct synthesis

The obtained composition of 5, 10, 15 and 18TiN-SBA-15 were prepared by the loading amount of TiN as shown in Table A1. The percentage of TiN measurement by WDXRF was less than the loading amount almost 0.6 times for all samples. Owing to the characteristic of TiN which is poor aqueous solubility so the particles may aggregate and separate from the gel solution during the synthesis and washing step.

Table A1 Chemical composition of TiN-SBA-15

Sample	Amount of TiN loading (wt%)	Composition by WDXRF (wt%)		$TiN^*/TiN_{loading}$
		Ti	TiN*	
5TiN-SBA-15	8	3.8	4.9	0.61
10TiN-SBA-15	15	7.2	9.3	0.62
15TiN-SBA-15	22	11.2	14.5	0.66
18TiN-SBA-15	28	13.9	17.9	0.64

***calculation:** Ti 47.87 g containing in TiN 61.874 g/mol

Ti 3.8 g = (61.874*3.8)/47.87 = 4.9 g

- TEOS MW 208.33 g/mol and SiO_2 MW 60.08 g/mol

Basis 8.5 g of TEOS

Therefore, weight of SiO_2 = (8.5g/208.33g.mol^{-1})*60.08 g/mol = 2.45 g

Example; 5TiN-SBA-15 was obtained from 8 wt% of TiN loading

Based on 100 g of catalyst; the catalyst composition of 8 wt% TiN loading is containing 92 g of SiO_2 and 8 g of TiN

For 2.45 g of SiO_2;

Required TiN = (8*2.45)/92 = 0.22 g

Therefore, 5TiN-SBA-15 was prepared by loading 0.22 g of TiN into 8.5 g of TEOS.

2. Preparation of Ni/TiN-SBA-15 by impregnation

- $Ni(NO_3)_2.6H_2O$ MW 292 g/mol

Example; 10Ni/5TiN-SBA-15 was obtained from 10 wt% of Ni loading.

Based on 100 g of catalyst; the catalyst composition of 10 wt% Ni loading is containing 90 g of 5TiN-SBA-15 and 10 g of Ni

For 1 g of 5TiN-SBA/15;

Required Ni = (10*1)/90 = 0.11 g

The required Ni was prepared from $Ni(NO_3)_2.6H_2O$ as follow;

Ni 58.69 g containing in $Ni(NO_3)_2.6H_2O$ 292 g

Ni 0.11 g containing in $Ni(NO_3)_2.6H_2O$ = (292*0.11)/58.69 = 0.55 g

Therefore 10Ni/5TiN-SBA-15 was prepared by loading 0.55 of $Ni(NO_3)_2.6H_2O$ into 1 g of 5TiN-SBA/15.

APPENDIX B

Additional details of Catalyst activity

Catalyst 0.05 g

Average catalyst bed high = 2 cm

Diameter inside stainless tube = 0.35 cm

Volume of bed = πr^2 x catalyst bed high (cm)

= 3.14 x $(0.35)^2$ x 2 = 0.77 cm^3

GSHV = Gas volumetric flow rate[1]/Volume of bed

= 20 (ml/min)/ 0.77 ml

= 25.97 min^{-1} x 60 $min.h^{-1}$ = 1558 h^{-1}

at STP; Gas volumetric flow rate = volumetric flow rate[1] *((273.25+T)/(273.15))

T = room temperature

Table A2 Data of dry reforming reaction with and without Ni catalyst at 700°C.

Catalyst	H_2 yield (%)		CO yield (%)		H_2/CO	
	1h	4h	1h	4h	1h	4h
No catalyst	(-)	(-)	(-)	(-)	(-)	(-)
5TiN-SBA-15	(-)	(-)	(-)	(-)	(-)	(-)
10TiN-SBA-15	(-)	(-)	(-)	(-)	(-)	(-)
15TiN-SBA-15	(-)	(-)	(-)	(-)	(-)	(-)
18TiN-SBA-15	(-)	(-)	(-)	(-)	(-)	(-)
2.5Ni/SBA-15	(-)	(-)	5.2	(-)	(-)	(-)
2.5Ni/5TiN-SBA-15	(-)	(-)	9.5	(-)	(-)	(-)
2.5Ni/10TiN-SBA-15	(-)	(-)	9.4	(-)	(-)	(-)
2.5Ni/15TiN-SBA-15	12.2	(-)	24.1	(-)	0.51	(-)
2.5Ni/18TiN-SBA-15	23.1	15.1	35.1	25.1	0.66	0.66
5Ni/SBA-15	(-)	(-)	8.63	(-)	0.34	(-)
5Ni/5TiN-SBA-15	31.4	29.3	39.5	39.2	0.80	0.75
5Ni/10TiN-SBA-15	29.0	23.4	37.0	33.2	0.78	0.70
5Ni/15TiN-SBA-15	25.4	12.4	34.6	22.2	0.73	0.56
5Ni/18TiN-SBA-15	22.1	12.8	33.6	22.3	0.66	0.58
7.5Ni/SBA-15	26.6	11.7	31.1	18.9	0.86	0.62
7.5Ni/5TiN-SBA-15	32.1	29.9	39.3	40.0	0.82	0.75
7.5Ni/10TiN-SBA-15	32.9	31.8	38.9	39.7	0.85	0.80
7.5Ni/15TiN-SBA-15	28.5	21.3	37.1	30.5	0.77	0.70
7.5Ni/18TiN-SBA-15	31.9	30.9	36.1	37.3	0.88	0.83
10Ni/SBA-15	31.9	29.2	39.2	38.9	0.81	0.75
10Ni/5TiN-SBA-15	33.7	32.7	41.0	38.6	0.82	0.85
10Ni/10TiN-SBA-15	31	29.6	39.8	39.7	0.78	0.75
10Ni/15TiN-SBA-15	32.3	30.1	37.3	38.1	0.80	0.79
10Ni/18TiN-SBA-15	31.4	29.5	39.2	39.1	0.87	0.75
(-) < 5%						

The H_2 and CO selectivity of DRM at 4 h reaction.

- H_2 selectivity (2.5–10 wt% of Ni)

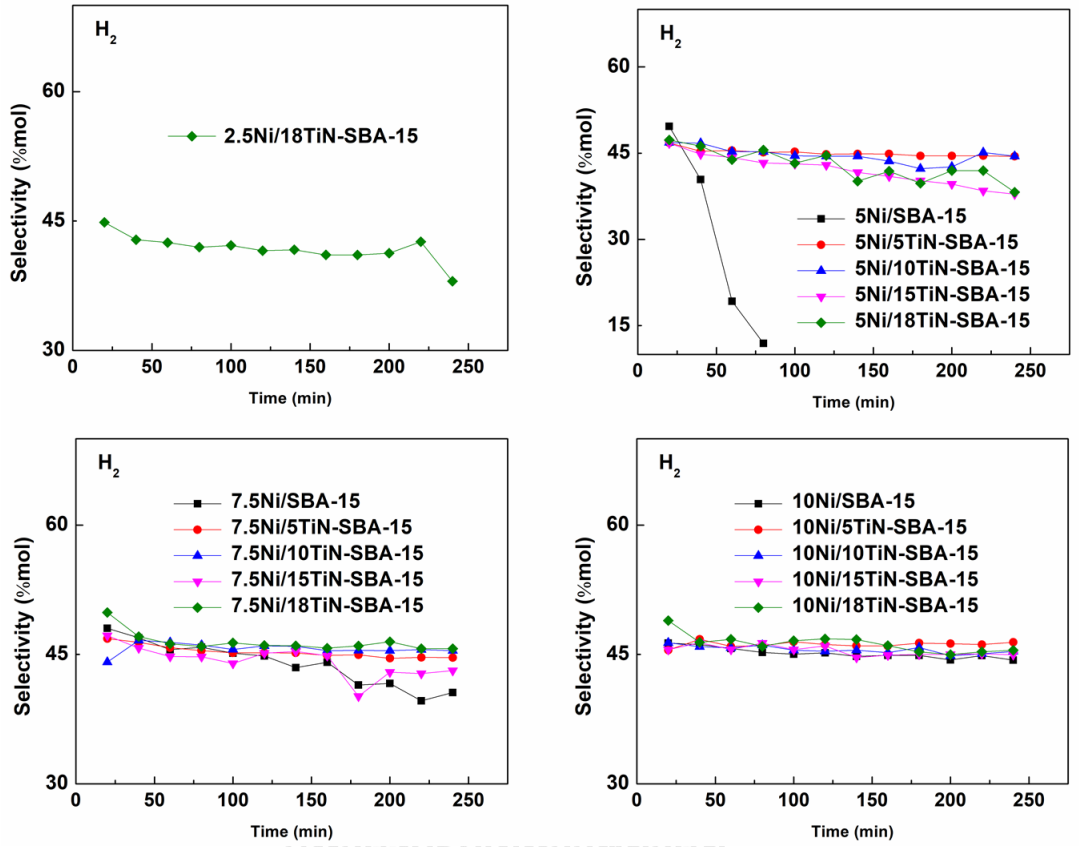

- CO selectivity (2.5–10 wt% of Ni)

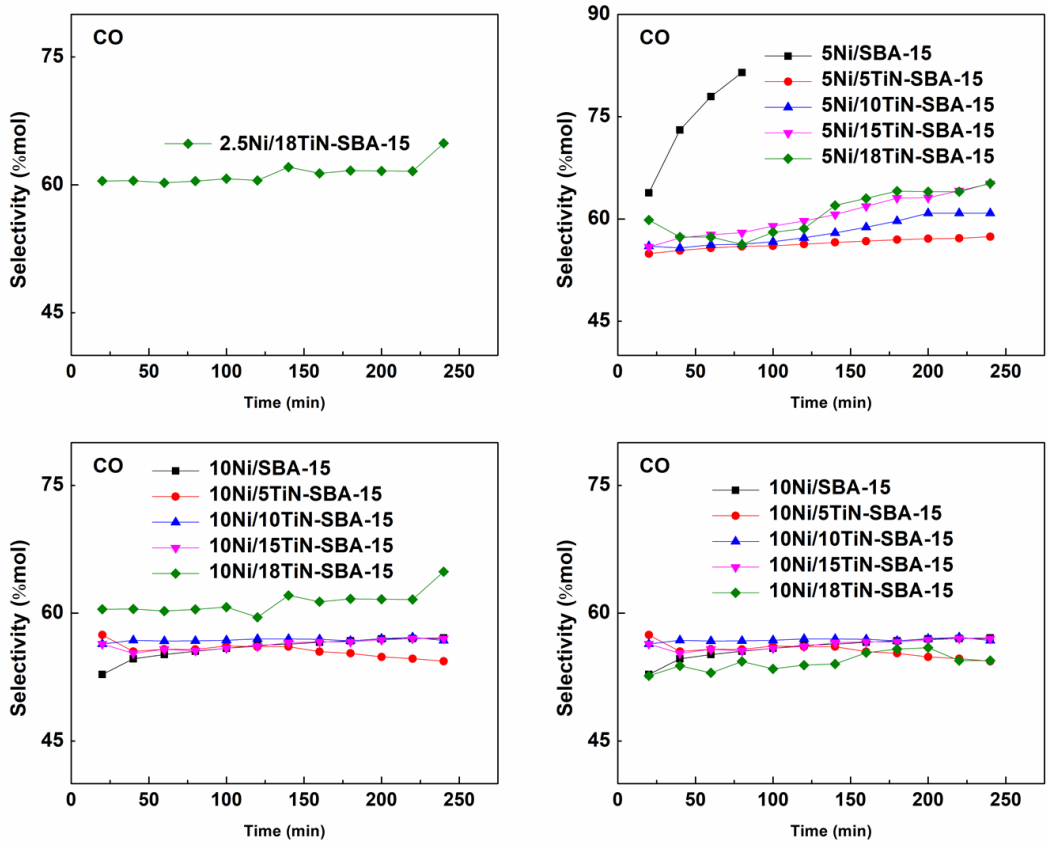

VITA

Miss Maslin Chotirach was born on August 30, 1984 in Songkhla, Thailand. She received her Bachelor degree of Science in Chemistry from Prince of Songkla University in 2007. She continued her study in Master's degree, majoring in Petrochemistry and Polymer Science, Faculty of Science, Chulalongkorn University, Bangkok, Thailand since 2007 and finished her study in 2009. She has been a Ph.D. student in Program of Petrochemisty, Faculty of Science, Chulalongkorn University, Bangkok, Thailand since 2012 and finished her studied in 2017.

Publication

Chotirach, M.; Tantayanon, S.; Tungasmita, S.; Kriausakul, K., Zr-based intermetallic diffusion barriers for stainless steel supported palladium membranes. Journal of Membrane Science 2012, 405-406, 92-103.

Chotirach, M.; Tantayanon, S.; Tungasmita, D.N; Sun, J.; Wang, X.; Tungasmita, S., Direct synthesis of TiN confined in the framework of ordered mesoporous SBA-15. (Manuscript)

Chotirach, M.; Tantayanon, S.; Tungasmita, D.N; Tungasmita, S.,TiN promoted Ni-based SBA-15 catalyst for dry reforming of methane (Manuscript)